Functional characteristics of periodontitis and peri-implantitis lesions in humans

Carlotta Dionigi

Department of Periodontology

Institute of Odontology

Sahlgrenska Academy

University of Gothenburg

UNIVERSITY OF GOTHENBURG

Gothenburg 2023

carlotta.dionigi@gu.se

ISBN 978-91-8069-465-0 (PRINT)
ISBN 978-91-8069-466-7 (PDF)
http://hdl.handle.net/2077/78885

Printed in Borås, Sweden 2023
Printed by Stema Specialtryck AB

To my family

"Alone we can do so little, together we can do so much."
– H. Keller

Abstract

In the current series of studies functional characteristics of periodontitis and peri-implantitis lesions in humans were investigated. Cell markers for antimicrobial activity were used to evaluate differences between periodontitis and peri-implantitis lesions (**Study I**), while epigenetic and oxidative stress markers were used to compare periodontitis lesions in smokers and non-smokers (**Study II**). The occurrence and localization of titanium micro-particles were assessed in tissue samples obtained from dental implant sites with and without peri-implantitis and the influence of titanium particles on gene expression profiles was investigated in peri-implantitis lesions (**Study III)**. Gene expression profiles were analyzed in tissue samples obtained from dental implant sites with and without peri-implantitis by integrating spatial transcriptomics and RNA-sequencing data (**Study IV**).

It was demonstrated that:

- Peri-implantitis lesions were larger and presented with significantly larger densities of cells with antimicrobial activity than periodontitis lesions. In both lesions, cellular densities were higher in the inner zone, lateral to the pocket epithelium, than in the outer compartment of the lesion The non-infiltrated connective tissue in peri-implantitis specimens showed significantly higher densities of cells with antimicrobial activity than that in periodontitis specimens (**Study I**).

- Although periodontitis lesions did not differ in size between smokers and non-smokers, differences in cellular functions were observed. Periodontitis lesions in smokers presented with diminished antimicrobial activity and lower levels of epigenetic markers than lesions in non-smokers (**Study II**).

- Densities of titanium micro-particles in peri-implant tissues varied across patients but not between dental implant sites with and without peri-implantitis within the same individual. The titanium micro-particles were of similar size and morphology and mainly located in a 2-mm wide tissue zone close to the implant, in samples with and without peri-implantitis. Out of >36000 analyzed genes, only 14 were differentially expressed when comparing peri-implantitis specimens with high and low densities of titanium micro-particles (**Study III**).

- A clear association was observed between distinct gene clusters and specific compartments in peri-implant tissues. Peri-implantitis specimens showed overall higher levels of gene activity than specimens from reference implant sites. Several pathways specific for the activation of the host response towards bacterial insults were clearly dysregulated in peri-implantitis specimens (**Study IV**).

Keywords: periodontitis, peri-implantitis, biopsy, immunohistochemistry, oxidative stress, epigenetics, titanium micro-particles, proton-induced X-rays emission, RNA-sequencing, spatial transcriptomics.

Sammanfattning på svenska

I föreliggande avhandlingsserie analyserades funktionella egenskaper i inflammationsprocesser i vävnadsprover från patienter med parodontit och periimplantit. Cellmarkörer för inflammationsreaktiva ämnen och epigenetiska markörer användes för att studera skillnader mellan parodontit- och periimplantitlesioner (**Studie 1**) och mellan parodontitlesioner hos rökare och icke-rökare (**Studie 2**). Mikropartiklar av titan i periimplantära vävnader från områden med och utan periimplantit karakteriserades och deras effekt på cellreaktioner i periimplantitlesioner analyserades i **Studie 3**. Nya molekylärbiologiska tekniker användes i **Studie 4** för att utforska specifika mönster i genuttryck i vävnadsprover från områden med och utan periimplantit.

Resultaten visade att

- Lesionerna vid periimplantit var större och innehöll högre andel celler med antimikrobiell aktivitet än de vid parodontit. Vid båda sjukdomstillstånden var celltätheten var högre i den delen av lesionerna som gränsade mot fickepitelet. I de delar av vävnadsproven från periimplantit som definierats vara utanför lesionens område var densiteten av celler med inflammationsreaktiva ämnen markant högre än i motsvarande vävnadsområden från parodontit (**Studie 1**).

- Även om parodontitlesionerna var lika stora hos rökare och icke-rökare fanns skillnader beträffande inflammationscellernas funktion. Parodontitlesioner hos rökare visade minskad antimikrobiell aktivitet och lägre nivåer av epigenetiska markörer. (**Studie 2**).

- Den proportionella förekomsten av titanpartiklar i periimplantära vävnader varierade mellan patienter men inte mellan tandimplantatområden med och utan periimplantit inom samma individ. Mikropartiklarna var av samma storlek och huvudsakligen lokaliserade till en 2 mm bred vävnadszon intill implantatet vid områden med och utan periimplantit. Endast 14 gener av totalt >36 000 analyserade s.k. transcripts identifierades som avvikande vid jämförelse av periimplantit-vävnadsprover med hög respektive låg procentuell förekomst av titanpartiklar (**Studie 3**).

- Ett tydligt samband noterades mellan distinkta genkluster och specifika områden i periimplantära vävnader. En högre andel aktiverade gener noterades i vävnadsprover från implantatområden med periimplantit jämfört med områden utan periimplantit. Avvikelserna i genuttryck mellan de två grupperna av vävnadsprover var kopplade till olika komponenter i aktiveringskedjan för vävnadsförsvaret mot bakteriella infektioner (**Studie 4**).

List of papers

This thesis is based on the following studies, referred to in the text by their Roman numerals:

I. Dionigi C., Larsson L., Carcuac O. & Berglundh T.
Cellular expression of DNA damage/repair and reactive oxygen/nitrogen species in human periodontitis and peri-implantitis lesions.
Journal of Clinical Periodontology 2020; 47 (12): 1466–1475.

II. Dionigi C., Larsson L., Difloe-Geisert J.C., Zitzmann N. & Berglundh T.
Cellular expression of epigenetic markers and oxidative stress in periodontitis lesions of smokers and non-smokers.
Journal of Periodontal Research 2022; 57 (5): 952–959.

III. Dionigi C., Nagy G., Ichioka Y., Derks J., Tomasi C., Larsson L., Primetzhofer D. & Berglundh T.
Titanium micro-particles in soft tissues around dental implants.
In manuscript.

IV. Dionigi C., Larsson L. & Berglundh T.
Spatial transcriptomic assessments of gene expression profiles in human peri-implant lesions.
In manuscript.

Content

Abbreviations

CP	Chronic periodontitis
PI	Peri-implantitis
PI-M	Peri-implant mucositis
PPD	Probing pocket depth
BOP	Bleeding on probing
SOP	Suppuration on probing
MBL	Marginal bone level
IHC	Immunohistochemistry
ILM	Inverted light microscopy
FFPE	Formalin-fixed paraffin-embedded
H&E	Hematoxylin & eosin
RONS	Reactive oxygen/nitrogen species
ROI	Region of interest
ICT	Infiltrated connective tissue
PE	Pocket epithelium
NCT	Non-infiltrated connective tissue
RNA-seq	RNA sequencing
ST	Spatial transcriptomics
mRNA	Messenger RNA
gDNA	Genomic DNA
cDNA	Complementary DNA
UMI	Unique molecular identifier
μ-PIXE	Micro-Proton-Induced X-Ryas Emission
TEM	Transmission electron microscopy
Ti	Titanium
MeV	Mega electron volt
KeV	Kilo electron volt

Introduction

Periodontitis is an inflammatory disease characterized by complex host-microbial interactions that lead to progressive loss of the supporting apparatus around teeth, ultimately resulting in tooth loss (Papapanou et al., 2018). The latest classification of periodontitis, introduced at the 2017 World Workshop, provides a model useful not only for the characterization of patients with the disease, but also for the planning of efficient treatment strategies (Caton et al., 2018; Tonetti et al., 2018; Tonetti & Sanz, 2019; Sanz et al., 2020; Herrera et al., 2022). While keeping a straight-forward structure, the new classification highlights that periodontitis is a complex condition. In fact, the classification emphasizes the need for assessing the extension and severity of the disease together with additional factors that influence the risk for progression and the response to treatment.

Despite efforts in recognizing early stages of disease, implementing preventive programs, and developing new treatment modalities, severe periodontitis remains the 6th most common disease in man (Kassebaum et al., 2017). Concomitantly, the number of dental implants installed annually worldwide is increasing, with estimations up to a magnitude of >20 million each year. The use of dental implants is therefore considered to be a safe procedure in replacing lost teeth, as clinical studies have reported survival rates of dental implants between 92% and 97% at 10 years (Jung et al., 2012; Pjetursson et al., 2012). Recent studies, however, revealed that complications in implant dentistry are not uncommon and that the number of implants in need for further treatment is also growing (Karlsson et al., 2020).

Peri-implant diseases include peri-implantitis and peri-implant mucositis and constitute a major problem in dentistry. Peri-implantitis is defined as "a plaque-associated pathological condition characterized by inflammation in the peri-implant mucosa and subsequent loss of supporting bone" (Berglundh et al., 2018; Schwarz et al., 2018). The absence of bone loss is, instead, what distinguishes peri-implant mucositis from peri-implantitis (Berglundh et al., 2018; Heitz-Mayfield & Salvi, 2018). It is estimated that severe forms of peri-implantitis affect approximately 15% of patients restored with dental implants after 9 years in function (Derks et al., 2016a).

Thus, the formation of a bacterial biofilm on a tooth or implant surface and the resulting inflammatory response in adjacent soft tissues are respectively recognized as "the key etiological factor" and "the primary biological mechanism" in the pathogenesis of both periodontal and peri-implant diseases.

Periodontal and peri-implant lesions

The fact that accumulation of microbial plaque on implants promotes an inflammatory response in the soft tissues similarly to what happens at teeth is a well-established concept, as shown in pre-clinical (Berglundh et al., 1992; Lindhe et al., 1992; Abrahamsson et al., 1998; Carcuac et al., 2013) and clinical studies (Pontoriero et al., 1994; Zitzmann et al., 2001).

Already 3 weeks after plaque accumulation, soft tissues surrounding dental implants and teeth presented with analogous reactions (Berglundh et al., 1992). Consistent observations of higher numbers of leukocytes, increased vascular densities and decreased collagen proportions were reported. These early stages of disease, namely gingivitis and peri-implant mucositis, are initially located within the marginal portion of the gingival/mucosal connective tissue compartment and appear to be reversible. In fact, re-establishment of healthy conditions can be achieved both at tooth and implant sites once optimal oral hygiene measures are re-introduced (Salvi et al., 2011). On the other hand, if left untreated, the lesions may progress with time and develop into more severe pathological stages where inflammation progresses together with loss of supporting tissues (Zitzmann et al., 2001; Jepsen et al., 2015; Chapple et al., 2018).

Redness, swelling, bleeding on probing and increased probing depths are all typical clinical signs found both in periodontal and peri-implant diseases, while radiographic examinations are used to detect marginal bone loss. Despite these similar features, peri-implantitis appears to "progress with a faster and non-linear pattern compared to periodontitis" (Fransson et al., 2010; Derks et al., 2016b; Berglundh et al., 2018; Schwarz et al., 2018). In addition, findings reported in pre-clinical studies also pointed to differences between the two diseases. While the infiltrated connective tissue (ICT) was 4 to 6 times larger in peri-implantitis than in periodontitis, the lesion in peri-implantitis was located closer to the bone crest and contained larger amounts of neutrophils and osteoclasts. The epithelial lining in peri-implantitis was commonly ulcerated in its apical portion, allowing a direct contact between the microbial biofilm and the lesion (Lindhe et al., 1992; Carcuac et al., 2013).

In the last two decades, studies on human biopsy material confirmed the findings of impaired and exaggerated inflammatory reactions in peri-implantitis compared to periodontitis (**Table 1**). In fact, peri-implantitis samples consistently contained

significantly higher numbers and densities of plasma cells, neutrophils and macrophages (Carcuac & Berglundh, 2014; Galindo-Moreno et al., 2017). Further characterizations of macrophage phenotypes revealed that higher numbers of pro-inflammatory "M1" species, but similar levels of pro-healing "M2" macrophages, were noted in peri-implantitis lesions (Fretwurst et al., 2020). In addition, levels of proteolytic enzymes and pro-inflammatory cytokines were significantly enhanced in peri-implantitis (Konttinen et al., 2006; Venza et al., 2010; Ghighi et al., 2018). Other studies also demonstrated different gene-expression profiles between samples from peri-implantitis and periodontitis sites (Wu et al., 2013; Becker et al., 2014; Liu et al., 2020; Cho et al., 2020; Zhou et al., 2020; Figueiredo et al., 2020).

Although analyses of human tissue biopsies represent one of the most valuable models in pathophysiology research, the interpretation of results from most of the above-mentioned studies is limited by small sample sizes and a vast heterogeneity of case definitions.

Fundamental anatomical and structural differences between periodontal and peri-implant tissues may contribute to differences in disease progression. The different orientation of collagen fibers, the diverse vasculature arrangement, and the different type of attachment towards the implant surface (Berglundh et al., 1991; Lang et al., 2011; Carcuac & Berglundh, 2014) are all factors which may influence the apical progression of the inflammatory reaction around dental implants.

In addition, studies on the oral microbiome introduced the concept of "dysbiosis" to indicate the capacity of oral bacteria to manipulate the immune response and to promote a self-perpetuating inflammatory loop (Hajishengallis et al., 2020). In a recent clinical study, specific microbial signatures correlated with increased disease severity in peri-implantitis sites. In addition, sites with deep pockets showed higher levels of dysbiotic microbiota than sites with shallow pockets (Kroger et al., 2018).

The observation that peri-implantitis is characterized by enhanced numbers and densities of neutrophils (Carcuac & Berglundh, 2014) seems to be partly in line with the idea of a dysbiotic alteration of the host-microbe homeostasis. Peri-implantitis lesions are, in fact, characterized by the lack of an epithelial lining in the apical portion of the tissue facing the biofilm residing in the pocket area. This exposure leads to the recruitment of neutrophils and macrophages towards the

unprotected tissue portion. The findings of large numbers of neutrophils in central portions of peri-implantitis lesions (Gualini & Berglundh, 2003; Berglundh et al., 2004) corroborate observations on greater severity and extension of tissue breakdown in peri-implantitis than in periodontitis.

Although presenting with similar clinical features, periodontal and peri-implant diseases appear to have profound pathological differences. Further studies with adequate sample size are therefore needed. In a continuing evaluation of human soft tissue biopsies (Carcuac & Berglundh, 2014), **Study I** was performed to evaluate differences in cellular expressions of DNA-damage/repair and oxidative stress markers between periodontitis and peri-implantitis lesions.

Table 1. Comparisons of periodontitis and peri-implantitis lesions in humans (n=19 studies)

Study	N of patients	Methods & Markers	Main findings
Bullon et al., 2004	15 subjects: 5 with AP 5 with PI 5 healthy peri-implant controls	Histology & Immunohistochemistry: CD1a CD3 CD20 CD34 Factor-VIII VEGF bcl2 p53 Mib1	Thin non-keratinized junctional epithelium partly ulcerated in PI. In ICT: significantly more CD34, Factor-VIII and VEGF in PI than in AP sites. Similar levels of bcl2 and p53 in the three groups.
Konttinen et al., 2006	30 subjects: 10 with PI 10 with CP 10 healthy periodontal controls	Histology & Immunohistochemistry: TNF-α IL-1a IL-6 PDGF-A TGF-a	Significantly higher levels of IL-1a and IL-6 but lower levels of TNF-α in PI than in CP. Multinuclear giant cells only found in PI.
Kuula et al., 2008	28 subjects: 6 with CP 5 with AP 11 with PI 6 healthy periodontal controls	Histology, Immunohistochemistry, Immunofluorescence, RT-PCR & Western blotting: MMP-25 MMP-26 CD68 HBD-1 HBD-2	In PI, MMP-25 observed in plasma cells and PMN cells. MMP-26 could be observed in PI and CP. HBD-1 detected in endothelial cells and peri-vascular areas of PI, CP and AP. Low expression levels of selected markers in all groups.
Roediger et al., 2009	48 subjects: 16 with PI 16 with CP 16 healthy periodontal controls	RT-q-PCR: Collagen type IV Integrin b1 Integrin b4 Integrin a6 HPRT1	mRNA expression of Collagen type IV up-regulated in PI compared to CP. No differences in mRNA levels of Integrin b1 and Integrin b4 between PI and CP. Up-regulated mRNA levels of Integrin a6 in PI (5.3-fold) and in CP (11.6-fold) compared to healthy controls. 18 up-regulated and 8 down-regulated DEGs found when comparing PI and CP.

Study	N of patients	Methods & Markers	Main findings
Venza et al., 2010	170 subjects: 53 with PI 82 with CP 35 healthy periodontal controls	Real-time q-PCR & Western blotting: TNF-α IL-6 IL-8 MCP-I CCR1 CCR2 CCR3 CCR4 CCR5 CXCR1 CXCR2 CXCR3	Significantly higher levels of TNF-α, IL-8, CCR5 and CXCR3 in PI than in CP.
Wu et al., 2013	30 subjects: 10 with PI 10 with CP 10 healthy periodontal controls	q-PCR: Fibronectin (cFn)	Lower mRNA expression of cFn in CP compared to healthy controls. Higher mRNA expression of cFn in PI samples compared to healthy controls.
Becker et al., 2014	22 subjects: 7 with PI 7 with CP 8 healthy periodontal controls	Transcriptome Analysis	136 unique transcripts found in PI when compared to CP and healthy controls.
Buffoli et al., 2014	18 subjects: 3 with PI 3 with CP 3 healthy periodontal controls 3 healthy peri-implant controls 3 with “healed” CP 3 with “healed” PI	Histology, Immunohistochemistry, Polarized light microscopy & Immunofluorescence: Sirius Red staining AQP1 CD141	Changes in collagen fibers organization and elevated areas of inflammatory cells in CP and PI compared to healthy controls. After healing, organization of collagen fibers was partially restored both in PI and CP, and numbers of inflammatory cells were significantly decreased.
Carcuac & Berglundh, 2014	80 subjects: 40 with PI 40 with CP	Histology & Immunohistochemistry: CD3 CD20 CD138 CD68 MPO	Significantly larger ICT in PI compared to CP. Significantly higher levels of CD138-, CD68- and MPO-positive cells in PI than in CP. In PI, larger densities of vascular structures in the area lateral to the ICT than within the infiltrate.

Study	N of patients	Methods & Markers	Main findings
Galindo-Moreno et al., 2017	30 subjects: 15 with PI 15 with CP	Histology & Immunohistochemistry: CD45 CD68 CD38 MPO CD34	Inflammatory infiltrate more pronounced in PI than in CP. Higher proportions of plasma cells in PI than in CP. Abundant monocytes/macrophages and neutrophils near the pocket epithelium in both groups. Similar densities of CD34-positive cells in PI and CP. CD38-positive cells more pronounced in PI than CP.
Ghighi et al., 2018	31 patients: 11 with PI 10 with CP 10 healthy periodontal controls	Multiplex immunoassay: Cytokines MMP TIMP RANKL OPG Histology & Immunohistochemistry: CD68 CD20 CD3 CD45 IL-10 MPO OPG RANKL TIMP-2	Higher TIMP-2 and CD3-positive cells in PI compared to CP. Greater numbers of CD3, CD20 and CD68-positive cells in PI than in controls. TIMP-2, MMP-2, -8, -12 and -13 significantly increased in PI and CP compared to controls. Elevated levels of IL-10 in PI compared to controls. RANKL/OPG ratio, MMP-10 levels increased in CP compared to controls.
Kasnak et al., 2018	38 patients: 12 with PI 13 with CP 13 healthy periodontal controls	Histology & Immunohistochemistry: 8-OHdG PARK7/DJ-1 NFE2L2/NRF2 KEAP1	Disrupted epithelium and loss of spinous layer thickness in PI. Pronounced inflammatory infiltrate in PI compared to CP. Higher proportions of 8-OHdG-positive cells in the epithelium in PI and CP compared to controls. Elevated numbers of PARK7/DJ-1-positive cells in PI and CP compared to controls.

Study	N of patients	Methods & Markers	Main findings
Liu et al., 2020	30 subjects: 10 with PI 10 with CP 10 healthy periodontal controls	Microarray & qRT-PCR	434 up-regulated and 569 down-regulated DEGs in PI compared to CP. Higher levels of LINC00525, MGAT4C, BMP5, RANKL and MZB1 in PI compared to CP. Lower levels of UOX, EPHA7 DRD5, OPG and MMP7 in PI compared to CP. Up-regulated osteoclast differentiation in PI compared to CP.
Cho et al., 2020	20 subjects: 10 with PI 10 with CP	RNA-sequencing	1490 DEGs found comparing PI and CP. No major differences found in Gene Ontology analysis between PI and CP.
Karatas et al., 2020	60 patients: 15 with PI 15 with PI-M 15 with CP 15 healthy periodontal controls	Histology & Immunohistochemistry: Fibroblasts Inflammatory cells HIF-1a COX2 iNOS PH MMP8 TIMP-1 CD68-iNOS CD68-CD206	Highest numbers of fibroblasts and lowest counts of inflammatory cells, found in healthy controls followed by PI-M sites. Similar counts of fibroblasts and inflammatory cells in PI and CP. Significantly lower levels of HIF-1a, COX2 and iNOS in PI-M compared to PI and CP.
Fretwurst et al., 2020	14 patients: 7 with PI 7 with CP	Immunofluorescence: CD68-iNOS CD68-CD206	Higher numbers of CD68-positive cells in PI compared to CP. Higher levels of M1 macrophages in PI compared to CP. Similar levels of M2 macrophages in PI and CP.
Taskan & Gevrek, 2020	45 subjects: 15 with PI 15 with CP 15 healthy periodontal controls	Histology & Immunohistochemistry: PPAR-y RXR-a VDR COX-2	Higher numbers of inflammatory cells in PI and CP compared to controls. Higher numbers of fibroblasts in controls compared to PI and CP. Higher numbers of PPAR-y- and COX-2-positive cells in PI and CP compared to controls. Higher levels of RXR-a and VDR in controls compared to PI and CP.

Study	N of patients	Methods & Markers	Main findings
Zhou et al., 2020	15 subjects: 5 with PI 5 with CP 5 healthy periodontal controls	RNA-sequencing	Several differentially expressed mRNAs, miRNAs and lncRNAs in PI compared to CP. Genes FAM126B, SORL1, PRLR, CPEB2, RAP2C and YOD1 were the most differentially expressed. Gene Ontology and Reactome analyses revealed that "muscle filament sliding", "rhythmic process" and "cytokine secretion" were enriched in PI compared to CP.
Figueiredo et al., 2020	80 subjects: 20 with PI 20 with CP 20 healthy peri-implant controls 20 healthy periodontal controls	qPCR: IL-6 IL-1β TNF-α MMP-1 MMP-2 MMP-8 MMP-9 TIMP-1 TIMP-2 GAPDH	Higher mRNA levels of IL-1β in PI compared to the other groups. Higher mRNA levels of IL-6 in PI and CP compared to controls.

Peri-implantitis (PI)
Peri-implant mucositis (PI-M)
Chronic periodontitis (CP)
Aggressive periodontitis (AP)

Tobacco smoking and periodontitis

Although a causal relationship between accumulation of oral microbiota on teeth and subsequent inflammatory host responses has been established, susceptibility to periodontal diseases vary greatly among individuals. The concept of an "individual disease expression" is nowadays used to describe intricate interactions among behavioral, environmental, genetic and epigenetic factors that contribute to the susceptibility of the disease (Loos & Van Dyke, 2020).

Tobacco smoking is recognized as one of the most important risk factors for periodontitis. In fact, past epidemiological studies demonstrated that smoking affects both the prevalence and the severity of the disease (Tomar & Asma, 2000; Nociti et al., 2015; Leite et al., 2018). In addition, findings from clinical studies showed that periodontal treatment is less effective in smokers when compared to non-smokers (Tomasi et al., 2007; Kotsakis et al., 2015).

The mechanisms by which smoking affects the host response in patients with periodontitis, however, are not fully understood. It is suggested that the numerous chemical substances found in tobacco products have genotoxic effects that directly affect the inflammatory response (Goncalves et al., 2011; Nociti et al., 2015). After smoke exposure, *in vitro* experiments demonstrated an impairment of chemotaxis and phagocytosis of polymorphonuclear cells together with augmented levels of reactive oxygen species (ROS) and proteolytic enzymes in the extra-cellular environment (Palmer et al., 2005; Johnson & Guthmiller, 2007).

Comparative studies on human biopsy material (**Table 2**) mainly demonstrated altered levels of inflammatory mediators when comparing periodontitis lesions in smokers and non-smokers. In fact, dysregulated levels of cytokines, interleukins, metalloproteinases and other inflammatory mediators were found in gingival tissues of smokers with periodontitis when compared to non-smokers (Cesar-Neto et al., 2007; Katz et al., 2007; Gultekin et al., 2008; Mouzakiti et al., 2011; Moeintaghavi et al., 2017; Senturk et al., 2018). These findings support the hypothesis that high levels of oxidative stress products and free radicals after smoke exposure lead to an impaired host response and enhanced tissue damage (White et al., 2018).

On the other hand, reports on cellular composition and vascular densities of periodontitis lesions in smokers and non-smokers are scarce (**Table 2**). Immunohistochemical assessments of phenotypes markers in soft tissue biopsies obtained from 46 patients with severe periodontitis revealed that no major differences could be observed in regard to size, number and densities of cells of the host response between smokers and non-smokers (Schmidt et al., 2020). A similar study demonstrated that lower levels of CD83-positive cells were found in the smoker group (Souto et al., 2014). Another report on soft tissue biopsies obtained from 50 patients with periodontitis demonstrated that smokers presented with significantly lower levels of CD4- and CD8-positive cells after periodontal treatment when compared to non-smokers (Orbak et al., 2003). However, in the study from Orbak et al. (2003) no clear information on the periodontal conditions of the patients were reported. The vasculature of periodontitis tissues is also affected by smoking, as the ICT in smokers was reportedly found to contain fewer but larger vessels than the one found in non-smokers (Mirbod et al., 2001; Rezavandi et al., 2002; Schmidt et al., 2020).

Only few studies have analyzed the role of smoking on epigenetic mechanisms in periodontitis. Epigenetics is the study of those "reversible mechanisms that, together, participate in the regulation of gene expression without directly altering the DNA sequence" (Feinberg, 2007). In 2011 Breitling and coworkers (Breitling et al., 2011) discovered differences in whole blood DNA-methylation levels among smokers, former smokers and non-smokers. Since then, DNA-methylation was used as a long-term marker for smoke exposure.

Although DNA-methylation was the most frequently analyzed epigenetic mechanism in relation to periodontitis (Larsson et al., 2015), only few studies analyzed samples from patients with smoking habits. A study comparing gingival biopsies from 12 smokers and 11 non-smokers with chronic periodontitis found no differences in methylation levels in the promoter region of the toll-like receptor 2 and 4 between groups (De Oliveira et al., 2011). Another study compared gene expression profiles and DNA-methylation levels in soft tissue biopsies collected from 5 smokers and 5 non-smokers with periodontitis. In this case, where RNA-sequencing techniques were used, a magnitude of differentially expressed genes (2901) and differentially methylated sites (96) were observed between the groups (Cho et al., 2017).

In general, a high level of heterogeneity can be found among studies on epigenetic markers in relation to study design, type of samples (e.g., cells, fluids, tissues) and laboratory techniques (e.g., flow cytometry, ELISA, qPCR) (Khouly et al., 2020). Since results on gene expression profiles and epigenetic markers are highly influenced by tissue-specific variability, this type of studies should be performed on those tissues that best represent the condition under exam (Jiang et al., 2020). Thus, more studies on appropriate tissue samples and with adequate sample size are needed to investigate the role of tobacco smoking on the host response in periodontitis lesions. In a continuing evaluation of soft tissue biopsies obtained in humans (Schmidt et al., 2020), periodontitis lesions from smokers and non-smokers were analyzed with oxidative stress and epigenetic markers (**Study II**).

Table 2. Comparisons of periodontitis lesions in smokers and non-smokers (n=15 studies)

Study	N of patients	Methods	Main findings
Mirbod et al., 2001	17 subjects with CP: 5 smokers 12 non-smokers	Histology & Immunohistochemistry: H&E CD34	Similar vascular densities between groups. Higher proportions of smaller blood vessels and lower proportions of larger blood vessels in smokers compared to non-smokers.
Rezavandi et al., 2002	34 subjects with CP: 17 smokers 17 non-smokers	Histology & Immunohistochemistry: ICAM-1 E-selectin Human von Willebrand factor	Significantly lower numbers of vessels in inflamed than in non-inflamed areas found both in smokers and non-smokers. Higher levels of ICAM-1 and E-selectin in sites with inflammation compared to sites without inflammation both in smokers and non-smokers.
Orbak et al., 2003	50 subjects with CP: 25 smokers 25 non-smokers	Flow-cytometry: CD4 CD8	Before and after treatment, lower numbers of lymphocytes in smokers compared to non-smokers.
Sonmez et al., 2003	74 subjects with CP: 38 smokers 36 non-smokers	Histology & Immunohistochemistry: Fibronectin Number of vessels (NVES) Vascular surface density (VSD)	No differences in fibronectin distribution, NVES and VSD between smokers and non-smokers.
Cesar-Neto et al., 2006	50 subjects with CP: 25 smokers 25 non-smokers 12 non-smoking healthy controls	qPCR & ELISA: INF-γ	Higher levels of INF-γ in CP compared to controls. Higher levels of INF-γ in smokers compared to non-smokers.
Katz et al., 2007	10 subjects with CP : 5 smokers 5 non-smokers	RT-PCR & Western Blotting: RAGE	Higher RAGE levels (x1.4) in smokers compared to non-smokers.

Study	N of patients	Methods	Main findings
Cesar-Neto et al., 2007	50 subjects with CP: 25 smokers 25 non-smokers 10 non-smoking healthy controls	qRT-PCR & ELISA: MMP-2 MMP-8 IL-1α IL-1ra IL-8 IL-10 TNF-α RANKL Osteoprotegerin	Higher levels of all markers (apart from MMP-8 and Osteoprotegerin) in inflamed tissues compared to healthy controls. Lower levels of IL-1α, IL-8, IL-10, TNF-α, MMP-8 and Osteoprotegerin in smokers compared to non-smokers. Higher levels of IL-6 and IL-1ra in smokers compared to non-smokers.
Gultekin et al., 2008	20 subjects with CP: 10 smokers 10 non-smokers 20 subjects with GI: 10 smokers 10 non-smokers 20 healthy controls: 10 smokers 10 non-smokers	Histology & Immunohistochemistry: H&E PCNA Ki67	Higher levels of PCNA and Ki67 in smokers compared to non-smokers.
De Oliveira et al., 2011	23 subjects with CP: 12 smokers 11 non-smokers 10 healthy non-smokers	qPCR: TLR2 TLR4	No differences in methylation levels among the three groups.
Mouzakiti et al., 2011	30 subjects with CP: 15 smokers 15 non-smokers 30 healthy controls: 15 smokers 15 non-smokers	RT-PCR: MMP-1 MMP-3 MMP-8 MMP-9 MMP-13 TIMP-1 GAPDH	Lower levels of MMP-1, lower MMP-1/TIMP-1 ratios, but higher levels of MMP-9 and TIMP-1 in smokers with CP compared to non-smokers with CP. MMP-8 levels, MMP-8/TIMP-1 and MMP-1/TIMP-1 ratios elevated in non-smokers with CP compared to healthy non-smokers.

Study	N of patients	Methods	Main findings
Souto et al., 2014	45 subjects with CP: 24 smokers 21 non-smokers	Histology & Immunohistochemistry: H&E Factor XIIIa CD1a CD83 Cytometric bead array	Lower levels of CD83-positive cells in smokers compared to non-smokers. No differences in cytokines levels between groups.
Cho et al., 2017	10 subjects with CP: 5 smokers 5 non-smokers 10 healthy controls: 5 smokers 5 non-smokers	RNA-seq	2901 DEGs observed comparing smokers and non-smokers with CP (1298 up-regulated and 1603 down-regulated in smokers). 96 sites with different DNA methylation levels observed comparing smokers and non-smokers with CP (30 hyper-methylated and 66 hypo-methylated in smokers).
Moeintaghavi et al., 2017	20 subjects with CP: 10 smokers 10 non-smokers 21 healthy controls: 10 smokers 11 non-smokers	qPCR: IL-1β IL-12	Higher IL-1β levels in non-smokers with CP compared to healthy non-smokers. Lower IL-1β levels in smokers with CP compared to non-smokers with CP.
Senturk et al., 2018	40 subjects with CP: 20 smokers 20 non-smokers 40 healthy controls: 20 smokers 20 non-smokers	Histology & Immunohistochemistry: MMP-2 MMP-9	Higher MMP-2 and MMP-9 levels in non-smokers with CP compared to healthy non-smokers. Lower levels of MMP-2 in smokers with CP compared to non-smokers.
Schmidt et al., 2020	46 subjects with CP: 25 smokers 21 non-smokers	Histology & Immunohistochemistry: CD3 CD20 CD138 MPO CD68 CD34	Similar ICT areas in smokers and non-smokers. No significant differences in densities of inflammatory cells between smokers and non-smokers. Higher vascular density in non-smokers than in smokers.

Chronic periodontitis (CP)
Gingivitis (GI)
Infiltrated connective tissue (ICT)

Titanium particles in peri-implant tissues

Although different morphological characteristics have been identified when comparing peri-implant and periodontal tissues (Berglundh et al., 1991; Lang et al., 2011), the reasons behind the enhanced inflammatory reactions found in peri-implantitis are still not fully understood. As suggested at the 2017 World Workshop, the role of several "non-plaque related factors" remains to be clarified (Berglundh et al., 2018). Among those factors, degradation products derived from dental implants (namely, titanium particles) have been suggested to influence peri-implant inflammation (Noronha Oliveira et al., 2018).

Different hypotheses have been proposed on mechanisms involved in the detachment of metal particles from the implant body. First of all, the mechanical friction generated during implant installation between the implant surface and the bony wall of the osteotomy site may dislodge titanium particles that become trapped in the surrounding tissues. Results from pre-clinical *in vivo* experiments support this concept, as small metal-like granules were detected in newly formed peri-implant bone after implant installation (Schliephake et al., 1993, Martini et al., 2003; Franchi et al., 2004; Meyer et al., 2006; Suarez-Lopez Del Amo et al., 2017). In addition, dark pigments and black particles of varying size were noted in human soft tissue biopsies obtained at sites covering submerged titanium implants before abutment connection (Schlegel et al., 2002; Flatebo et al., 2006). Similar findings were also reported in orthopedic studies. Analogous discolorations were found in the soft tissues surrounding titanium miniplates/implants that were used to stabilize fractured bone fragments (Kim et al., 1997; Voggenreiter et al., 2003).

A second mechanism called "tribo-corrosion" (i.e., the degradation process deriving from the dual action of electrochemical and mechanical stimuli) is thought to contribute to the detachment of metal particles from the implant body (Apaza-Bedoya et al., 2017). In this context, it should be noted that titanium is known for its high resistance to corrosion. In fact, due to a great affinity towards oxygen, an external thin but stable passive oxide layer (TiO_2) is formed on the implant surface, thereby protecting the bulk material from reactive species and chemical compounds (Asri et al., 2017). *In vitro* experiments, however, demonstrated that high concentrations of acidic elements (e.g., lactic acid, hydrogen peroxide, citric acid, or fluoride) were corrosive and able to induce

morphological changes to the surface of the tested implants (Souza et al., 2015; Wheelis et al., 2016). Studies also demonstrated that the destruction of the TiO_2 layer on the implant surface resulted in the release of metal particles into the surrounding environment (Khan et al., 1996). In addition, wear-accelerated corrosion was more effective than corrosion alone in damaging the protective TiO_2 film on the implant surface (Revathi et al., 2017). In a recent *in vitro* study, Olander et al. (2022) observed titanium particles of varying size [0.2-95.3 μm] after exposing different implant/abutment materials to the dual action of cycling loading and corrosive immersion.

The influence of detached metal particles on the host response in peri-implant tissues has been debated extensively. Most of the available evidence, however, derives from *in vitro* observations. The exposure of fibroblasts to titanium particles resulted in genotoxic effects and changes in histone acetylation in a dose-dependent way (Setyawati et al., 2013). At high concentrations of titanium, cell viability was reduced together with signs of necrotic cell death. Furthermore, Ti-ions were shown to enhance the inflammatory reactions induced by the presence of bacterial endotoxins (Makihira et al., 2010). Interestingly, the size of the metal particles was found to be important, as nano-size particles produced more DNA-damage than larger ones (Toyooka et al., 2012). Lastly, the exposure of cells to titanium ions/particles influenced the production of several signaling cytokines, such as nuclear factor-kB ligand (RANKL) and osteoprotegerin (OPG) (Koide et al., 2003), chemokine ligand 2 (CCL2) (Wachi et al., 2015) and IL-1β (Pettersson et al., 2017).

Available publications on metal elements found in human peri-implant soft tissue biopsies are presented in **Table 3**. Few studies with relatively small sample size revealed that the ICT in peri-implantitis specimens occasionally contained titanium particles (Wilson et al., 2015; Fretwurst et al., 2016; Rakic et al., 2022). The significance of such observations, however, is unclear as no biopsies were obtained from reference peri-implant sites. In other studies where samples from healthy peri-implant or periodontitis-affected sites were used as controls, results were inconsistent whether the presence or content of titanium particles was unique for peri-implantitis tissues (Olmedo et al., 2013, Pettersson et al., 2019).

It is important to mention that only adequate and reliable methods should be used to assess metal elements in tissue biopsies. Evaluations of metal particles using, for example, polarized light microscopy (e.g., Fretwurst et al., 2016; Rakic

et al., 2022) may be questionable. This method, in fact, does not allow the elemental characterization of the particles under exam. Other techniques such as inductive coupled plasma mass spectrometry (ICP-MS) are relatively cheap, quick and reliable in terms of broad quantification of metal content within a tissue, but require the enzymatic homogenization and nebulization of samples (e.g., Olmedo et al., 2013; Mercan et al., 2014; He et al., 2016; Pettersson et al., 2017; Pettersson et al., 2019; Safioti et al., 2017). The chemical digestion of the tissue leads to the complete loss of any spatial information relative to the metal debris. Analyses of metal elements within biological samples should preferably rely on methods such as scanning electron microscopy with energy-dispersive X-ray spectroscopy (SEM-EDX), proton-induced X-ray emission (PIXE), or synchrotron radiation X-ray fluorescence spectroscopy (SR-XRF) (e.g., Passi et al., 2002; Fretwurst et al., 2016; Petterson et al., 2019; Nelson et al., 2020; Rakic et al., 2022). In fact, these techniques allow (to different degrees) both the characterization and the precise localization of metal particles within intact specimens. Lastly, the type of samples should also be carefully considered. Results from evaluations of submucosal plaque or crevicular fluid specimens (e.g., Tawse-Smith et al., 2017; Safioti et al., 2017; Daubert et al., 2023) risk to be inconsistent or highly influenced by external contaminations.

Altogether, the results are inconclusive regarding the overall occurrence, size and distribution of titanium particles in peri-implant tissues and whether implant characteristics, installation protocols or healing time influenced results (Mombelli et al., 2018; Ivanovski et al., 2022). Thus, in **Study III** we evaluated differences in occurrence and localization of titanium particles between human soft tissue samples obtained from dental implant sites with and without peri-implantitis. The influence of titanium particles on gene expression in peri-implantitis tissues was also investigated.

Table 3. Evidence of metal particles found in peri-implant samples in humans (n=17 studies)

Study	N of subjects/implants	Samples & Methods	Main Findings
Arys et al., 1998	8 subjects 15 "failed" implants (early loss)	Soft tissue biopsies Light microscopy, SEM & XPS	Encapsulated ICT commonly found with fibroblasts, plasma cells, lymphocytes, macrophages and giant multinucleated cells. Iron granular particles observed in the tissues. Phosphorous was found in all samples, titanium in two samples and zinc in one sample. Traces of copper, tin, silicon and fluorine could also be detected in few samples.
Passi et al., 2002	4 subjects 1 implant removed due to PI 3 implants removed due to fracture	Soft tissue biopsies PIXE	Small titanium deposits found occasionally in peri-implant tissues. Aluminum leaked diffusely in peri-implant tissues. Vanadium traces not found in the samples.
Flatebo et al., 2006	13 subjects 13 healthy implants	Soft tissue biopsies Light microscopy	No giant-cells could be detected in any of the samples. Dense dark particles of different size noted in different layers of the samples with varying densities.
Tawse-Smith et al., 2012	4 subjects 4 implants with PI	Soft tissue biopsies Light microscopy & SEM-EDX	Numerous deposits of granular foreign material found within the ICT. The presence of metal particles was confirmed by SEM-EDX. The size of Ti particles ranged from 2 to 15 µm. Other particles (aluminum, phosphorous, sulfur) found in few samples.
Olmedo et al., 2012	153 subjects 153 healthy implants (cover screws)	Soft tissue biopsies Light microscopy	41% of the samples showed metal particles in different layers of the sections. Particles varied greatly in size and numbers. Macrophages and T-lymphocytes were associated with metal particles.

Study	N of subjects/implants	Samples & Methods	Main Findings
Olmedo et al., 2013	30 subjects 15 with PI 15 healthy controls	Oral exfoliative cytology smears Light microscopy & ICP-MS	Metal-like particles observed inside and outside epithelial cells and macrophages in PI samples. No particles found in samples from controls.
Mercan et al., 2014	30 subjects 20 subjects (22 healthy implants – cover screws) 10 subjects with healthy gingiva (controls)	Soft tissue biopsies ICP-MS	Higher titanium levels in samples from implant cover screws (50 µg/g ± 23.5) compared to gingival samples (37.1 µg/g ± 1.0).
Paknejad et al., 2015	N of subjects not specified 96 healthy implants (cover screws)	Soft tissue biopsies Light microscopy & EDS	Higher content of metal particles found in sections in proximity of the implant cover screws. Particles varied in size and number.
Wilson et al., 2015	31 subjects 36 implants with PI	Soft tissue biopsies Light microscopy & SEM-EDX	In 4 cases giant cells identified in the samples. Radiopaque particles (diameter 9-54 µm) found in 34 samples. Ti particles found in 7 samples. Zirconium, silico or aluminum particles found in 19 samples.
Fretwurst et al., 2016	12 subjects 12 implants with PI	Soft & bone tissue biopsies Light microscopy & SRXRF	Titanium and iron particles were noted in 9 samples. Metal particles observed in the soft tissue surrounding dental implants. Lymphocytes and M1 macrophages observed in the tissues.
Pettersson et al., 2017	3 subjects 3 implants with PI 3 healthy implants	Soft tissue biopsies & crevicular fluid samples ICP-MS	Ti concentrations varied from 7.3 to 38.9 µM. IL-1β range from 13.0 to 268.9 pg/ mL in PI.
Safioti et al., 2017	30 subjects 20 implants with PI 20 healthy implants	Submucosal plaque samples ICP-MS	Higher levels of Ti (0.85 ± 2.47) in PI compared to healthy sites (0.07 ± 0.19).

Study	N of subjects/implants	Samples & Methods	Main Findings
Tawse-Smith et al., 2017	16 subjects N of implants not specified	Exfoliative cytology smears Light microscopy, SEM-EDX & ICP-MS	Higher levels of Ti found at the implant-abutment interface. No signs of inflammation found around metal particles.
Daubert et al., 2019	40 subjects 21 implants with PI 24 healthy implants	Plaque samples & crevicular fluid samples ELISA & ICP-MS	Epigenetic modifications more pronounced in PI samples. A 1-unit increase in Ti levels was positively associated with a 0.09 increase in methylation levels.
Pettersson et al., 2019	24 subjects 13 with PI 11 with CP	Soft tissue biopsies Light microscopy, ICP-MS, SEM-EDX & TEM	Higher levels of Ti particles in PI compared to CP. The mean size of Ti particles was $10.9 \pm 35.7\ \mu m^2$.
Nelson et al., 2020	N of subjects/implants not specified Implants with PI at titanium implants Implants with PI at ceramic implants	Soft tissue biopsies XRF & XANES	Ti particles found in all samples from Ti implants. The frequency of Ti particles varied among samples. Traces of Nb, Bi, Pb and As noted in the samples from Ti implants. Traces of Zr, Y, Hf and Sr noted in samples from ceramic implants.
Rakic et al., 2022	74 subjects 39 implants with PI 35 controls with CP (not analyzed for metal content)	Soft tissue biopsies Light microscopy & SEM-EDX	Ti particles found in all PI samples. Ti particles had a mean size of $8.9 \pm 24.8\ \mu m^2$. Traces of Si, Fe, Rb and Yr found in some samples. No signs of macrophages or multinucleated giant cells.

Peri-implantitis (PI); Chronic periodontitis (CP); Titanium (Ti)

Functional characteristics

Understanding the pathogenesis of a disease is not only an important prerequisite to make a precise diagnosis, but also a fundamental step to develop correct treatment strategies. In pathophysiology, the term "functional" refers to the study of how a disease may disrupt normal physiological processes. By examining changes in functional characteristics, the nature and/or progression of a condition can be better understood. The analysis of biological systems, however, is a complex challenge. Intricate mechanisms and interactions among molecules, cells and tissues make the understanding of underlying processes and functions difficult. In addition, as disease manifestation and susceptibility vary among individuals, the identification of functional characteristics becomes even more complicated.

The use of *in vitro* experiments and pre-clinical *in vivo* models greatly contributes to the understanding of biological processes. They serve the purpose to isolate specific variables and investigate causal relationships between different factors or outcomes. On the other hand, experimental pre-clinical studies lack the possibility to fully replicate the complexity of human pathophysiology. Thus, access to human samples being specific for the disease of interest (possibly together with matched controls) is considered the most appropriate model to study the pathogenesis of a disease. The restricted availability to such samples is in most cases the biggest limitation in this type of research.

The current series of studies investigated specific characteristics of periodontitis and peri-implantitis lesions in humans. Epigenetic and oxidative stress markers were used to evaluate differences in periodontitis and peri-implantitis lesions (**Study I**) or to compare periodontitis lesions in smokers and non-smokers (**Study II**). The occurrence and localization of titanium particles in peri-implant tissues were also investigated together with the influence of titanium particles on gene expression in peri-implantitis sites (**Study III**).

In **Study IV** we further analyzed the samples obtained in Study III. The purpose was to evaluate gene expression profiles in peri-implant tissues with and without peri-implantitis using a novel approach integrating spatial transcriptomics and RNA-sequencing.

Historically, immunohistochemistry (IHC) was the most used method to investigate pathological features of peri-implantitis tissues in humans (**Table 4**). Studies were designed to include sites with peri-implantitis and sites presenting with either clinically healthy conditions or peri-implant mucositis. As expected, IHC analyses revealed elevated numbers of inflammatory cells in peri-implantitis samples when compared to healthy controls (Seymour et al., 1989; Sanz et al., 1991; Cornelini et al., 2001; Mardegan et al., 2017; de Araujo et al., 2017) or peri-implant mucositis (Gualini & Berglundh, 2003; Duarte et al., 2009; Lucarini et al., 2019).

Despite being a powerful and well-established method, IHC requires the selection of specific markers to detect targeted proteins in cells. Although the method allows the recognition and analysis of a multitude of cell phenotypes and biomarkers, the approach is restricted to the preselection procedure. Advances in laboratory systems include new techniques such as RNA-sequencing and transcriptome analysis. These so called "new generation sequencing" (or "omics") techniques enable the study of large-scale data, providing insights into structures, functions and interactions of molecules in different biological complexes (Rao et al., 2021).

Among these new technologies, spatial transcriptomics is a cutting-edge technique which was introduced in 2016 by Ståhl and coworkers (Stahl et al., 2016). This method allows high-throughput analysis of gene expression profiles within the context of tissue organization, almost at the single-cell level. In contrast to RNA-sequencing, where whole tissue biopsies need to be homogenized, spatial transcriptomics allows the visualization of gene expression within intact tissue samples.

Until today, only a single study used spatial transcriptomics to investigate gene expression profiles in human periodontal tissues (Lundmark et al., 2018). Studies applying spatial transcriptomics in the analysis of peri-implantitis lesions are lacking. Thus, in **Study IV** we combined RNA-sequencing and spatial transcriptomics to further elucidate functional characteristics of peri-implant lesions.

Table 4. Methods used to analyze peri-implant soft tissue biopsies in humans (n=18 studies)

Study	N of patients	Methods
Seymour et al., 1989	13 subjects: 9 implants with PI 18 healthy implants	Light microscopy & Immunohistochemistry
Sanz et al., 1991	12 subjects: 6 with PI 6 healthy peri-implant controls	Light microscopy & TEM
Cornelini et al., 2001	15 subjects: 10 implants with PI 10 healthy implants	Light microscopy & Immunohistochemistry
Gualini & Berglundh, 2003	16 subjects: 6 with PI 10 with PI-M	Light microscopy & Immunohistochemistry
Borsani et al., 2005	14 subjects: 5 with PI 4 healthy periodontal controls 5 healthy peri-implant controls	Light microscopy & Immunohistochemistry
Duarte et al., 2009	48 subjects: 11 with healthy implants 15 with PI-M 10 with “initial” PI 12 with “severe” PI	PCR
Luo et al., 2013	20 subjects: 12 with PI 8 healthy peri-implant controls	Light microscopy, Immunohistochemistry & RT-qPCR
de Araujo et al., 2014	18 subjects: 9 with PI 9 healthy peri-implant controls	Light microscopy, Immunohistochemistry & ELISA
Schminke et al., 2015	14 subjects: 12 with PI 2 healthy peri-implant controls	Microarray, qRT-PCR, Cell sorting & Western blot

Study	N of patients	Methods
Konermann et al., 2016	25 subjects: 21 with PI 2 healthy peri-implant controls 2 healthy periodontal controls	Light microscopy & Immunohistochemistry
Mardegan et al., 2017	40 subjects: 20 with PI 20 healthy peri-implant controls	RT-PCR
de Araujo et al., 2017	28 subjects: 18 with PI 10 healthy peri-implant controls	Light microscopy & Immunohistochemistry
Bastos et al., 2018	35 subjects: 20 with PI 15 healthy peri-implant controls	RT-PCR
Lucarini et al., 2019	48 subjects: 16 with PI 16 with PI-M 16 healthy peri-implant controls	Light microscopy & Immunohistochemistry
Mijiritsky et al., 2019	40 subjects: 20 with PI 20 healthy peri-implant controls	Light microscopy, Immunohistochemistry, Immunofluorescence, TEM & RT-PCR
Zhang et al., 2020	16 subjects: 8 with PI 8 healthy peri-implant controls	Western Blot & Immunofluorescence
Giro et al., 2021	35 subjects: 20 with PI 15 healthy peri-implant controls	RT-PCR
Martin et al., 2022	7 subjects: 4 with PI 3 healthy peri-implant controls	RNA-sequencing
Martins et al., 2022	35 subjects: 20 with PI 15 healthy peri-implant controls	RT-PCR

Aims

The current series of studies aimed at evaluating functional characteristics of periodontitis and peri-implantitis lesions in humans.

Specific aims:

- To evaluate differences in the cellular expression of DNA damage/repair markers and reactive oxygen/nitrogen species between periodontitis and peri-implantitis lesions in humans (**Study I**).
- To evaluate differences in the cellular expression of epigenetic and oxidative stress markers in periodontitis lesions of current smokers and non-smokers (**Study II**).
- To assess the occurrence and localization of titanium particles in human tissue samples obtained from dental implant sites with and without peri-implantitis. (**Study III**).
- To investigate the influence of titanium particles on gene expression profiles in peri-implantitis lesions (**Study III**).
- To analyze gene expression profiles in human tissue samples obtained from dental implant sites with and without peri-implantitis (**Study IV**).

Material and Methods

The current series of studies was based on the analysis of human soft tissue biopsies obtained in conjunction with the surgical therapy of periodontitis and/or peri-implantitis affected sites.

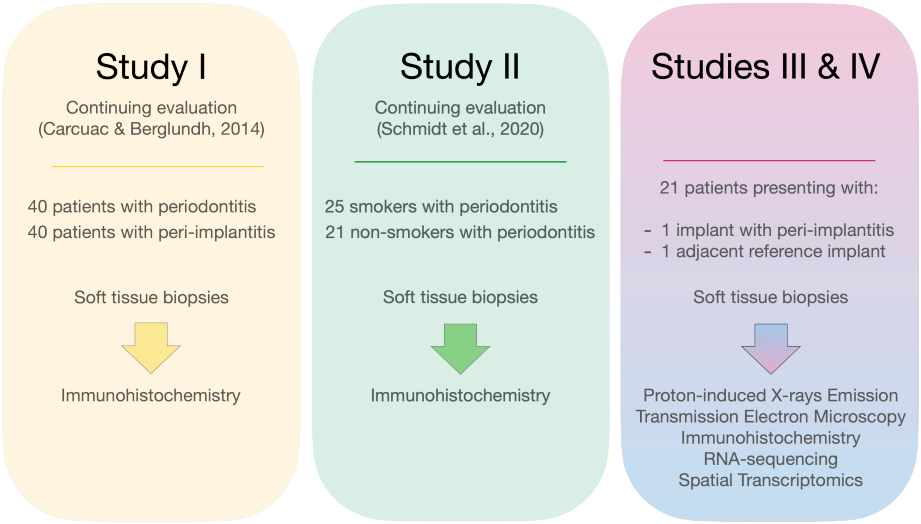

Figure 1. Overview of the series of studies.

Study population

Before enrolment, all subjects received information about the study protocol and signed an informed consent. Patients were excluded if they had undergone periodontal or peri-implant therapy during the last 6 months (**Studies I** & **II**), if they already received peri-implant surgical interventions (**Studies III** & **IV**) and if they presented any systemic disease that could have affected the periodontal and/or peri-implant tissue conditions. All patients received a detailed and individualized case presentation, oral hygiene instructions and a professional supra-gingival cleaning prior to study initiation.

In **Study I**, 40 patients with generalized severe periodontitis and 40 patients with severe peri-implantitis were recruited from the Clinics of Periodontics in

Gothenburg and Mölndal, Public Dental Services, Region Västra Götaland, Sweden.

Table 5. Patient characteristics and case definitions - Study I

	Case definition	N of patients	Age		Gender (n)		Smoking (%)	
			Mean	Range	F	M	Yes	No
Periodontitis	Bone loss ≥50 % PPD ≥7 mm BoP+	40	64	40-89	24	16	27.5	72.5
Peri-implantitis	Bone loss ≥3 mm PPD ≥7 mm BoP/SoP+	40	70	46-93	23	17	27.5	72.5

In **Study II**, 46 patients with generalized severe periodontitis were recruited from the Department of Periodontology, Endodontology and Cariology, and from the undergraduate clinic at the School of Dental Medicine, University Centre for Dental Medicine, University of Basel, Switzerland.

Table 6. Patient characteristics and case definitions - Study II

		N of patients	Age		Gender (n)		N of cigarettes	Cotinine
			Mean	Range	F	M		(μg l-1)
Periodontitis Bone loss ≥30% PPD ≥5 mm BoP+	**Non-smokers**	21	54	35-75	12	9	Never smoker / <100 cig/lifetime	<10
	Smokers	25	49	33-69	13	12	≥10 cig/day for 3 years / ≥1.5 pack-years	376 ± 188

In **Studies III** & **IV**, 21 patients with ≥1 implant with peri-implantitis and ≥1 adjacent reference implant with either peri-implant mucositis or clinically healthy conditions were consecutively recruited from the Specialist Clinic of Periodontics in Gothenburg, Public Dental Services, Region Västra Götaland, Sweden. Patients were excluded if the target implants differed in terms of time of installation and/or implant system.

Table 7. Patient characteristics and case definitions - Studies III & IV

	Case definition	N of patients	Age		Gender (n)		Smoking (n)	
			Mean	Range	F	M	Yes	No
Peri-implantitis	Bone level ≥3 mm PPD ≥7 mm BoP/SoP+	21	72	45-90	18	3	3	18
Reference implants	Bone level <3 mm PPD ≤5 mm							

Biopsy retrieval

When feasible, implant supra-constructions were disconnected prior to initiation of the surgical intervention.

Following local anesthesia, a crestal incision was made and, prior to flap elevation, a soft tissue biopsy about 3-5 mm wide and extending from the mucosal margin to the bone crest was carefully dissected from the target sites. At diseased sites, remaining inflamed tissues were removed and the implant/tooth surface was mechanically instrumented. Bone recontouring was performed under continuous irrigation with saline, if needed. Flaps were replaced and sutured.

Histological processing (Studies I, II & III)

After retrieval, the specimens were rinsed with saline, mounted in plastic cassettes (Tissue-Tek Paraform Sectionable Cassette System; Sakura Finetek Europe, Netherlands) and placed in 4% buffered formalin for 48 hours. Tissue samples were stored in 70% ethanol, kept at 4°C, subsequently dehydrated and embedded in paraffin until further processing.

Figure 2. Biopsy retrieval and processing - schematic illustration.
Soft tissue biopsies are collected, mounted in plastic cassettes, fixed in 4% formalin, dehydrated in ethanol, embedded in paraffin, sectioned and mounted on glass slides.

From each formalin-fixed paraffin-embedded (FFPE) tissue block, 5-µm-thick sections were produced in a microtome, mounted on glass slides, dewaxed and incubated in DIVA antigen-retrieval solution (Biocare Medical, Histolab, Concord, CA, USA) at 60°C overnight.

Following blocking of endogenous peroxidase and application of 4% bovine serum albumin (BSA), sections were incubated with primary antibodies. Incubation was then performed with Envision horseradish peroxidase (HRP)-labelled polymer (Agilent, Santa Clara, CA, USA) for 30 minutes. Positive cells were detected using DAB substrate (Agilent). Counterstaining was performed with hematoxylin. Lastly, the sections were cover slipped. Negative controls were produced by substituting the primary antibody with non-immune serum.

Table 8. Primary antibodies used in Study I

Antibody	Origin	Type	Isotype	Dilution	Company	Target/Meaning
y-H2AX	Rabbit	Monoclonal	9F3	1:300	EMD	DNA double-strand breaks
8-OHdG	Mouse	Monoclonal	IgG2b	1:8000	GeneTex	ROS oxidative stress
Chk2	Rabbit	Polyclonal	IgG	1:400	Abcam	DNA repair
MPO	Rabbit	Polyclonal	IgG	1:1500	Agilent	PNMs
CD68	Mouse	Monoclonal	IgG3	1:200	Agilent	Macrophages
iNOS	Rabbit	Polyclonal	IgG	1:50	Abcam	Antimicrobial NO
NOX2	Mouse	Monoclonal	IgG1	1:500	Abcam	Antimicrobial NADPH
MPO/PAD4	Rabbit	Polyclonal	IgG	1:100 / 1:1500	Abcam	NETs

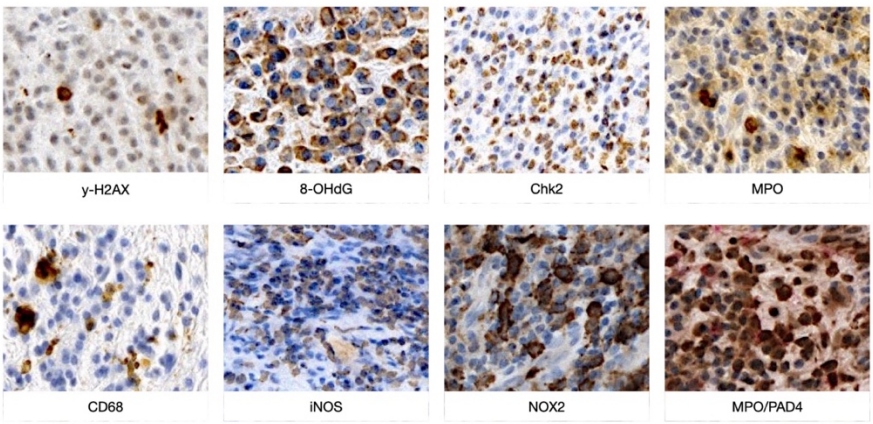

Figure 3. Immunohistochemical preparations in Study I. Magnification 400x.

Table 9. Primary antibodies used in Study II

Antibody	Origin	Type	Isotype	Dilution	Company	Target/Meaning
DNMT1	Mouse	Monoclonal	IgG1k	1:5	SC Biotech	DNA methylation
TET2	Mouse	Monoclonal	IgG1k	1:50	Active Motif	DNA de-methylation
AcH3	Rabbit	Monoclonal	IgG	1:500	CS Tech	Histone 3 acetylation
AcH4	Rabbit	Monoclonal	IgG	1:800	Abcam	Histone 4 acetylation
HDAC1	Rabbit	Polyclonal	IgG	1:500	Abcam	Histone de-acetylation
HDAC2	Rabbit	Monoclonal	IgG	1:100	Abcam	Histone de-acetylation
y-H2AX	Rabbit	Polyclonal	IgG	1:100	Active Motif	DNA double-strand breaks
8-OHdG	Mouse	Monoclonal	IgG2b	1:8000	GeneTex	ROS oxidative stress
iNOS	Rabbit	Polyclonal	IgG	1:10	ThermoFisher	Antimicrobial NO
NOX2	Mouse	Monoclonal	IgG1	1:50	Abcam	Antimicrobial NADPH oxidase

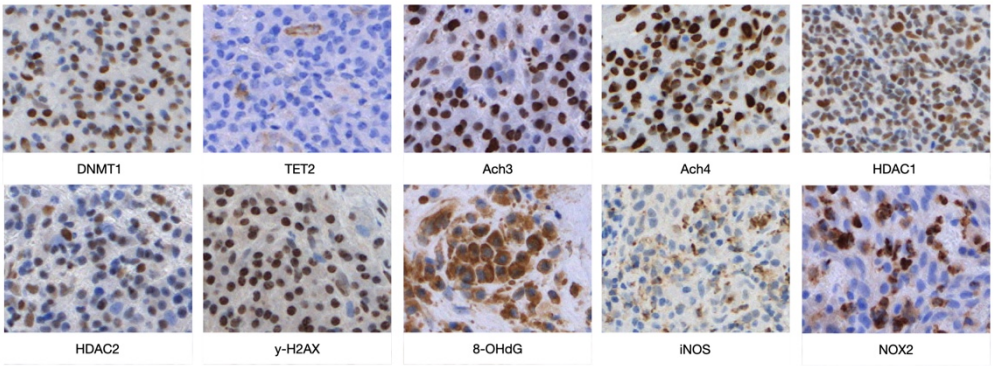

Figure 4. Immunohistochemical preparations in Study II. Magnification 400x.

Table 10. Primary antibodies used in Study III

Antibody	Origin	Type	Isotype	Dilution	Company	Target/Meaning
ALOX12	Rabbit	Polyclonal	aa618-650	1:75	LS-Bio	Lipoxygenase family
ARG1	Rabbit	Polyclonal	IgG	1:100	Invitrogen	Collagen synthesis
C4BPA	Rabbit	Polyclonal	aa470-499	1:150	LS-Bio	Component of complement cascade
NLRP2	Rabbit	Polyclonal	IgG	1:35	LS-Bio	Component of inflammasome
RASGRP2	Rabbit	Polyclonal	IgG	1:250	GeneTex	GTPase signal transduction

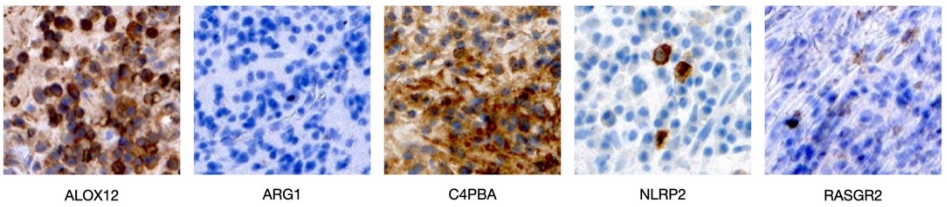

Figure 5. Immunohistochemical preparations in Study III. Magnification 400x.

Image acquisition & analysis

Histological evaluations were performed under a light microscope (Leitz DM-RBE microscope, Leica, Wetzlar, Germany). Each section was scanned by the Glissando Desktop Scanner (Objective Imaging Inc., Kansasville, WI, USA) with a 20x magnification. The acquired images were transferred to the computerized image analysis software Image-Pro Premier (IPP, version 10; Media Cybernetics Inc., Rockville, MD, USA) that was used for qualitative and quantitative analyses. The different regions of interest (ROIs) were outlined with a mouse cursor.

In **Study I** the entire area of the infiltrated connective tissue (ICT) and the pocket epithelium (PE) were depicted as ROIs. In addition, the ICT was further divided into two equivalent sub-regions: one inner area, facing the PE (ICT-1), and one outer area (ICT-2). A non-infiltrated connective tissue area (NCT) of about 0.10–0.50 mm^2 was also selected as ROI.
In **Studies II** & **III**, only the ICT was depicted as the designated ROI for IHC analysis.

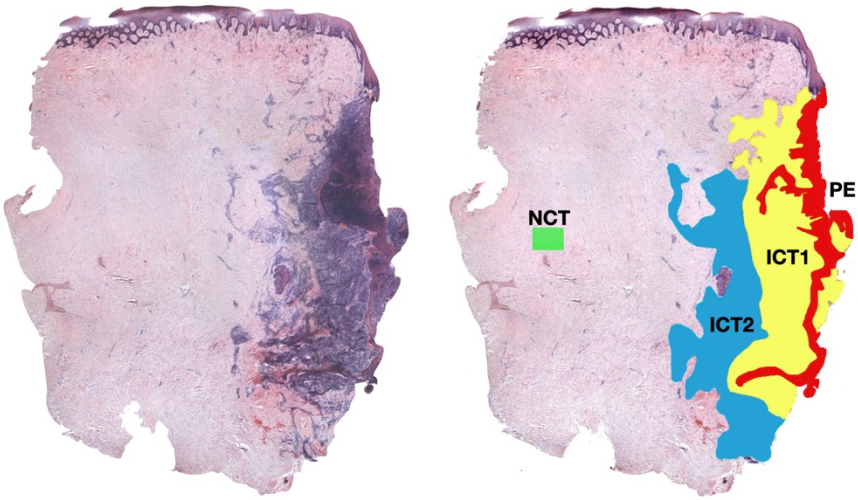

Figure 6. Example of the outlined ROIs. Magnification 20x.
On the left: original section stained with hematoxylin & eosin.
On the right: pocket epithelium (PE - red); infiltrated connective tissue (ICT – yellow and blue); non-infiltrated connective tissue (NCT - green).

Specific algorithms for each marker (based on analysis of color, intensity, morphology and size) were created to identify positive cells using the IPP "smart segmentation" tool.

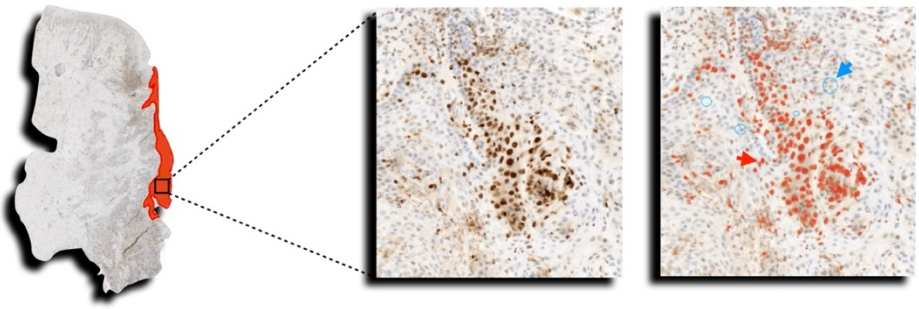

Figure 7. Illustration of the smart segmentation tool from the IPP Software. After depicting the ROI of choice (red area, left image), positive cells are isolated (red arrow, right image) from the background (blue arrow and circles, right image). Magnification 20x.

The total area of the ROI was measured (μm^2 or mm^2) together with the area occupied by positive cells, which was expressed in μm^2 (or mm^2) and as percentage area of the ROI (%).

The average size of cells (μm^2) was also assessed for each marker from 10-20 randomly selected positive cells in 10 different sections.

The number of positive cells in the different ROIs was arithmetically computed (number of cells = area of positive cells / average cell size). Cell numbers were expressed as total number (n) and as density of cells (number of cells/mm^2) within the different ROIs (densities of cells = number of cells * 1.000.000 / tot ROI area in μm^2).

Data analysis

Mean values, standard deviations, medians, inter-quartile ranges and 95% confidence intervals were calculated for each variable. Due to a non-normal distribution of the cellular densities, the non-parametric Mann-Whitney U test for independent variables was used for comparisons between patient groups (e.g., peri-implantitis vs periodontitis in Study I). Wilcoxon signed-rank test was used for paired intra-group comparisons (e.g., ICT-1 vs ICT-2 in Study I). Significance level was set at $p<0.05$.

Proton-induced X-rays Emission (Study III)

In **Study III**, micro-PIXE (μ-PIXE) was used for the quantification, localization and characterization of titanium (Ti) micro-particles in soft tissue samples obtained from peri-implantitis and reference implants sites. The analysis was performed in collaboration with the **Tandem Laboratory**, Department of Nuclear Physics, Uppsala University, Sweden.

Micro-PIXE belongs to the family of ion-beam based analytical methods, in which a proton beam (2 MeV H^+) is focused down to the micrometer lateral scale and used to scan target samples. The X-rays generated due to the sample-beam interaction are detected using an energy dispersive detector. Since the X-rays are characteristic for each chemical species, elemental mapping of intact tissue samples becomes possible with information on their spatial distribution.

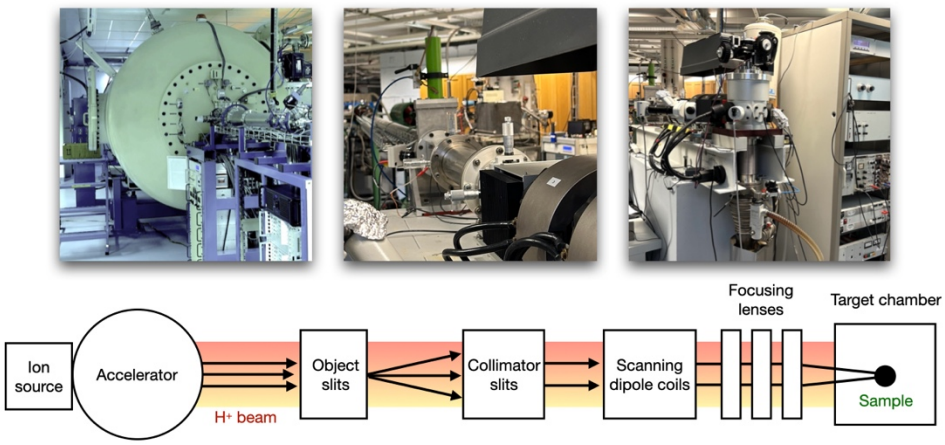

Figure 8. Photographs & schematic drawing of the Uppsala scanning nuclear microprobe.

- *The ion source generates keV H+ ions that are accelerated to MeV energies in the electrostatic accelerator.*
- *The resulting 2 MeV H+ ion beam is focused onto the sample via quadrupole focusing lenses.*
- *The sample-beam interaction causes the emission of characteristic X-rays that are measured through a detector positioned inside the target chamber.*

Image acquisition

From each FFPE biopsy (n=42), a 20- to 50-μm-thick section was obtained with a microtome equipped with a stainless-steel knife. Each section was individually mounted on clean 1x1 cm silico-crystal holders and dewaxed at 60°C overnight.

All sections were first imaged under an inverted light microscope (Leica, Wetzlar, Germany) at 5x magnification and then transferred to the Tandem Laboratory in Uppsala for further analysis. Samples from three patients had to be excluded due to complications during sample preparation. Thus, a total of 36 paired samples were fully mapped and included in the final analysis. Three additional sections from archive material obtained from patients with severe periodontitis (from Study I) were used as negative controls.

For an efficient characterization, the scanning system of the nuclear microprobe was modified to combine beam scanning and stage scanning in a so-called "mosaic-scan way" (Nagy et al., 2022). Thus, samples up to several cm^2 in size could be effectively mapped without any need for operator intervention.

The samples were placed into the vacuum chamber and irradiated with the proton microbeam. The entire specimens were raster-scanned with 1x1 mm sequential tiles and a spot-focusing of 4-5 μm. The sampling voltage analysis (SVA) mode was used to record scanned coordinates for mapping.

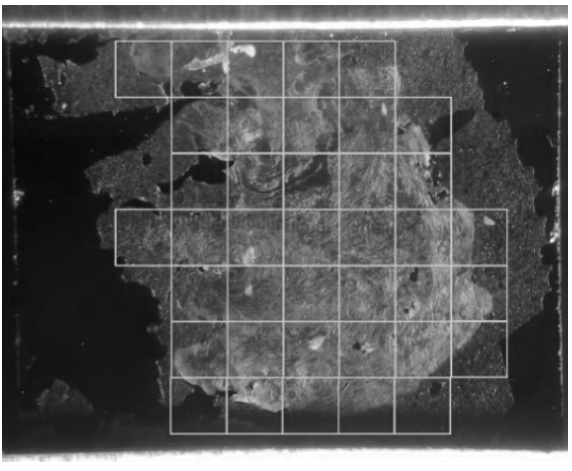

Figure 9. Mosaic imaging of a tissue section mounted on a silico-crystal wafer (1x1 cm).

Tile dimensions: 1x1mm. Spot-focusing: 1-2 μm.

During the mapping of the samples, Ti micro-particles were automatically imaged using the "Hough-transformation based object-identification" algorithm. Single-particle maps were generated and high statistics PIXE analysis was performed on selected micro-particles. This was done to further characterize the objects of analysis and to obtain threshold levels where all the counts originating from noise were vanished. Background subtraction was performed using the GeoPIXE software (version 8.6, CSIRO, Australia) on the full-sample maps, resulting in clean, background-free elemental maps.

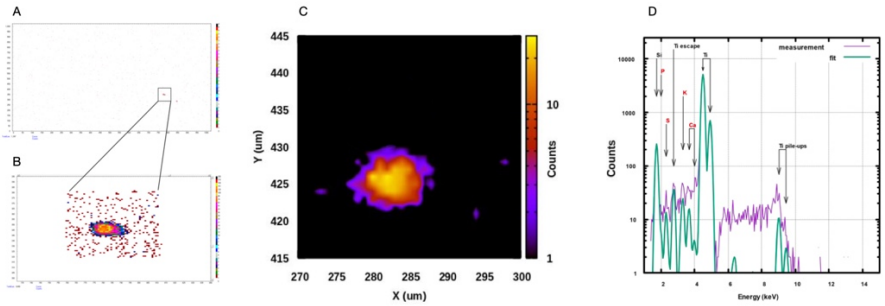

Figure 10. Single-particle identification (left image) and characterization (central image). Example of the characteristic X-ray spectrum of one representative titanium micro-particle (right image).

Image analysis

The elemental composite maps were analyzed with the computerized image analysis software Image-Pro Premier (IPP, version 10, Media Cybernetics Inc., Rockville, MD, USA).

Images obtained by the inverted light microscope and sulfur elemental maps were used to depict the entire outline of each specimen with a mouse cursor. The outline of the specimen was then transferred to the corresponding titanium composite map. To avoid any image distortion, matching sulfur and titanium maps were imaged with identical size and with fixed resolution. Linear calibration was performed manually on each composite image using the side of a single tile as reference (side of 1 tile = 1 mm).

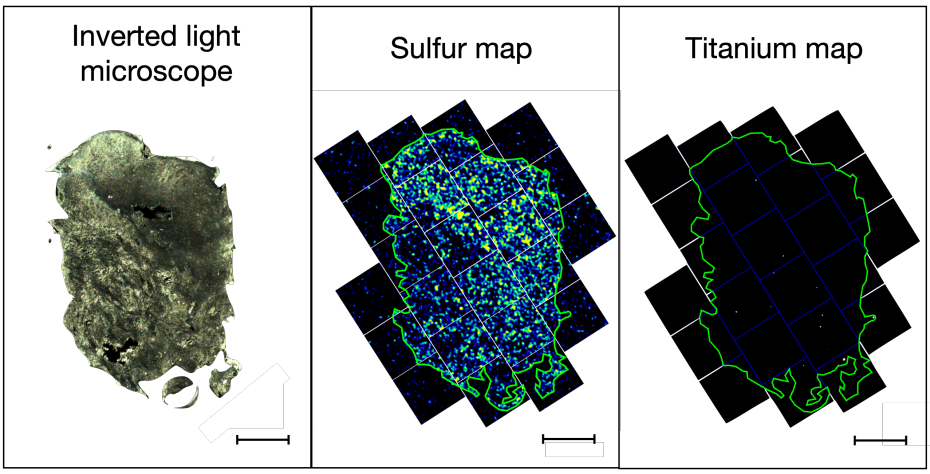

Figure 11. Schematic illustration of the image analysis process.
Images from the ILM and the sulfur maps are used to outline the entire ROI which is then transferred to the titanium map (green line). Scale bars 1 mm.

Different ROIs were depicted for the analysis. The initial examination was focused on the "**entire specimen**" ROI, where the total area of the specimen was analyzed as a whole. To further characterize the spatial distribution of titanium particles within tissues, different sub-analyses were conducted.

Thus, the "entire specimen" ROI was divided into three different zones, depending on the distance to the implant/tissue interface. "**Zone 1**" encompassed the tissue portion from the implant/tissue interface up to 1 mm, "**zone 2**" from

1 mm to 2 mm, and "**zone 3**" from 2 mm onwards. It must be noted that three sections from reference implant sites presented with a width that did not encompass zone 2.

Two additional ROIs were depicted in the connective tissue portions characterized by the presence/absence of an inflammatory infiltrate. To do so, a "**zone with inflammation**" as well as a "**zone without inflammation**" were outlined. The selection was performed by superimposing the titanium maps with images obtained from sequential 5-µm-thick sections previously stained with hematoxylin & eosin (H&E). Any portion of the tissue characterized by epithelial lining was excluded.

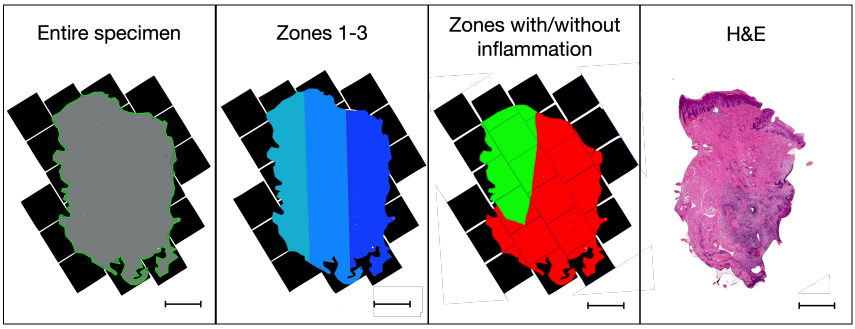

Figure 12. Schematic illustration of the image analysis process. Depiction of the different ROIs.

From the left: "Entire specimen" (in grey), "Zone 1" (in dark blue), "Zone 2" (in blue), "Zone 3" (in light blue), "Zone with inflammation" (in red), "Zone without inflammation" (in green), Hematoxylin & Eosin micrograph with magnification 20x. Scale bars 1 mm.

The "smart segmentation" tool of the IPP software was used to generate an algorithm for the identification of Ti micro-particles, similarly to what was done for IHC analyses in Studies I & II. Thus, the area (mm^2) and volume (= area of ROI x biopsy thickness, mm^3) of the ROIs, the number of Ti micro-particles (n) and the percentage area occupied by Ti micro-particles were measured. Volumetric densities were mathematically computed and expressed as number of particles/mm^3.

In addition, a comprehensive analysis of all the Ti micro-particles was performed. Thus, information on each particle-specific area (μm²), diameter (μm), Feret diameters (μm) and circularity (values 0-1) were obtained.

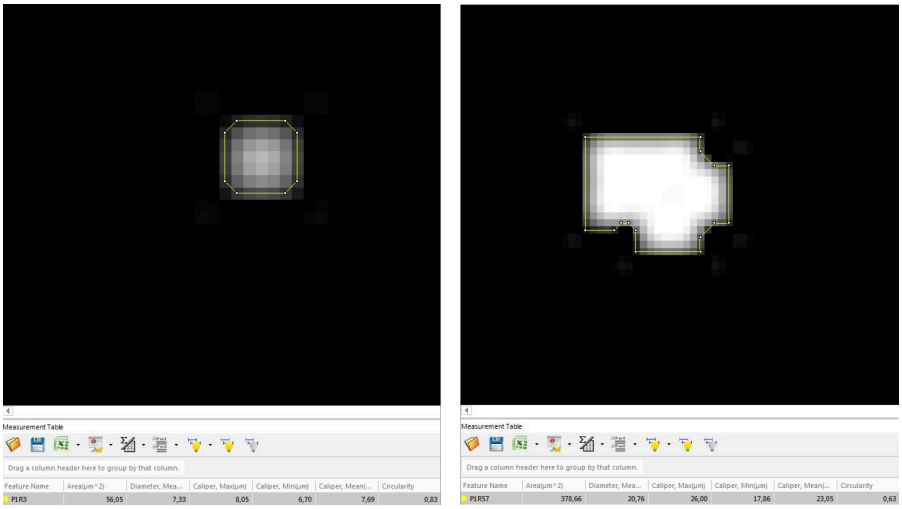

Figure 13. Illustration of two titanium micro-particles analyzed with the "smart segmentation" tool and the different measurements obtained for each particle.

Lastly, linear vertical distances (μm) from the mucosal margin and linear horizontal distances from the implant/tissue interface were measured for each particle. After tracing two reference lines corresponding to the implant/tissue interface and to the mucosal margin, perpendicular (= minimum) distances were automatically traced and measured for each particle using the "relative minimum distance between objects" tool of the IPP software. The maximum width (μm) and depth (μm) of the specimens were also recorded.

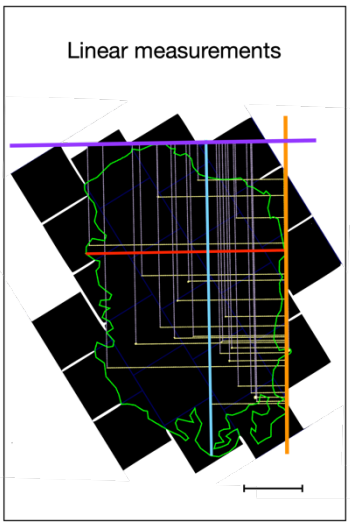

Figure 14. Schematic illustration of the image analysis process. Linear measurements.

Orange line: implant/tissue interface.
Purple line: mucosal margin.
Blue line: max depth of sample.
Red line: max width of sample.
Scale bar 1 mm.

Data analysis

Mean values, standard deviations, medians, inter-quartile ranges and 95% confidence intervals were calculated for each variable. Due to non-normal distribution of data, the non-parametric Wilcoxon pairwise signed-rank test was used for comparisons between peri-implantitis and reference implant sites. A linear regression analysis was performed to investigate the influence of implant characteristics (independent variables) and clinical measurements (PPD, MBL) on the volumetric density of titanium micro-particles (dependent variable). Statistical significance was set at $p<0.05$.

In **Studies III** & **IV**, after flap elevation, an additional soft tissue biopsy (about 1-2 mm^3) was dissected both at diseased and reference implant sites (n=42). The tissue portion was harvested at the same "FFPE sample" collection site from the connective tissue previously facing the implant body.

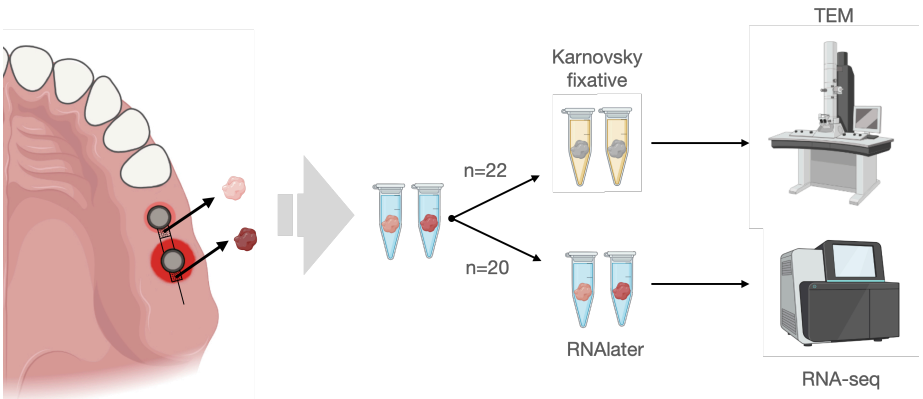

Figure 15. Biopsy retrieval and processing - schematic illustration.
Soft tissue biopsies (≈1-2 mm^3) are collected from target sites and prepared for TEM or RNA-seq analysis.

All tissue samples were rinsed with saline and immediately placed in Eppendorf tubes according to the following outline:

i) Samples from the initial 11 patients (n=22) were immersed in Karnovsky fixative, kept at 4°C, and prepared for transmission electron microscopy (TEM).

ii) Samples from the last 10 patients (n=20) were immersed in RNAlater (AMBION, US), kept at 4°C for 48 hours and stored at -80°C until further processing for RNA-sequencing.

Transmission Electron Microscopy (Study III)

After retrieval, samples were washed with saline and immersed in Eppendorf tubes with Karnovsky fixative (using EM-grade fixative quality) for 1 hour at 4°C. The specimens were then transferred to the **Core Facility** - **Cellular Imaging** (Sahlgrenska Academy, University of Gothenburg, Sweden) for further processing and analysis.

All samples were moved into new tubes containing 1:10 diluted Karnovsky fixative with cacodylate buffer 0.1 M at 4 °C for a maximum of 14 days before being processed. Post-fixation was performed with a combination of 1% osmium tetra-oxide (OsO4 - EMS, US) and 1% potassium ferrocyanide (Sigma-Aldrich, Germany) for 45 min in 0.05 M cacodylate buffer at room temperature (RT).

The samples were then processed with the Leica EM AMW Automatic Microwave Tissue Processor (Leica, Austria) using the following protocol:

- Immersion in 1% thio-carbo-hydrazide (EMS, US) in water at RT for 10 minutes.
- Profuse washes with distilled water (5 times, 10 minutes each).
- Immersion in 1% OsO4 in water at 37°C for 20 minutes.
- Profuse washes with distilled water (5 times, 10 minutes each).
- Incubation with 1% Uranyl Acetate (Fisher Scientific, UK), at RT for 30 minutes.
- Profuse washes with distilled water (5 times, 10 minutes each).
- Stepwise dehydration with increasing concentrations of ethanol (Fisher Scientific, UK).
- Stepwise dehydration with propylene oxide (Fisher Scientific, UK).
- Perfusion with increasing concentrations of Hard-Plus epoxy resin (EMS, US) without accelerator.
- Profuse washes with distilled water.
- Embedding in 100% Hard-Plus epoxy resin with accelerator.
- Polymerization at 60°C for 16 hours.

The polymerized specimens were trimmed with a 45° trimming diamond knife (Diatome, Switzerland) with a clearance angle of 6° into a pyramid shape to obtain a rectangular flat cutting surface.

Figure 16. Orthogonal projections of one representative resin-embedded specimen trimmed into pyramid shape (left and center). Illustration of 70-nm-thick sections collected onto copper grids ready for TEM analysis (right).

Alternate 70-nm-thick sections were produced using the UC6 ultramicrotome (Leica, Austria) equipped with a 45° diamond knife and clearance angle of 6°. The cutting was performed with a speed of 0.8mm/s. The sections were collected onto 150-mesh copper formvar/carbon-coated grids (Agar Scientific Ltd, UK).

Grids were imaged using the Talos L120C transmission electron microscope (Thermofisher Sc., US) operating at 120 KeV. Micrographs for qualitative evaluations of metal-like deposits were acquired with a CMOS 4Kx4K Camera (Gatan, UK) using the TIA Software (Zeiss, Germany) at various magnifications (range: 1600x - 28000x).

RNA-sequencing (Studies III & IV)

In **Study III**, RNA-sequencing was used to investigate the influence of Ti micro-particles on gene expression in peri-implantitis samples (n=9). Samples were divided into "Ti-low" (n=6) and "Ti-high" (n=3) groups depending on volumetric densities of Ti micro-particles being lower or higher than the mean.

In **Study IV**, RNA-sequencing was used for differential gene expression analysis between peri-implantitis and reference implant specimens obtained in 10 patients (n=20).

After retrieval, all samples were washed with saline, individually immersed in Eppendorf tubes with RNAlater (AMBION, US), kept at 4°C for 48 hours and subsequently stored at -80°C until further processing.

Sample preparation

The RNeasy Plus Micro Kit (Quiagen, Germany) was used for the extraction of total RNA following the manufacturer's instructions. In brief, the protocol included:

- Lysis and homogenization of samples in a highly denaturing guanidine-isothiocyanate-containing buffer using TissueRuptor II.
- Centrifugation for 3 minutes at maximum speed in the RNeasy spin column.
- Supernatant removal by pipetting.
- Removal of any genomic DNA by a new centrifugation cycle together with an optimized high-salted buffer.
- Removal of contaminants by addition of ethanol.
- Elution of total RNA content in 14 μl of RNAse-free water.
- Storage at -80°C.

The specimens were then transferred to the **Core Facility** - **Genomics** (Sahlgrenska Academy, University of Gothenburg, Sweden) for quality check and RNA-sequencing.

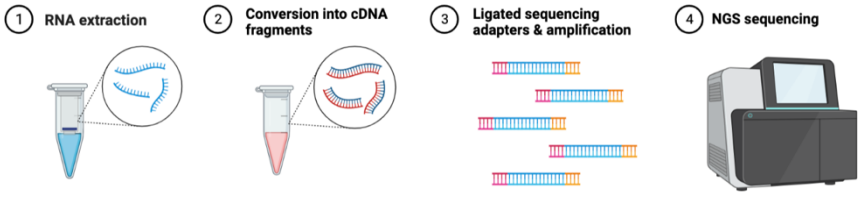

Figure 17. Schematic illustration of the RNA-sequencing protocol.

The integrity and size distribution of total RNA were checked with the Tapestation 4200 system (Agilent, USA). Quality check revealed that all samples presented with optimized concentrations of total RNA [range 34-463 ng/μL] and RIN scores ≥5 [range 5-9].

Library preparation

The Illumina Stranded mRNA Prep Ligation protocol (Illumina, USA) was used for library preparations as follows:

- mRNAs (with polyA tails) were captured by oligo(dT) magnetic beads.
- mRNA was fragmented and primed for first strand complementary DNA (cDNA) synthesis.
- The hexamer-primed RNA fragments were reverse transcribed including actinomycin D, granting RNA-dependent synthesis and improved strand specificity while preventing spurious DNA-dependent synthesis.
- The RNA template was then removed, and a replacement strand was synthesized to generate blunt-ended, double-stranded cDNA fragments.
- Deoxyuridine triphosphate was incorporated, and an adenine nucleotide was added to the 3′ ends of the blunt fragments.
- A corresponding thymine nucleotide on the 3′ end of the adapter was used for ligating the adapter to the fragment.
- Pre-index anchors were ligated to the ends of the double-stranded cDNA fragments to prepare them for dual indexing.
- After 11 PCR cycles and purification of the adapter-ligated fragments with magnetic beads, the libraries were normalized down to 1 nM, pooled together, diluted to 0.5 nM and standard run on a S2 flowcell on the NovaSeq 6000 (Illumina, USA).

Libraries were sequenced with an average depth of approximately 59.3 (±11.4) Mreads/sample.

Data analysis

Differential gene expression analysis was performed in collaboration with the **Core Facility** - **Bioinformatics** (Sahlgrenska Academy, University of Gothenburg, Sweden).

The quality of the reads was examined using fastqc/0.11.9, and the resulting quality reports were summarized using MultiQC/1.9. The reads were quality filtered using Trim Galore/0.4.0 and adapters were removed using Cutadapt/1.9. The quality-filtered reads were aligned towards the human reference genome GRCh38.109 using STAR/2.7.10b. Infer experiment within RSeQC/5.0.1 was used to extract the strandness of the data. Featurecounts within the subread/2.0.4 package was used to gather the gene counts.

The differential expression analysis was run in the R/4.1.3 package DESeq2/1.34.0. Genes were considered differentially expressed with adjusted *p* values <0.05. Log-fold change was used to identify the magnitude of change in gene expression between groups. Threshold levels of $Log_2FC \geq 1$ and $Log_2FC \leq -1$ were applied to identify the most significantly differentially expressed genes.
The package pheatmap/1.0.12 was used to generate heatmaps, while ClusterProfiler/4.2.2 was used to perform the overrepresentation analysis for Gene Ontology and Reactome.

Spatial Transcriptomics (Study IV)

Spatial transcriptomics was used for differential gene expression analysis and visualization between peri-implantitis and reference implant specimens obtained in 2 patients (n=4). Sample and library preparations were performed in collaboration with the **SciLife Laboratory - National Genomics Infrastructure** (Karolinska Institute and Stockholm University, Sweden).

Sample preparation

Four FFPE tissue sections were prepared following the Visium CytAssist spatial gene expression workflow (CG000518, 10x Genomics). The protocol included:

- Sectioning of the FFPE tissue blocks in 5-μm-thick sections using a microtome equipped with a stainless-steel knife.
- Collection of the sections in a Milli-Q or ultrapure water bath at 42°C to allow optimal expansion.
- RNA quality assessment on additional tissue sections by calculating the percentage of total RNA fragments >200 nucleotides (DV200) using the RNAEasy FFPE Kit (Agilent, USA) and the RNA 6000 Pico Kit (Agilent, USA) following the manufacturer's instructions. All FFPE sections presented with DV200 values ≥70% and were accepted for further processing.
- Placement of the sections on superfrost plus microscope slides (Fischer Scientifics, UK).
- Drying of the sections in a slide drying rack or desiccator by incubation for 3 hours at 42°C and subsequent incubation at room temperature overnight.
- Deparaffinization by sequential Xylene and decreasing Ethanol (from 100% to 70%) baths.
- Hematoxylin & eosin immunostaining and imaging of the sections with a V200 Slide Scanner Olympus Microscope (Evident, Japan) at x5 magnification.
- Decrosslinking and tissue permeabilization with a thermocycler at 95°C for 1 hour.
- Loading of glass slides together with the Visium CytAssist Spatial Gene Expression v2 Slides (6.5mm) into the Visium CytAssist instrument and placement into close proximity.

The CytAssist Spatial Gene Expression Slides present with 2 capture areas (6.5 x 6.5 mm) each including ~5000 barcoded spots. Each spot includes: 1 Illumina TruSeq partial read sequencing primer, 16 nucleotide (nt) Spatial Barcode, 12 nt unique molecular identifier (UMI) and 30 nt poly(dT) sequence (captures ligation product).

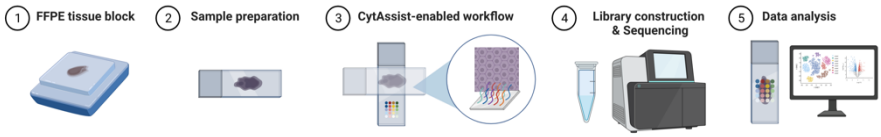

Figure 18. Schematic illustration of the Visium CytAssist spatial gene expression for FFPE workflow.

Library preparation

The Visium CytAssist spatial gene expression workflow (CG000518, 10x Genomics) was followed for library preparation. The protocol included:

- Probe hybridization: addition of the human whole transcriptome probe panel (= a pair of specific probes for each targeted gene) to the tissues. Probe pairs hybridize to their complementary target RNA.
- Probe ligation: ligase addition to seal the junction between the probe pairs, forming a ligation product.
- Probe release: release of ligated products from the tissue using the CytAssist Enabled RNA Digestion & Tissue Removal.
- Probe capture: capture of released ligated probes on the Visium CytAssist Spatial Gene Expression v2 Slides via spatially barcoded oligonucleotides present on the Visium slide surface.
- Probe extension: addition of UMI, Spatial Barcode and partial Read 1.
- Pre-amplification and indexing: collection of barcoded ligation products for qPCR to determine Sample Index PCR cycle number for generating final library molecules.
- Cleaning of final libraries by SPRIselect, assessment on bioanalyzer, quantification, and sequencing.

The final libraries comprised standard Illumina paired-end constructs which began and ended with P5 and P7 adaptors. Once quantified and normalized, the

libraries were denatured and diluted as recommended for Illumina sequencing platforms.

All samples were sequenced on NovaSeq6000 (NovaSeq Control Software 1.8.0/RTA v3.4.4) with a 151nt(Read1)-19nt(Index1)-10nt(Index2)-151nt(Read2) setup using "NovaSeqXp" workflow in "S4" flowcell mode.

Raw sequencing data were demultiplexed and converted to FastQ. The Bcl to FastQ conversion was performed using "bcl2fastq_v2.20.0.422" from the CASAVA software suite. The quality scale used was "Sanger / phred33 / Illumina 1.8+". Standardized bioinformatics quality control checks were performed including yield, sequence read quality and cross-sample contamination checking (accredited under ISO/IEC 17025).

Libraries from all samples were sequenced with library depths ≥114 Mreads [114.24 - 167.74] and presented with a ≥87% aggregated percentage of bases quality score >30.

Image alignment, demultiplexing on spatial barcodes and basic Visium quality checks were performed using Space Ranger and Loupe Browser (10xGenomics).

Data analysis

Data analysis was performed in collaboration with the **Core Facility – Bioinformatics** (Sahlgrenska Academy, University of Gothenburg, Sweden). Filtered gene spot matrix and high-resolution fiducial aligned images were used for downstream data analysis in Seurat (version 4.9.9.9045).

Each sample was filtered according to the following protocol: cells were filtered if the percentage of mitochondrial genes was higher than 20% and if the number of unique molecular identifier (UMI) counts per spot was less than 130. Samples were individually normalized and variance-stabilized using regularized negative binomial regression with the R package "SCTransform" (version 0.3.5) where the percentage of mitochondrial expression was regressed out and the number of variable genes was set to 6000 out of 18000 total available genes.

The number of variable genes was further used to create anchors for integration between samples in order to reduce batch affect and resolve for possible

differences in sample tissue quality. PCA npcs=10, FindNeighbors, Clustering with resolution set to 0.6 and UMAP dimensionality reduction using 10 dimensions were then used to identify 12 stable clusters across peri-implantitis and reference implant samples. Identifying differentially expressed markers for disease-specific clusters compared to reference was done using the "FindMarker" function from Seurat. Genes were considered differentially expressed with adjusted *p* values <0.05. Log-fold change was used to identify the magnitude of change in gene expression between groups. Threshold levels of $Log_2FC \geq 2$ and $Log_2FC \leq -2$ were applied to identify the most significantly differentially expressed genes.

Immune cell populations were identified using the R package "SingleR" (version 2.2.0) which is based on automatic annotations based on a reference dataset with known labels from "celldex" (version 1.10.1). A combination of the "Human Primary Cell Atlas Data" and "DICE" was used as reference in order to maximize the number of labeled cells. "ClusterProfiler" (version 4.2.2) was used to perform the overrepresentation analysis for Gene Ontology and Reactome.

The level of agreement between spatial transcriptomics and RNA-sequencing was investigated by comparing DEGs identified by spatial transcriptomics in the ICT-specific clusters and DEGs found by RNA-sequencing. Sensitivity and specificity were calculated comparing genes consistently present in both datasets and exhibiting significant dysregulation (adjusted *p* values <0.05). Sensitivity quantified the ability of RNA-sequencing to accurately identify genes up-regulated in spatial transcriptomics, while specificity indicated the precision in detecting down-regulated genes.

Radiographic assessments (Study III)

In **Study III** intra-oral radiographs were obtained by long-cone parallel technique prior to the surgical intervention (≤4 weeks).

Linear measurements were performed using the Fiji image analysis software (ImageJ 2.0.0-rc-69/1.52n, National Institutes of Health). Known inter-thread distances were used for linear calibration. Marginal bone levels (mm) were assessed at mesial and distal sites of each implant, using the implant shoulder as reference point. The mean value of mesial and distal measurements was used for the analysis. The length (mm) and diameter (mm) of each implant were also measured.

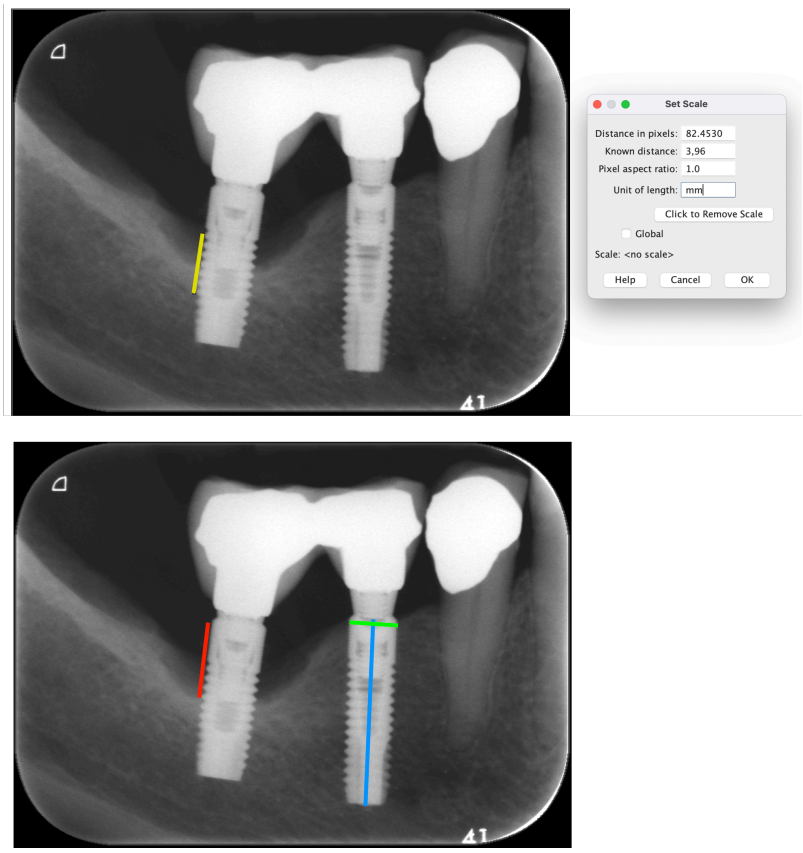

Figure 19. Illustration of the image calibration process with known inter-thread distance (yellow line). Measurements: marginal bone level at distal site (red line); implant length (blue line); implant diameter (green line).

Error of methods

Histological, immunohistochemical and radiographical measurements were repeated in Study I and Study III for accuracy assessments. Agreement levels are reported as inter-class coefficients (ICC) and confidence intervals (CI).

Study	Target		Intra-examiner agreement	
			ICC	[C.I.]
I	TOT ROI Area (μm²)	ICT	0.96	0.87-0.99
III	TOT ROI Area (μm²)	ES	0.99	0.98-0.99

Histological analysis: the infiltrated connective tissue (ICT) and the "entire specimen" (ES) ROIs were outlined with a mouse cursor and the total ROI area was re-assessed in 20 randomly selected sections.

Study	Target		Intra-examiner agreement	
			ICC	[C.I.]
I	Positive cells area (μm²)	ChK2	0.94	0.74-0.98
III	Ti micro-particles area (μm²)	Ti	0.99	0.99-0.99

Immunohistochemical analysis: the algorithms for assessing areas occupied by positive cells and titanium micro-particles (in the ICT or in the ES, respectively) were re-created and measurements were repeated in 20 randomly selected sections.

Study	Target		Intra-examiner agreement	
			ICC	[C.I.]
III	MBL	M sites (mm)	0.99	0.98-0.99
III	MBL	D sites (mm)	0.99	0.98-0.99

Radiographic analysis: marginal bone levels at mesial (M) and distal (D) sites were re-measured in 10 randomly selected radiographs.

Ethical considerations

Ethical approvals

The protocol for **Study I** was approved by the local Human Review Board of Gothenburg, Sweden (Dnr 245-10).

The protocol for **Study II** was approved by the local Human Review Board of the University of Basel, Switzerland (EK: 159/06).

The protocol for **Studies III** & **IV** was approved by the Swedish Ethical Review Authority (Dnr 2021-00508).

Data protection

Data from all studies were regarded as "sensitive personal data", as they derived from analyses of human biological samples. Pseudonymization was applied (only code numbers were used) in all studies. The code keys were stored in a locked safe accessible only by authorized personnel.

In **Studies III** & **IV**, access to the Bianca Cluster was granted for storage and analysis of human RNA-sequencing and spatial transcriptomic datasets. For this purpose, an agreement was signed (Dnr sens2023510) with the Uppsala Multidisciplinary Center for Advanced Computational Science (UPPMAX) and with the National Academic Infrastructure for Supercomputing in Sweden (NAISS, former Swedish National Infrastructure for Computing - SNIC).

Results

Periodontitis and peri-implantitis lesions in humans (Study I)

The total areas of the PE and ICT were significantly larger in peri-implantitis than in periodontitis samples.

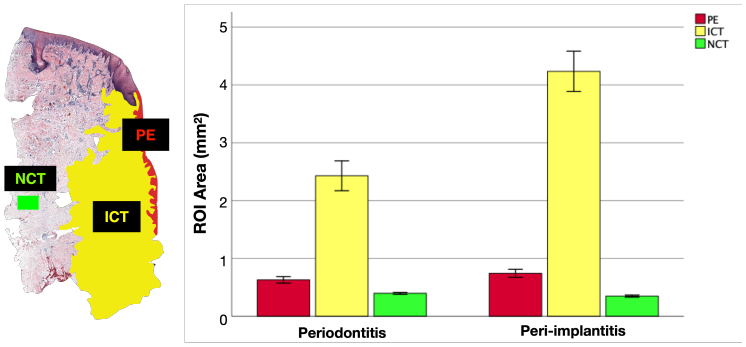

Figure 20. Micrograph representing the outlined ROIs (left). Bar graphs: total areas of ROIs (mm^2) in periodontitis and peri-implantitis sites (right). Mean and 95% CI.

In the **PE**, periodontitis sites presented with significantly higher densities and area proportions of 8-OHdG-positive cells compared to peri-implantitis. In addition, periodontitis sites contained significantly lower numbers of MPO-positive cells and higher numbers of 8-OHdG-positive cells than peri-implantitis sites.

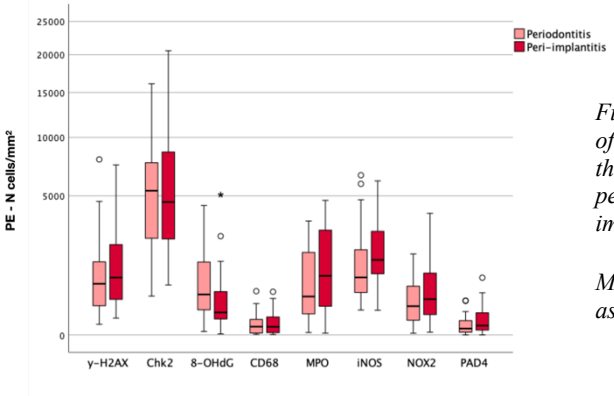

Figure 21. Boxplots: density of positive cells observed in the pocket epithelium of periodontitis and peri-implantitis sites.

Median and IQR. Circles and asterisks represent outliers.

In the **ICT**, peri-implantitis specimens exhibited significantly higher densities and area proportions of iNOS-, MPO-, and CD68-positive cells than periodontitis lesions. The density of MPO-positive cells was about 3 times larger in peri-implantitis than that in periodontitis. The numbers of γ-H2AX-, iNOS-, MPO-, PAD-4/MPO-, and CD68-positive cells were significantly higher in peri-implantitis than in periodontitis sites.

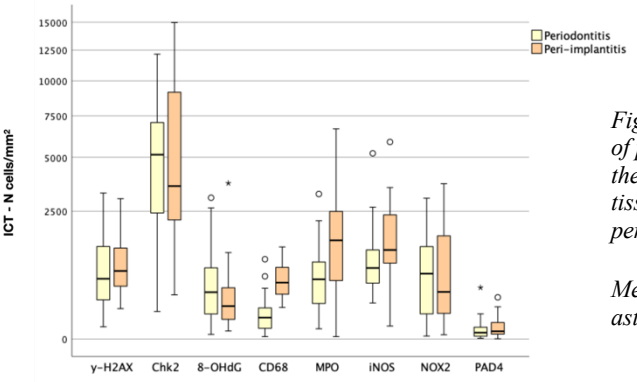

Figure 22. Boxplots: density of positive cells observed in the infiltrated connective tissue of periodontitis and peri-implantitis sites.

Median and IQR. Circles and asterisks represent outliers.

In the **NCT**, area proportions and densities of γ-H2AX-, iNOS-, NOX2-, MPO- and PAD4/MPO-positive cells were significantly greater in peri-implantitis than in periodontitis sites. The density of NOX2-positive cells was almost 6 times larger in peri-implantitis than in periodontitis lesions. Peri-implantitis sites exhibited a significantly larger number of γ-H2AX-, MPO-, PAD4/MPO-, and CD68-positive cells than periodontitis sites.

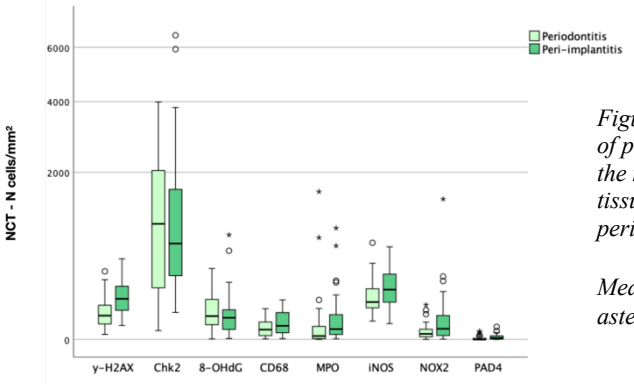

Figure 23. Boxplots: density of positive cells observed in the non-infiltrated connective tissue of periodontitis and peri-implantitis sites.

Median and IQR. Circles and asterisks represent outliers.

Intra-group comparisons showed no significant differences between **ICT-1** and **ICT-2** areas, both in periodontitis and peri-implantitis sites (method validation).

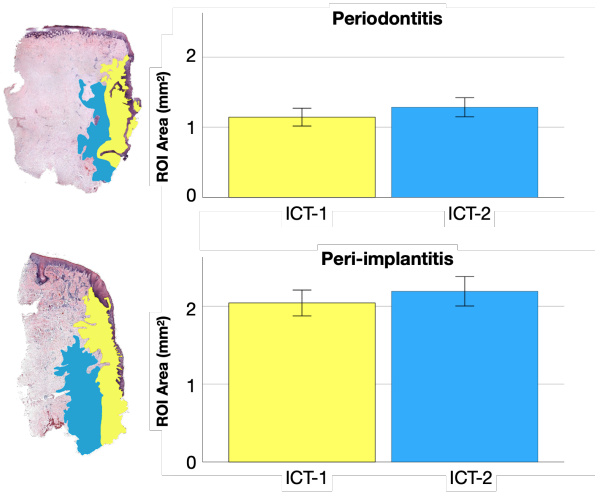

Figure 24. Micrograph representing the outlined ROIs (left). Bar graphs: total areas of ICT-1 and ICT-2 in periodontitis and peri-implantitis sites (right). Mean and 95% CI.

Statistically significant intra-group differences in cellular densities for all markers were found between the ICT-1 and the ICT-2 in both periodontitis and peri-implantitis sites. Overall, the ICT demonstrated a gradient of the cellular infiltrate towards the pocket epithelium, with ICT-1 exhibiting about 1.5–3 times higher cellular densities than the ICT-2.

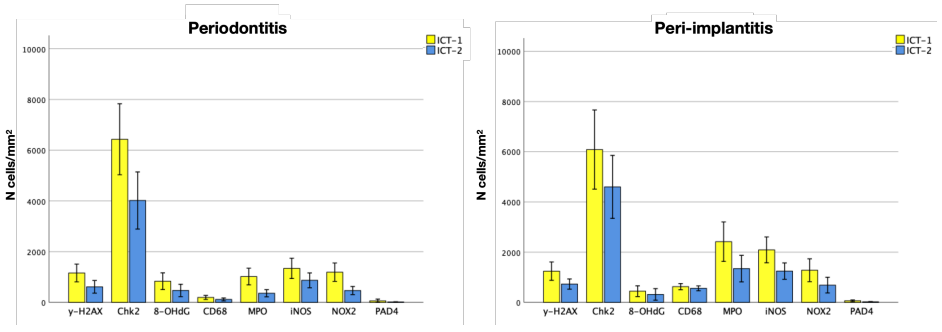

Figure 25. Bar graphs: density of positive cells observed in ICT-1 and ICT-2 of periodontitis (right) and peri-implantitis sites (left). Mean and 95% CI.

The proportion of smokers (27.5%) was equally distributed between periodontitis and peri-implantitis groups. No significant differences in cellular densities between smokers and non-smokers were observed for any of the markers in periodontitis and peri-implantitis lesions.

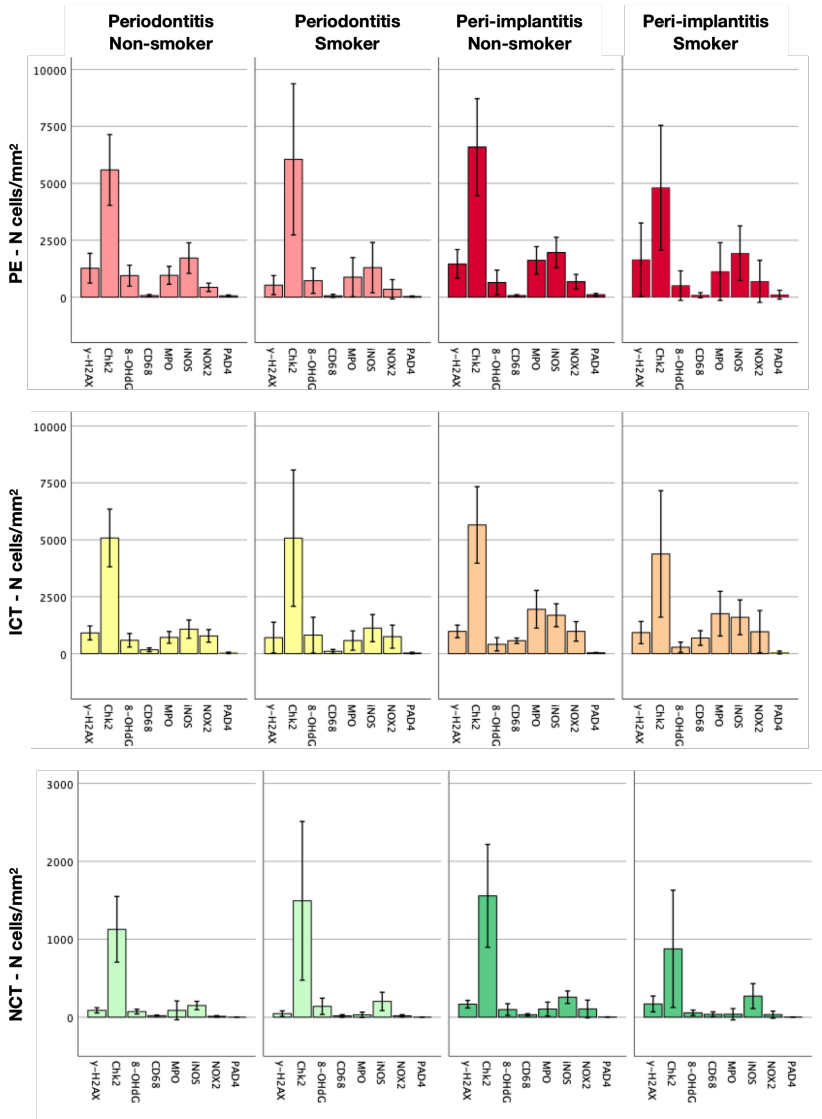

Figure 26. Bar graphs: density of positive cells in the different patient groups divided by ROI. Mean and 95% CI.

Periodontitis lesions in smokers and non-smokers (Study II)

No differences in ICT areas were detected between non-smokers and current smokers.

Figure 27. Micrographs representing the outlined ROIs (sides). Bar graphs: ICT areas (mm2) in non-smokers and current smokers. Mean and 95% CI.

In the ICT, non-smokers showed significantly higher densities and area proportions of DNMT1-, AcH3-, iNOS-, and NOX2-positive cells than current smokers. The largest difference in cellular densities between the two groups was noted for the DNMT1- and NOX2-markers. The total number of DNMT1- and NOX2-positive cells were significantly higher in specimens from non-smokers than from current smokers.

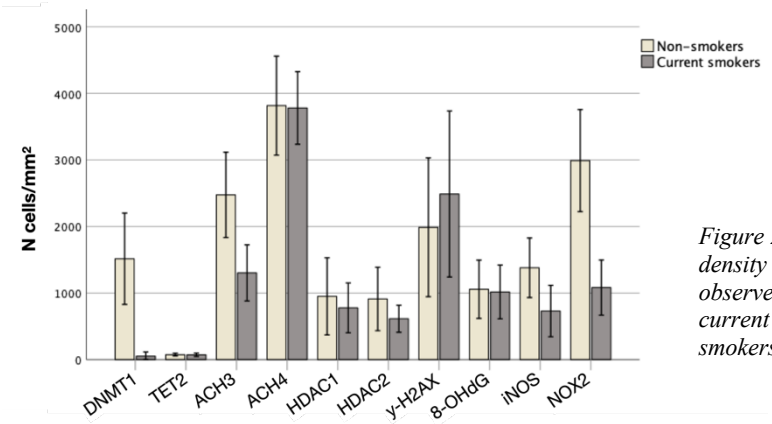

Figure 28. Bar graphs: density of positive cells observed in the ICT of current smokers and non-smokers. Mean and 95% CI.

Titanium micro-particles in peri-implant tissues (Study III)

Localization and quantification

In the "**entire specimen**" ROI, areas and volumes of the soft tissue biopsies were significantly larger in peri-implantitis than in reference implant sites (Table 2, manuscript of Study III). However, no differences were found in terms of number of Ti micro-particles, percentage area occupied by Ti micro-particles or volumetric densities of Ti micro-particles between samples with or without peri-implantitis.

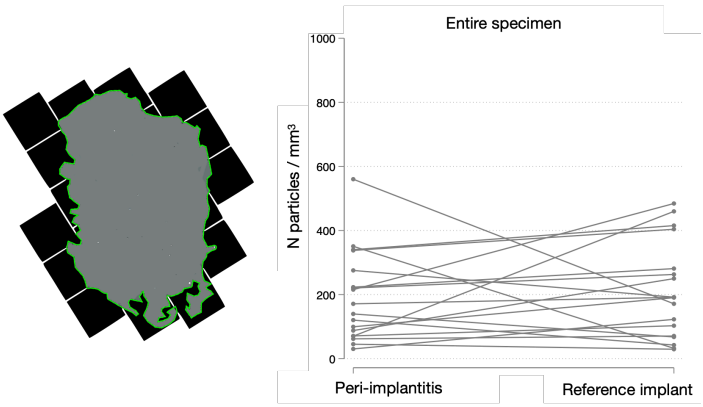

Figure 29. Outlined ROI (left). Strip plots: volumetric densities of titanium micro-particles in the "entire specimen" ROI of peri-implantitis and reference implant sites. Each dot represents one implant and paired implants from the same patient are connected by lines.

In the ROIs "**zone 1**" and "**zone 2**", no differences in volumetric densities of Ti micro-particles were found between sites with or without peri-implantitis.
In the "**zone 3**" ROI, although differences were small in magnitude, the percentage area occupied by Ti micro-particles was statistically lower in reference implant samples than in peri-implantitis specimens (0.06% ±0.10 vs 0.10% ±0.12,

respectively; $p<0.05$). However, no differences in volumetric densities were observed in "zone 3" between sites with or without peri-implantitis.

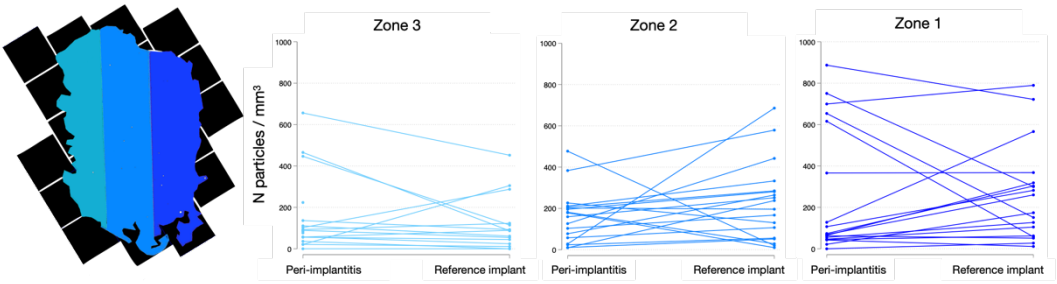

Figure 30. Outlined ROIs (left). Strip plots: volumetric densities of titanium micro-particles in "zone 3"," zone 2" and "zone 1" in peri-implantitis and reference implant sites. Each dot represents one implant and paired implants from the same patient are connected by lines.

Comparisons between the ROIs "**zone with inflammation**" and "**zone without inflammation**" did not demonstrate any significant difference in volumetric densities of Ti micro-particles, both in peri-implantitis and in reference implant sites.

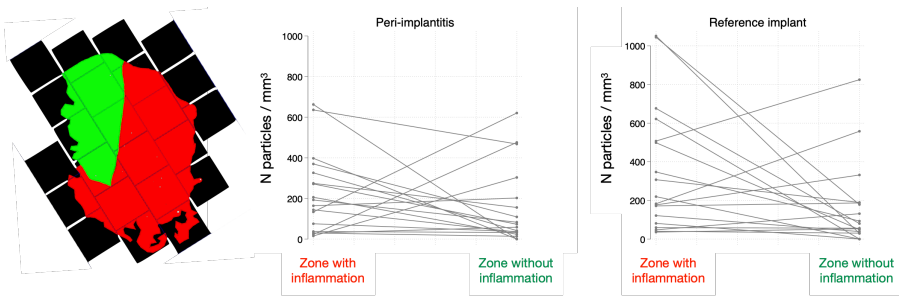

Figure 31. Outlined ROIs (left). Strip plots: volumetric densities of titanium micro-particles in "zone with inflammation" & "zone without inflammation" in peri-implantitis and reference implant sites. Each dot represents one implant.

Among the implant-related characteristics, the "implant system" variable significantly influenced the density of Ti particles in the "zone 1" ROI. As the different implant systems were not equally represented among the 18 patients, the least represented systems were collectively merged into a new category named "Others". Thus, Astra OsseoSpeed implants demonstrated significantly lower volumetric densities of Ti micro-particles when compared to Nobel TiUnite and "Others" implant systems in the "zone 1" ROI ($p = 0.024$ and 0.047, respectively).

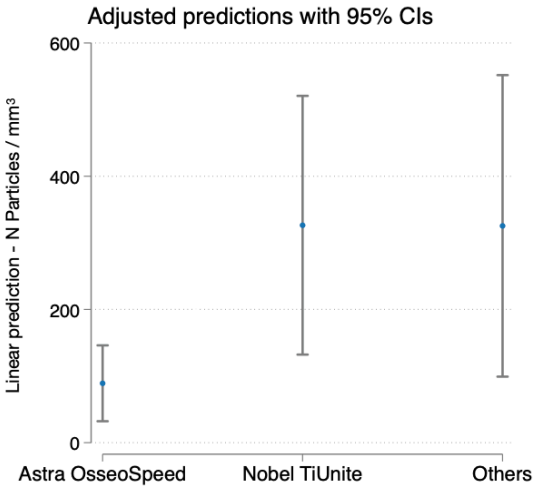

Figure 32. Predicted volumetric densities of Ti micro-particles in the "zone 1" ROI by implant system.

No titanium micro-particles were observed in the connective tissue of negative controls from periodontitis affected sites in patients with no dental implants. Few isolated Ti micro-particles were observed in the pocket epithelium.

Characterization

A total of 1228 and 663 Ti micro-particles were characterized in peri-implantitis and reference implant sites, respectively. No differences in particle-related characteristics (area, diameter, Feret caliper diameters, circularity) could be observed between samples with or without peri-implantitis. In both groups, approximately 60-65% of the Ti micro-particles presented with a diameter ≤15 μm and with a circularity value >0.6.

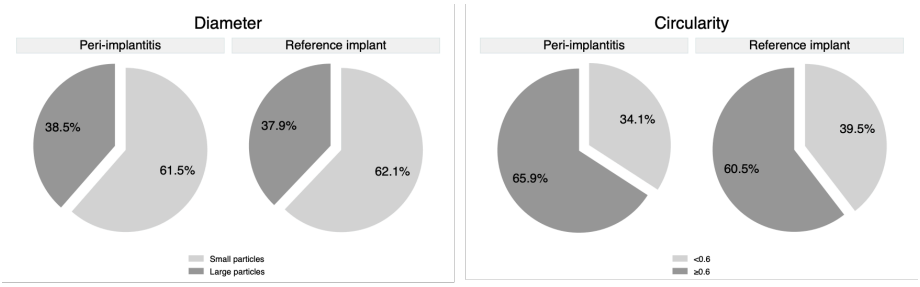

Figure 33. Distribution of diameter (small: ≤15μm; large: >15μm) and circularity (range 0-1) of titanium micro-particles in peri-implantitis and reference implant sites.

Results from the linear measurements showed similar horizontal (from implant/tissue interface) and vertical (from mucosal margin) distributions of Ti micro-particles between samples with and without peri-implantitis.

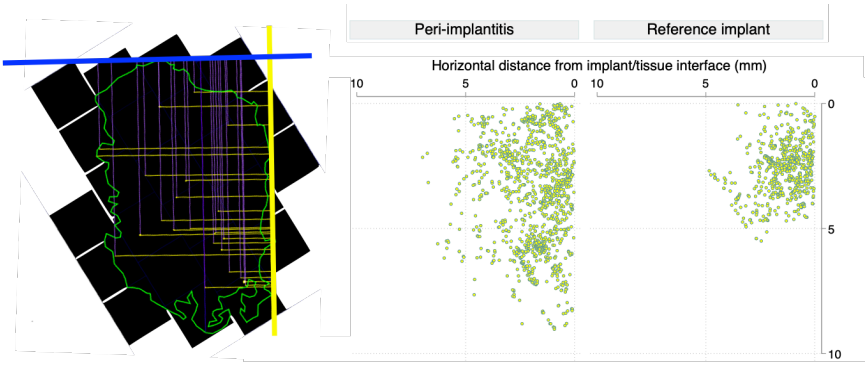

Figure 34. Linear measurements (left). Scatterplots: absolute horizontal and vertical distances of micro-particles in peri-implantitis and reference implant sites. Each dot represents one Ti micro-particle.

Comparison between the distribution of small (diameter ≤15 μm) and large (diameter >15 μm) Ti particles did not demonstrate any significant difference, both in peri-implantitis and in reference implant samples.

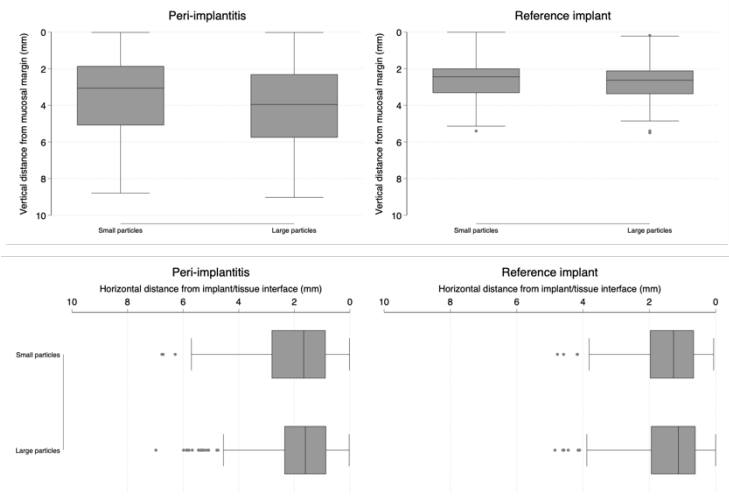

Figure 35. Boxplots: distribution of small and large particles at peri-implantitis and reference implant sites.

Median and IQR. Circles represent outliers.

Sporadic metal-like particles could be observed in TEM sections and exclusively in peri-implantitis samples. All the observed metal-like particles were located in the extracellular compartment. Sections from peri-implantitis sites exhibited evident signs of tissue degradation and elevated numbers of inflammatory cells. Well-oriented collagen fibers, numerous fibroblasts and occasional cells of the host response were found in sections obtained from reference implant sites.

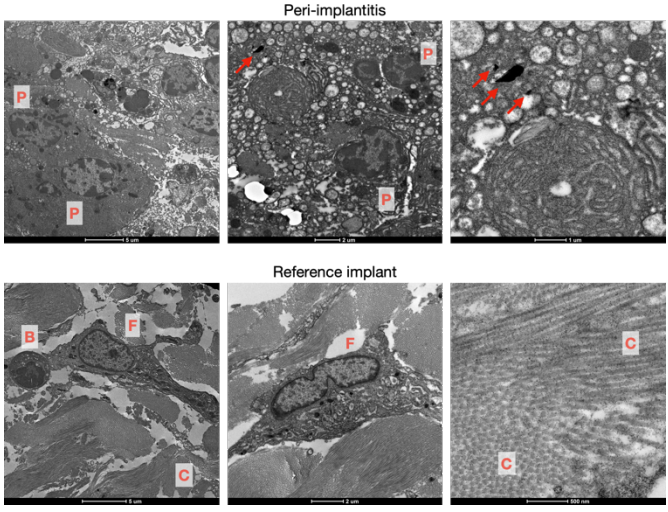

Figure 36. Representative TEM images illustrating sections from peri-implantitis and reference implant sites. Plasma cell (P); B-cell (B); fibroblast (F), collagen fibers (C). Red arrows indicate metal-like particles.

Influence on gene expression

A total of 9 peri-implantitis samples were analyzed with RNA-sequencing to investigate if Ti micro-particles influenced gene expression profiles.

The Supplementary Fig 1 in the manuscript of Study III displays the volume of the ROI "zone with inflammation" and the volumetric density of Ti micro-particles in the 9 FFPE samples corresponding to the "Ti-high" (n=3) and "Ti-low" (n=6) groups.

The RNA-seq analysis showed that, among a total of 36623 entries, only 16 significantly differentially expressed genes (DEGs) were identified between the two groups (adjusted *p* values <0.05). One up-regulated and one down-regulated DEGs were putative genes not registered with any specific gene ID.

Table 11. Differentially expressed genes between the two groups (Ti-high versus Ti-low).

Ensembl ID	Gene symbol	Gene name	Log2 fold change	*Adjusted p-value*
Up-regulated genes				
ENSG00000234925	-	-	3.95	1.9E-06
ENSG00000144820	ADGRG7	Adhesion G protein-coupled receptor G7	4.73	1.2E-05
ENSG00000123838	C4BPA	Complement component 4 binding protein alpha	3.96	0.0005
ENSG00000068831	RASGRP2	RAS guanyl releasing protein 2	1.76	0.032
Down-regulated genes				
ENSG00000159455	LCE2B	Late cornified envelope 2B	-0.60	1.9E-06
ENSG00000226278	-	-	-0.60	1.9E-06
ENSG00000187223	LCE2D	Late cornified envelope 2D	-0.59	3.43E-06
ENSG00000187173	LCE2A	Late cornified envelope 2A	-0.59	5.97E-05
ENSG00000129437	KLK14	Kallikrein related peptidase 14	-3.22	0.0016
ENSG00000204539	CDSN	Corneodesmosin	-1.16	0.019
ENSG00000135374	ELF5	E74 like ETS transcription factor 5	-2.20	0.019
ENSG00000108839	ALOX12	Arachidonate 12-lipoxygenase, 12S type	-2.51	0.019
ENSG00000022556	NLRP2	NLR family pyrin domain containing 2	-2.97	0.019
ENSG00000118520	ARG1	Arginase 1	-2.14	0.029
ENSG00000204538	PSORS1C2	Psoriasis susceptibility 1 candidate 2	-2.64	0.032
ENSG00000203782	LORICRIN	Loricrin cornified envelope precursor protein	-0.81	0.043

Three significantly up-regulated and 11 significantly down-regulated genes were found when comparing the Ti-high group to the Ti-low group. Among these DEGs, five genes (RASGRP2, C4BPA, NLRP2, ARG1 and ALOX12) were further investigated with gene-set enrichment analyses. Biological pathways related to "regulation of immune response", "complement activation" and "skin development" were found to be the most abundantly enriched in the Gene Ontology (GO) analysis.

Table 12. Gene Ontology enrichment analysis (Ti-high versus Ti-low).

GO term	Biological process	Adjusted p-value
Up-regulated pathways		
GO:0002924	Negative regulation of humoral immune response mediated by circulating immunoglobulin	0.021
GO:0008228	Opsonization	0.021
GO:0045916	Negative regulation of complement activation	0.021
GO:0002713	Negative regulation of B cell mediated immunity	0.021
GO:0002890	Negative regulation of immunoglobulin mediated immune response	0.021
GO:0002921	Negative regulation of humoral immune response	0.021
GO:0002923	Regulation of humoral immune response mediated by circulating immunoglobulin	0.021
GO:0030449	Regulation of complement activation	0.021
GO:0002920	Regulation of humoral immune response	0.034
GO:0002707	Negative regulation of lymphocyte mediated immunity	0.034
GO:0002708	Negative regulation of adaptive immune response based on somatic recombination of immune receptors built from immunoglobulin superfamily domains	0.034
GO:0002709	Negative regulation of adaptive immune response	0.034
GO:0002710	Regulation of B cell mediated immunity	0.034
GO:0002711	Regulation of immunoglobulin mediated immune response	0.034
GO:0002712	Negative regulation of leukocyte mediated immunity	0.034
GO:0002713	Cellular response to calcium ion	0.043
GO:0002714	Phagocytosis, recognition	0.047
GO:0002715	Complement activation, classical pathway	0.047
GO:0002716	Negative regulation of immune effector process	0.047
GO:0002717	Humoral immune response mediated by circulating immunoglobulin	0.049
Down-regulated pathways		
GO:0031424	Keratinization	3.52E-08
GO:0043588	Skin development	5.10E-07
GO:0030216	Keratinocyte differentiation	8.89E-07
GO:0008544	Epidermis development	8.89E-07
GO:0009913	Epidermal cell differentiation	3.93E-06
GO:0022408	Negative regulation of cell-cell adhesion	0.0094
GO:0007162	Negative regulation of cell adhesion	0.029

Reactome analysis revealed that the most significant differences between the two groups regarded the "regulation of complement cascade", "platelet activation", "platelet signalling" and "keratinization" pathways.

Table 13. Reactome enrichment analysis (Ti-high versus Ti-low).

Reactome ID	Description	Adjusted p-value
Up-regulated pathways		
R-HSA-392517	Rap1 signalling	0.017
R-HSA-114508	Effects of PIP2 hydrolysis	0.017
R-HSA-354192	Integrin signaling	0.017
R-HSA-76009	Platelet Aggregation (Plug Formation)	0.017
R-HSA-977606	Regulation of Complement cascade	0.017
R-HSA-166658	Complement cascade	0.018
R-HSA-2871837	FCERI mediated NF-kB activation	0.021
R-HSA-2454202	Fc epsilon receptor (FCERI) signaling	0.031
R-HSA-416476	G alpha (q) signalling events	0.044
R-HSA-76002	Platelet activation, signaling and aggregation	0.048
Down-regulated pathways		
R-HSA-6809371	Formation of the cornified envelope	6.45E-10
R-HSA-6805567	Keratinization	6.63E-09
R-HSA-70635	Urea cycle	0.022
R-HSA-9018677	Biosynthesis of DHA-derived SPMs	0.025
R-HSA-9018678	Biosynthesis of specialized proresolving mediators (SPMs)	0.025

The IHC analysis showed that, in the ICT, the Ti-high group presented with significantly higher cellular densities of RASGRP2-positive cells compared to the Ti-low group (p=0.0253). In addition, although the difference was not statistically significant, the density of C4PBA-positive was higher in the Ti-high than in the Ti-low group (p=0.0526).

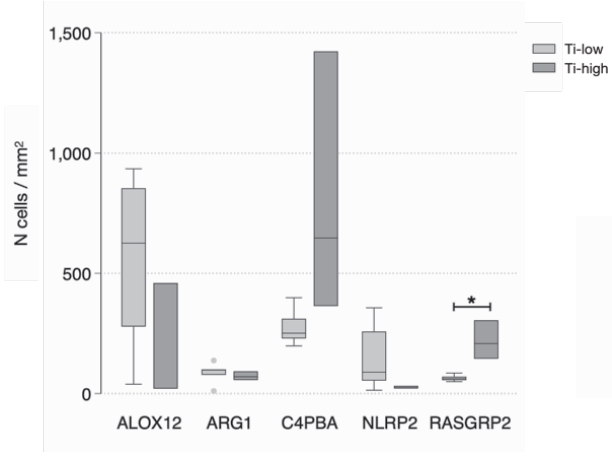

Figure 37. Boxplots: density of positive cells in Ti-low and Ti-high groups.

Median and IQR.
**p<0.05, Mann-Whitney U test.*

Gene expression profiles in human peri-implant lesions (Study IV)

Spatial transcriptomics

It was demonstrated that oral/pocket epithelium and infiltrated connective tissue areas presented with higher gene activity (number of transcript/spot) compared to non-infiltrated connective tissue portions in both peri-implantitis and reference implant sites. In addition, peri-implantitis samples showed overall higher degrees of gene activity when compared to reference implant specimens.

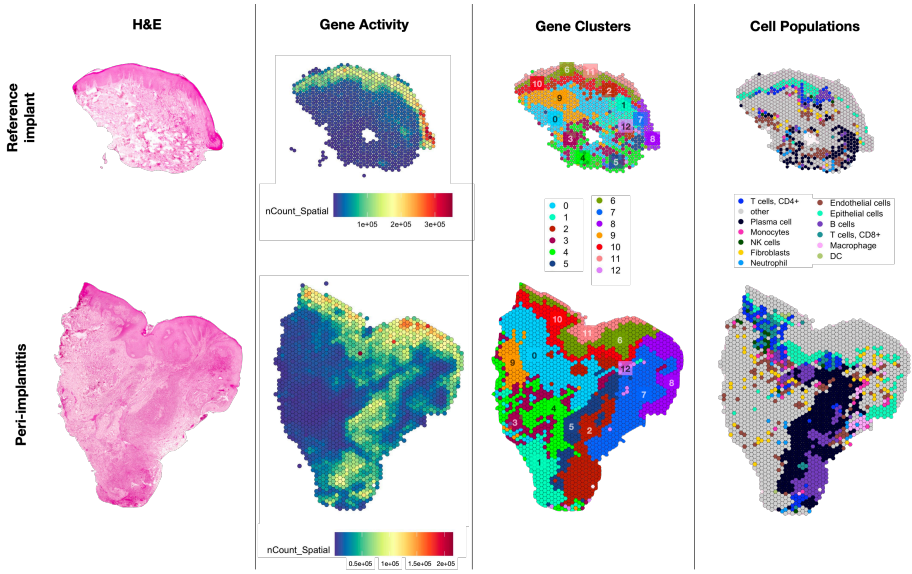

Figure 38. Spatial transcriptomic results. From left to right: H&E-stained sections of one pair of samples (Magnification 5x); visualization of gene activity; gene clusters; cell populations identified in peri-implantitis and reference implant samples. The implant/tissue interface is found on the right side of the samples.

Twelve distinct clusters of differentially expressed genes (DEGs) were identified and a clear association between clusters and specific regions in the tissues was observed. Thus, clusters 2, 5, 7 and 12 were distinctly located within the ICT compartment; clusters 6, 8, 10 and 11 matched oral epithelial tissues; clusters 0 and 9 were confined to NCT areas. No specific tissue areas were identified for clusters 1, 3 and 4. Stronger gene expression patterns were noticed in peri-

implantitis samples for all clusters except for cluster 9 when compared to reference implant specimens.

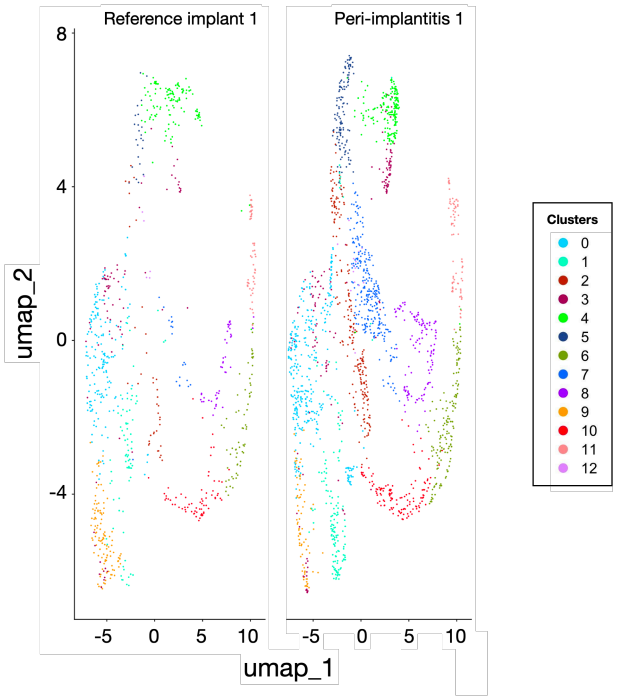

Figure 39. The 12 clusters identified in peri-implantitis and reference implant sites (in patient 1) by spatial transcriptomic analysis.

In total, the spatial transcriptomic analysis identified 3949 significantly down-regulated, and 349 significantly up-regulated genes when comparing peri-implantitis to reference implant specimens.

The analysis of the 4 clusters specific for the ICT areas identified a total of 188 up-regulated and 1247 down-regulated DEGs when comparing peri-implantitis specimens to samples from reference implant sites. Several DEGs were consistent among the 4 clusters.

Table 14. The most highly up-regulated and most highly down-regulated DEGs found when comparing peri-implantitis to reference implant sites in the 4 clusters specific for ICT areas ($Log_2FC \leq 2$ or ≥ 2 and p adjusted <0.05) by spatial transcriptomics.

Down-regulation			Up-regulation		
Gene symbol	*Gene name*	*Cluster(s)*	*Gene symbol*	*Gene name*	*Cluster(s)*
KRT13	Keratin 13	2	CHI3L1	Chitinase-3-like protein 1	2, 7
KRT6A	Keratin 6A	2, 5	IGLC7	Immunoglobulin lambda constant 7	2
KRT6B	Keratin 6B	2, 5	CXCL13	C-X-C Motif Chemokine Ligand 13	5
KRT1	Keratin 1	2, 7	MMP3	Matrix Metallopeptidase 3	7
KRT14	Keratin 14	2, 5	MMP1	Matrix Metallopeptidase 1	7
KRT6C	Keratin 6C	2, 5	G0S2	G0/G1 Switch 2	7
KRT7	Keratin 7	2	CHI3L2	Chitinase-3-like protein 2	7
KRT16	Keratin 16	2, 5	CXCL8	C-X-C Motif Chemokine Ligand 8	7
DSP	Desmoplakin	2	DERL3	Der1-Like Domain Family, Member 3	7
KRT5	Keratin 5	2, 5	CXCL6	C-X-C Motif Chemokine Ligand 6	7
SPRR1B	Small Proline Rich Protein 1B	5	TDO2	Tryptophan 2,3-Dioxygenase	7
KRT17	Keratin 17	5	PIM2	Serine/Threonine-Protein Kinase Pim-2	7
LY6D	Lymphocyte Antigen 6 Family Member D	5			
PI3	Peptidase Inhibitor 3	5			
COMP	Cartilage Oligomeric Matrix Protein	7, 12			
APOD	Apolipoprotein D	7, 12			
PRELP	Proline & Arginine Rich End Leucine Rich Repeat Protein	7			
ITGBL1	Integrin Subunit Beta Like 1	7			
OMD	Osteomodulin	7			
COL14A1	Collagen Type XIV Alpha 1 Chain	7			
THSD4	Thrombospondin Type 1 Domain Containing 4	7			
ABI3BP	ABI Family Member 3 Binding Protein	7			
CFD	Complement Factor D	7			
PRSS12	Serine Protease 12	12			
FABP4	Fatty Acid Binding Protein 4	12			
PODXL	Podocalyxin Like	12			
TIMP3	Tissue Inhibitor Of Metalloproteinases 3	12			
ECSCR	Endothelial Cell Surface Expressed Chemotaxis And Apoptosis Regulator	12			
SOX13	SRY-Box Transcription Factor 13	12			
PCDH18	Protocadherin 18	12			
CD200	CD200 Molecule	12			

Biological processes associated with ICT-specific DEGs were explored by gene ontology (GO) enrichment analysis. Pathways related to "B cell receptor signaling", "epidermal cell differentiation", "response to LPS", "humoral immune response" and "neutrophil chemotaxis" were found to be up-regulated in peri-implantitis specimens when compared to reference implant samples. On the contrary, pathways associated with "wound healing", "regulation of angiogenesis", "extracellular matrix organization", "connective tissue development", "collagen fibril organization" and "regulation of epithelial/endothelial cell apoptotic process" were found to be down-regulated.

Cell populations were identified by utilizing public transcriptomic datasets of pure cell types. Plasma cells and B cells were the most abundant cell types found in the ICT in both peri-implantitis and reference implant sites. Larger proportions of plasma cells, B cells, neutrophils, epithelial and endothelial cells were found in samples from peri-implantitis sites than in specimens from reference implant sites.

RNA-sequencing

Results from the RNA-sequencing analysis showed that 2878 significantly up-regulated and 2263 down-regulated genes were found when comparing peri-implantitis specimens to reference implant samples.

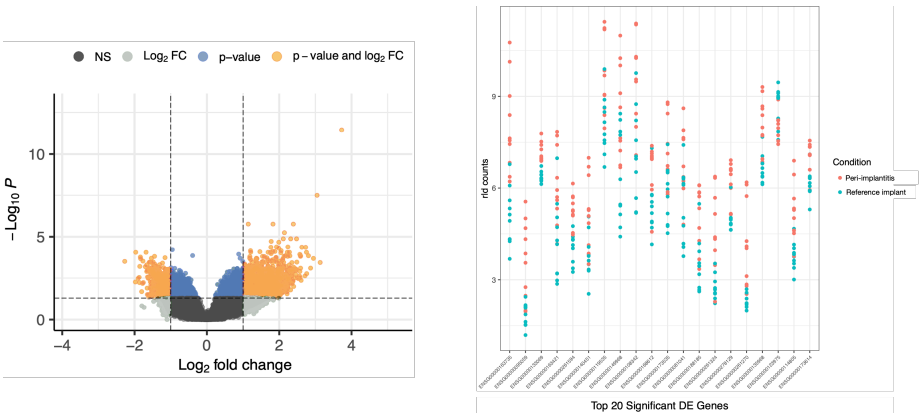

Figure 40. Volcano plot (on the left) illustrating the most dysregulated DEGs (orange color) found by using RNA-sequencing. Strip plots (on the right) illustrating the top 20 DEGs in peri-implantitis and reference implant specimens.

Table 15. The 10 most up-regulated and the 10 most down-regulated DEGs found when comparing peri-implantitis to reference implant sites by using RNA-sequencing.

Ensembl ID	Gene symbol	Genename	Log2 fold change	Adjusted *p*-value
Up-regulated genes				
ENSG00000163735	CXCL5	C-X-C motif chemokine ligand 5	3.73	3.55E-12
ENSG00000236871	LINC00106	Long intergenic non-protein coding RNA 106	3.13	0.00035
ENSG00000095059	DHPS	Deoxyhypusine synthase	3.05	3.17E-08
ENSG00000205702	-	-	2.95	0.00020
ENSG00000236529	LOC84214	Uncharacterized LOC84214	2.87	0.00077
ENSG00000291215	-	-	2.81	0.00014
ENSG00000170160	CCDC144A	Coiled-coil domain containing 144A	2.76	0.00166
ENSG00000196696	PDXDC2P-NPIPB14P	Nuclear pore complex-interacting protein	2.75	8.66E-05
ENSG00000261270	-	-	2.73	4.33E-05
ENSG00000291194	-	-	2.71	0.00232
Down-regulated genes				
ENSG00000242550	SERPINB10	Serpin family B member 10	-2.27	0.00031
ENSG00000255774	LINC02747	Long intergenic non-protein coding RNA 2747	-1.98	0.00541
ENSG00000173338	KCNK7	Potassium two pore domain channel subfamily K member 7	-1.97	8.66E-05
ENSG00000127129	EDN2	Endothelin 2	-1.90	0.00325
ENSG00000172867	KRT2	Keratin 2	-1.87	0.00278
ENSG00000082126	MPP4	Membrane palmitoylated protein 4	-1.86	0.00591
ENSG00000105048	TNNT1	Troponin T1, slow skeletal type	-1.86	0.00061
ENSG00000163331	DAPL1	Death associated protein like 1	-1.84	0.00017
ENSG00000186832	KRT16	Kratin 16	-1.83	0.00021
ENSG00000185038	MROH2A	Maestro heat like repeat family member 2A	-1.80	0.02053

Gene-set enrichment analyses were performed to explore the biological functions involved. Pathways associated with "immune response regulating-signaling", "histone modification", "activation of immune response" and "neutrophil degranulation" were found to be up-regulated in peri-implantitis samples when compared to reference implant samples.

Figure 41. Gene Ontology (GO) and Reactome enrichment analyses from RNA-sequencing data. On top: up-regulated pathways. On the bottom: down-regulated pathways.

In total, 1124 genes were found to be consistent between spatial transcriptomic and RNA-sequencing datasets. While all 1124 genes were differentially expressed (adjusted *p* values <0.05) in the spatial transcriptomic dataset, only 290 genes (25.8%) displayed significantly dysregulated levels in the RNA-sequencing dataset. The comparison of the 290 shared DEGs showed that the overall level of agreement between the two methods was high. However, RNA-sequencing showed higher levels of agreement for up-regulated genes (98%) than for down-regulated genes (66%) when compared to spatial transcriptomics.

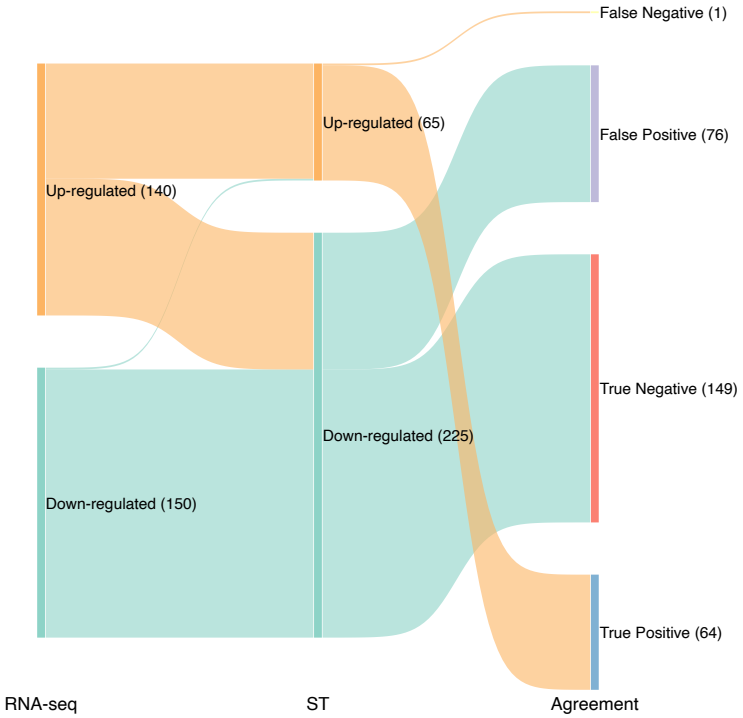

Figure 42. Alluvial plot illustrating the agreement between RNA-sequencing (RNA-seq) and spatial transcriptomics (ST) on the 290 shared DEGs. In parenthesis: number of DEGs in each category.

True positive: ST&RNA-seq up-regulated DEGs (98%).
True negative: ST&RNA-seq down-regulated DEGs (66%).
False positive: DEGs down-regulated in ST but up-regulated in RNA-seq.
False negative: DEGs up-regulated in ST but down-regulated in RNA-seq.

Main findings

Study I:

- Peri-implantitis lesions were significantly larger and presented with significantly higher densities of CD68-, MPO-, and iNOS-positive cells than periodontitis lesions.
- Cellular densities were higher in the inner zone of the lesion lateral to the pocket epithelium than in the outer compartment in both types of samples.
- The non-infiltrated connective tissue in peri-implantitis specimens comprised significantly higher densities of γ-H2AX-, NOX2-, iNOS-, MPO- and PAD4/MPO-positive cells than that in periodontitis specimens.

Study II:

- Although periodontitis lesions did not differ in size in current smokers and non-smokers, differences in cellular functions were observed.
- Periodontitis lesions in current smokers presented with significantly lower densities of DNMT1-, ACH3-, iNOS-, and NOX2-positive cells than lesions in non-smokers.

Study III:

- Volumetric densities of titanium micro-particles varied across patients but not between dental implant sites with and without peri-implantitis within the same individual.
- The titanium micro-particles had similar size and morphology and were mainly located in a 2-mm wide tissue zone close to the implant in samples with and without peri-implantitis.
- Out of >36000 analyzed genes, only 14 were differentially expressed when comparing peri-implantitis samples with high and low densities of titanium micro-particles.

Study IV:

- Peri-implantitis samples showed overall higher levels of gene activity than reference implant specimens.
- A clear association was observed between 12 distinct gene clusters and specific compartments in peri-implant tissues.
- Several pathways specific for the activation of the host response towards bacterial insults were clearly dysregulated in peri-implantitis specimens when compared to reference implant samples.

Concluding remarks

Methodological considerations

The field of biological science is characterized by a rapid and remarkable progress in laboratory techniques and software development. While advances in methods provide exceptional improvements in the precision of analysis of biological systems, the demand for enhanced and specific competences in different areas requires extensive collaboration between research teams. In the current series of studies, a methodological approach of introducing novel techniques was embraced. To achieve this goal, collaborations with research teams in University of Gothenburg and with other universities in Sweden were established.

Immunohistochemistry and image analysis

In **Studies I** & **II**, the full capacity of an image analysis software for the assessment of immunohistochemical sections was investigated. This led to a shift from conventional point-counting methods (e.g., Liljenberg et al., 1994; Zitzmann et al., 2001) to a semi-automated computer-assisted image analysis process based on the creation of specific algorithms for each applied marker. The semi-automated system was validated in Study I by comparing densities of CD68- and MPO-positive cells with findings previously obtained on the same specimens analyzed by conventional methods (Carcuac & Berglundh, 2014). In addition to a high level of agreement with results obtained from traditional methods, the computer-assisted analysis reduced operator-sensitive errors, and inconsistencies in qualitative assessment of staining intensities. The new method also provided analysis of larger regions of interest and reduced the overall time required for analysis. Similar observations were reported in a recent "proof-of-concept" study by Seyfang et al. (2022). It was reported that the computer-assisted method showed higher objectivity, repeatability levels and time efficiency than the manual point-counting procedure.

Although novel methods on cell-counting procedures were applied in Studies I and II, it should be realized that IHC evaluations are associated with limitations. Due to the cross-sectional nature of the analysis, ongoing processes or molecular productions may not be captured. Observations of dynamic changes or real-time

activities within tissues are not feasible using histological preparations of soft tissue samples obtained in humans. Therefore, temporal aspects of cellular processes cannot be assessed. Alternative techniques, such as real-time PCR or Western blotting, may analyze dynamic changes but do not provide information on the spatial localization and arrangement of cells and structures.

Differential gene expression analysis

In **Study III** we investigated the role of titanium micro-particles on the host response by integrating IHC with RNA-sequencing data. In this way, a more holistic perspective was used, as the choice of IHC markers was dictated by the evaluation of gene expression profiles of peri-implantitis lesions. At the same time, IHC served as a validation tool for gene expression, as the presence of targeted proteins in cells was evaluated.

The application of spatial transcriptomics in **Study IV** was made possible by recent advances in the method applicability (Gracia Villacampa et al., 2021) and the collaboration with the SciLife Laboratory - National Genomics Infrastructure (Karolinska Institute and Stockholm University, Sweden). While fresh-frozen specimens were the most used preparation method in the past, formalin-fixed paraffin-embedded (FFPE) sections have emerged as a novel preparation technique for spatial transcriptomics. Preliminary tests were made in collaboration with the Core Facility – Genomics (Sahlgrenska Academy, University of Gothenburg, Sweden) to ascertain the quality of total RNA content obtainable from FFPE samples. For this purpose, sections from archive FFPE specimens collected in the past were evaluated together with sections from freshly prepared FFPE samples. As expected, the RNA quality was found to be time dependent. Samples stored for 3, 2 or 1 years demonstrated DV200 values of 40-50%, 58-63% and >70%, respectively. Thus, spatial transcriptomic analysis of FFPE samples was judged as feasible and reliable if samples were collected and prepared not more than 1 year prior to analysis. Notably, the quality of the RNA content obtained in our tests was in accordance with published data investigating the quality of RNA content in FFPE samples when compared to fresh-frozen specimens (Wimmer et al., 2018, Gracia Villacampa et al., 2021).

The Visium CytAssist protocol (CG000518, 10xGenomics) was chosen in Study IV not only for the purpose of analyzing FFPE samples, but also because

sequencing-based methods are usually recommended in spatial transcriptomics for "hypothesis generating" analyses (Williams et al., 2022). The visualization of different clusters of gene expression profiles onto intact H&E-stained tissue sections represented one of the greatest advantages offered by spatial transcriptomics in Study IV. This possibility allowed us, not only to restrict our analysis to the clusters of major interest, but also to contextualize gene expression profiles in precise locations within tissues.

An analysis of the agreement levels between results from spatial transcriptomics and RNA-sequencing was also performed in Study IV. The two methods demonstrated high levels of agreement in identifying genes that were up- or down-regulated. Nevertheless, only 26% of the differentially expressed genes identified by spatial transcriptomics aligned with DEGs identified by RNA-sequencing. Variations in number of replicates, specimen size, sample preparation or library depth represent potential biological and technical factors that contributed to the observed differences. The biggest limitation of employing spatial transcriptomics and RNA-sequencing techniques resided in the substantial investment of both financial and time resources, which is reflected by the limited number of samples analyzed in Study IV.

Metal particles in biological tissue samples

In **Study III**, the question on the occurrence of titanium micro-particles in histological sections led to the development of an automated system for elemental mapping in samples up to several cm^2 in size (Nagy et al., 2022). As mentioned in the Introduction section, the selection of methods for the assessment of metal particles in tissues is of utmost importance. Micro PIXE was chosen for its high capacity and precision in detecting and localizing metal particles in intact tissue samples. In the past, one of the most frequently used technique for the analysis of metal content in peri-implant tissues was SEM-EDX (Table 3, Introduction). However, despite being a powerful tool for elemental analysis and imaging, SEM-EDX is mostly recommended for surface or "near-surface" investigations. In fact, SEM-EDX analysis, utilizing an electron beam with energy settings in the KeV range, is usually limited to a penetration depth of few micrometers (Mirani et al., 2021). In addition, biological samples analyzed by SEM-EDX require gold- or carbon-coating to avoid tissue charging. On the other hand, the 2 MeV proton beam that we used in Study III reaches a depth of approximately 64 micrometers

in biological samples (Fig. 43), resulting in a much larger penetration than the one offered by SEM-EDX (approximately 10 times more). Since the energy of the PIXE beam decreases while it penetrates into the specimen, a sample preparation with a maximum thickness of 50 micrometers was preferred in Study III.

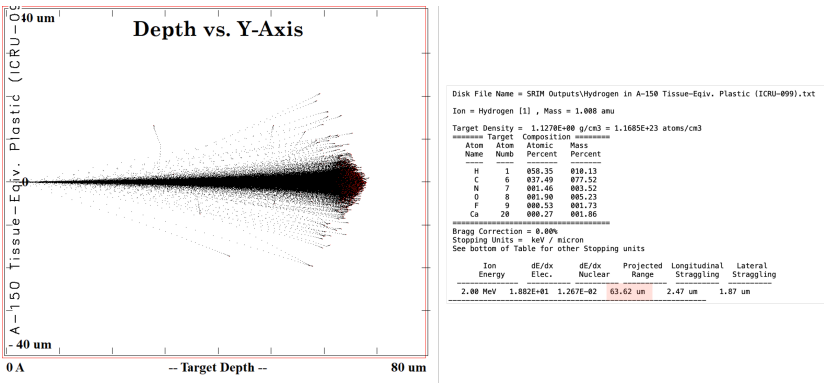

Figure 43. SRIM (Stopping and Range of Ions in Matter) simulation of a 2 MeV proton beam penetrating into the A-150 tissue equivalent plastic. The penetration depth is shown in the table, called "projected range" (highlighted in red).

It has to be remarked that other techniques might provide greater spatial resolution or penetration depth compared to μ-PIXE. For example, the spatial resolution achievable with synchrotron radiation allows the analysis of particles down to the nano-size scale (Nelson et al., 2020). The decision to adopt μ-PIXE in Study III was ultimately guided by considerations of both temporal and financial constraints, as a total of 39 samples (36 from peri-implant sites and 3 negative controls from periodontitis specimens) needed to be analyzed in their entirety.

It could be argued that other metals may occur in peri-implant tissues, as modern dental implants are not made only of commercially pure titanium (CP-Ti). The two most frequently used alloys in dental implants are Ti-6Al-4V and Ti-6Al-7Nb, which contain 6% aluminum together with either 4% vanadium or 7% niobium (Brunette et al., 2001). Taken together, 88–99.5% nominal weight of the dental implant composition is still made of titanium. The focus of our analysis was therefore to localize, characterize and quantify titanium micro-particles in peri-implant tissues.

Transmission electron microscopy (TEM) was used in Study III to evaluate the localization of metal-like particles at the single-cell level. Although TEM is a powerful technique for studying structures at a nanometer-scale resolution, very thin samples (70-nm-thick) are required (Nagashima et al., 2011). The likelihood of identifying metal particles within sections is thereby limited. In addition, TEM is primarily a morphological and ultra-structural imaging system and does not provide valuable information on the chemical composition of the particles. For these reasons, a very small number of metal-like particles was observed in the sections analyzed by TEM and only a descriptive characterization of the tissues was performed.

Findings

Periodontitis and peri-implantitis lesions

In **Study I** it was demonstrated that the ICT of peri-implantitis specimens contained significantly larger densities of macrophages (CD68), neutrophils (MPO) and iNOS-positive cells than the ICT of periodontitis samples. These results were in agreement with findings from other studies that compared human peri-implantitis and periodontitis lesions (Galindo-Moreno et al., 2017; Ghighi et al., 2018; Fretwurst et al., 2020).

In addition, the NCT area in peri-implantitis comprised significantly larger densities of γ-H2AX-, NOX2-, MPO-, iNOS-, and MPO/PAD4-positive cells when compared to periodontitis. By definition, the NCT area was selected as a reference region that was clearly separated from the ICT. A reverse difference was found for the cellular densities of 8-OHdG-positive cells that were significantly more expressed in the PE of periodontitis than peri-implantitis sites. These findings were in contrast with data presented by Kasnak et al. (2018) who reported on similar levels of 8-OHdG-positive cells in peri-implantitis and periodontitis specimens. The difference between our results and those presented by Kasnak et al. (2018) may be explained by the fact that we quantified the expression of cellular markers in the entirety of the regions of interest and not only in smaller selected areas, as done by Kasnak and co-workers.

A gradient-like distribution of the inflammatory infiltrate in the ICT towards the pocket area was also noted, with overall higher cellular densities in the inner ICT zone lateral of the PE (ICT- 1) than in the outer, deeply located ICT compartment (ICT-2).

Taken together, peri-implantitis lesions demonstrated elevated densities of inflammatory markers in the NCT, higher densities of CD68-, MPO- and iNOS-positive cells in the ICT, and decreased levels of 8-OHdG-positive cells in the PE compared to periodontitis sites. These findings further corroborate previous observations on the destructive nature of lesions in peri-implantitis when compared to those in periodontitis. These results were partly explained by enhanced secretions of antimicrobial enzymes in the uncovered apical portion of the ICT that faced the biofilm-coated implant surface.

Periodontitis lesions in smokers and non-smokers

In **Study II** it was demonstrated that, although the ICT of smokers and non-smokers did not differ in size, current smokers presented with significantly lower densities of DNMT1- and AcH3-positive cells. On the other hand, evaluations of markers for DNA damage (γ-H2AX), oxidative stress (8-OHdG), DNA de-methylation (TET2) and histone deacetylation (HDAC1/HDAC2) did not show any difference between the two groups.

The observation of decreased DNA-methylation levels (DNMT1-positive cells) in smokers with periodontitis was in accordance with data from other studies that investigated periodontitis samples from smokers and non-smokers (Richter et al., 2019; Cho et al., 2017). The results on cellular densities of γ-H2AX- and 8-OHdG-positive cells indicated that oxidative stress is a typical characteristic of periodontal inflammation, irrespective of the smoking status of the patient. This finding was in agreement with results from another study that compared salivary 8-OHdG levels in smokers and non-smokers with periodontitis (Hendek et al., 2015). While both groups of patients demonstrated a significant reduction in salivary levels of the marker after non-surgical periodontal therapy, no differences were observed between smokers and non-smokers at any time point.

Another interesting finding in Study II was that periodontitis lesions of smokers exhibited a suppressed antimicrobial capacity when compared to periodontitis lesions of non-smokers, as indicated by the lower densities of iNOS- and NOX2-positive cells. This observation seems to be partly in contrast with data presented in another study on healthy gingival and gingivitis samples (Ozdemir et al., 2016). It was reported that smokers presented with higher levels of iNOS-positive cells when compared to non-smokers. The difference between studies may be explained by the variation in tissue samples under exam.

Thus, taken together, Study II demonstrated that tobacco smoking induces an impairment of important components of the host response in periodontitis lesions.

Titanium particles in peri-implant tissues

In **Study III** it was demonstrated that titanium micro-particles were consistent findings in soft tissues surrounding dental implants. The density of titanium micro-particles varied between patients but not between samples obtained from diseased and reference peri-implant tissues in the same subject. The majority of titanium micro-particles were located in a 2-mm wide tissue portion from the implant/tissue interface, while a gradual decrease in density of micro-particles was observed in the deeper portions (>2 mm) of the samples. In addition, while most of the micro-particles displayed a circular-like appearance with diameters smaller than 15 micrometers, shape and size of titanium micro-particles did not differ between peri-implantitis and reference implant sites.

Comparable results were shown in a study utilizing synchrotron radiation to analyze severe peri-implantitis specimens collected in proximity to titanium or ceramic dental implants planned for explantation (Nelson et al., 2020). It was demonstrated that all samples collected in proximity to titanium implants consistently showed presence of titanium particles and that the density of particles varied considerably among patients. Notably, the densities of titanium particles reported in the study from Nelson et al. was much larger (magnitude of millions of particles per mm^3) than the one found in our study. Two possible explanations can justify such discrepancy in observed densities. First of all, the mathematical calculations used to infer particle densities is strongly influenced by the thickness of the sections under exam. In the study from Nelson and coworkers 5-μm-thick sections were analyzed, while in our study we preferred to analyze sections with a thickness of approximately 30 micrometers. On the other hand, the detection limit of synchrotron radiation is higher than the one offered by μ-PIXE, as particles in the micro- and nano-scale size can be identified by the former technique. Another study used SEM-EDX to analyze 36 tissue sections obtained from peri-implantitis sites (Wilson et al., 2015). Titanium particles were identified only in 7 samples and no quantitative data on occurrence of particles was reported. These findings corroborate the concept that SEM-EDX is a technique mostly recommended for "near-surface" analysis and, thus, is limited in detecting metal particles within tissue sections.

Another interesting finding in Study III was that "implant system" was the only implant-related characteristic that influenced the density of titanium micro-particles. This observation, however, must be interpreted with care. First of all,

the number of samples analyzed in Study III was limited and, thus, an uneven distribution of implant systems was found. In addition, the terminology "implant system" is not restricted to implant geometry and surface characteristics, but also reflects the protocols by which the implants are surgically installed. Not only a similar occurrence of titanium micro-particles was found in peri-implant samples with or without peri-implantitis, but also time in function of the implants did not influence the density of titanium micro-particles. These observations indicate that the micro-particles observed in Study III most probably derived from the friction between the bony wall and the dental implant that occurred during the installation procedure. Nevertheless, it must be realized that our analysis on human biopsies, based on a set of 18 paired samples, was not intended to delve deeply into specific characteristics and nuances of different implant systems. Experimental pre-clinical models are often more suitable to explore such differences. Thus, the exploration of what underlies variations in release of titanium micro-particles among different implants hold promise to future investigations.

Our research revealed a final interesting finding: the release of titanium micro-particles did not appear to impact the host response. As mentioned in the Introduction section, this topic has been extensively debated in the past (Mombelli et al., 2018; Ivanovski et al., 2022), but the majority of the available evidence derives from *in vitro* observations. In our analysis, not only paired samples from peri-implantitis and reference implant sites showed similar densities of titanium micro-particles, but also a minority of differentially expressed genes were observed when comparing tissue samples containing high and low densities of titanium micro-particles.

Taken together, results of Study III indicate that titanium micro-particles appear not to be a specific characteristic for peri-implantitis but rather an occurrence in peri-implant tissues in general.

Gene-expression profiles in peri-implant lesions

In **Study IV**, the spatial transcriptomic analysis revealed a clear association between distinct gene clusters and specific compartments in peri-implant tissues. Among the 1435 differentially expressed genes found in the 4 clusters that were specific for ICT areas, genes CHI3L1, IGL7, CXCL13, MMP3 and MMP1 were the most up-regulated in peri-implantitis tissues when compared to reference implant samples.

The strategy of using paired specimens obtained from the same patients served the purpose of reducing biological and technical variability among samples. The same strategy was employed by another recent study that utilized RNA-sequencing and RT-qPCR to compare samples obtained from peri-implantitis, periodontitis and healthy gingival tissues (Oh et al. 2023). The authors identified a total of 916 genes that were dysregulated in both diseased sites when compared to healthy controls (757 up-regulated and 159 down-regulated). Interestingly, several of the shared up-regulated genes between peri-implantitis and periodontitis sites (such as CXCL3, OSM, MEFV, A2M, MMP9, MMP13, TH1 and ICAM1) showed a greater increase in peri-implantitis samples than in periodontitis specimens and were correlated with the degree of inflammation found in tissues. In the study by Oh and coworkers (Oh et al., 2023), the gene-set enrichment analysis revealed that the two conditions showed similar molecular and biological pathways. However, the genes that were dysregulated only in peri-implantitis were mainly related to "receptor binding" and "signaling receptor" pathways.

In our study comparing peri-implant sites with and without peri-implantitis, Gene Ontology and Reactome enrichment analyses showed that the up-regulated genes in peri-implantitis were mainly associated with biological pathways specific for the activation of the host response, such as "B cell receptor signaling", "response to LPS", "humoral immune response" and "neutrophil chemotaxis".

Another study on transcriptome data (Kheder et al., 2023) reported that genes IL1B, CDK3, IL27 and CD86 were up-regulated in sites with severe peri-implantitis (termed "failed implants") as opposed to healthy gingival tissues at teeth. As no comparisons were made on gene expression profiles between peri-implantitis and reference implant sites, a direct comparison of the results presented in the study by Kheder et al. (2023) with data reported in Study IV is

not possible. Nevertheless, it is worth mentioning that, when evaluating inflammatory responses, an assessment of comparable samples is usually recommended. As such, the rationale of comparing inflamed peri-implant sites with healthy tissues around teeth is not fully understood.

The identification of cell populations reported in Study IV showed that plasma cells and B cells were the most representative cell types in the ICT of peri-implantitis lesions. In addition, larger proportions of plasma cells, B cells, neutrophils, epithelial and endothelial cells were noted in peri-implantitis sites than in specimens from reference implant sites. These results are, overall, strongly in agreement with findings from Study I and from previous IHC reports where peri-implantitis lesions consistently demonstrated larger proportions of inflammatory cells when compared to tissue samples representing peri-implant mucositis, healthy peri-implant tissues or periodontitis (Gualini & Berglundh, 2003; Bullon et al., 2004; Konttinen et al., 2006; Carcuac & Berglundh, 2014; Galindo-Moreno et al., 2017; Ghighi et al., 2018; Kasnak et al., 2018; Karatas et al., 2020; Fretwurst et al., 2020).

Interestingly, two of the most up-regulated genes found by spatial transcriptomics and RNA-sequencing in Study IV were CXCL13 and CXCL5, respectively. The CXCL13 gene is defined as "B lymphocyte chemoattractant" and plays a role in B cell activation and organization (Nakajima et al., 2008). The CXCL5 gene is also known as "epithelial-derived neutrophil-activating peptide 78" and participates in the regulation of neutrophil chemotaxis and in the activation of angiogenesis processes (Barros & Offenbacher, 2014). In the study from Nakajima and coworkers (2008), gingival biopsies from patients with periodontitis and gingivitis were analyzed. It was found that densities of CXCL13-positive cells were significantly higher in periodontitis than in gingivitis specimens.

In regard to the down-regulated DEGs found in Study IV when comparing peri-implantitis with reference implant sites, several genes were associated with keratin-encoding genes. Thus, pathways related to "wound healing", "regulation of angiogenesis", "extra-cellular matrix organization" and "collagen fibril organization" were down-regulated in peri-implantitis. These findings are explained by observations of exacerbated levels of tissue degradation found in peri-implantitis lesions, as reflected by the up-regulation of the MMP3 and MMP1 genes found in the ICT-specific clusters. In addition, there is robust evidence showing that the apical portion of the ICT in peri-implantitis lesions usually lacks

an epithelial lining and is left in direct contact with the bacterial biofilm residing on the implant surface (Lindhe et al., 1992; Carcuac et al., 2013, Carcuac & Berglundh 2014). In addition, similar results were observed in a study comparing soft tissue biopsies from patients with or without periodontitis (Kim et al., 2016). The transcriptome analysis revealed that KRT1, KRT2 and KRT27 were three of the most down-regulated genes in diseased gingival tissues. Lastly, immune cells, fibroblasts, and endothelial cells were reported to express keratin genes as a host defense mechanism in inflammation (Traweek et al., 1993; Katagata et al., 2002).

Taken together, the results of Study IV indicate that several biological pathways specific for the activation of the host response towards bacterial insults are clearly dysregulated in peri-implantitis when compared to reference implant sites.

Future studies might be able to reveal the intricate mechanisms that drive disease manifestation and susceptibility among individuals by incorporating complex data from oral microbiome analyses with findings from refined analyses (possibly at the single-cell level) of soft tissues biopsies collected in peri-implantitis sites in humans.

Acknowledgements

The studies included in this thesis were supported by grants from the Swedish Research Council (Vetenskapsrådet, Grant Number: 2016-0157) and the TUA research funding (TUAGBG-979431).

The Foundation Blanceflor Boncompagni Ludovisi, née Bildt (Stockholm, Sweden) provided funding for travel expenses to Uppsala University for conducting Study III.

Illustrations in this thesis were created with BioRender.com.
(Agreement numbers: OQ25ZGEALU, WU25ZGEKN3, BM25ZGEP19, EV25ZGERWR, XZ25ZGEVOA).

The author acknowledges:

- Gyula Nagy, Daniel Primetzhofer from the Tandem Laboratory, Department of Nuclear Physics, Uppsala University, for the access to the ion irradiation equipment and for the assistance with PIXE measurements and data analysis.
- Massimo Micaroni and the Centre for Cellular Imaging at the University of Gothenburg and the National Microscopy Infrastructure, NMI (VR-RFI 2019-00217), for the assistance with transmission electron microscopy, sample preparation and image analysis.
- Heidur Loftsdóttir, Catarina Mörck from the NGS team and the Genomics Core Facility platform at the Sahlgrenska University Hospital, for the assistance with RNA-sequencing library preparation.
- Sanna Abrahamsson, Alina Orozco from the Core Facility Bioinformatics at the University of Gothenburg, for the assistance with RNA-sequencing and spatial transcriptomic data analysis.
- The National Genomics Infrastructure in Stockholm funded by Science for Life Laboratory, the Knut and Alice Wallenberg Foundation and the Swedish Research Council, and SNIC/Uppsala Multidisciplinary Center for Advanced Computational Science, for the assistance with massively parallel sequencing and the access to the UPPMAX computational infrastructure.

My sincere and personal gratitude goes to:

- Asal Shikhan and Anna-Carin Ericson at the Department of Periodontology, University of Gothenburg, for the immunohistochemical preparation of all samples analyzed in the current thesis.

- Karolina Karlsson, Maria Welander and all the staff at the Specialist Clinic of Periodontics, Public Dental Services, Region Västra Götaland, for their contribution in collecting soft tissue biopsies for Studies III & IV.
- Yuki Ichioka, Ahmed Almohandes and Olivier Carcuac for their priceless example and encouragement during the realization of the studies in this thesis.
- Jan Derks at the Department of Periodontology, University of Gothenburg for his constant support in all moments of my PhD program.
- My co-supervisors Lena Larsson, Cristiano Tomasi and Ingemar Abrahamsson for their important contributions and constructive discussions.

The most significant appreciation and gratitude are reserved to my main supervisor Tord Berglundh. Your constant mentorship has been truly invaluable throughout this journey.

A final message to my family: you are my inspiration, my strength, my shield and my biggest support system. I hope to always make you proud.

References

Abrahamsson, I., Berglundh, T., & Lindhe, J. (1998). Soft tissue response to plaque formation at different implant systems. A comparative study in the dog. *Clin Oral Implants Res*, *9*(2), 73-79. https://doi.org/10.1034/j.1600-0501.1998.090202.x

Apaza-Bedoya, K., Tarce, M., Benfatti, C. A. M., Henriques, B., Mathew, M. T., Teughels, W., & Souza, J. C. M. (2017). Synergistic interactions between corrosion and wear at titanium-based dental implant connections: A scoping review. *J Periodontal Res*, *52*(6), 946-954. https://doi.org/10.1111/jre.12469

Arys, A., Philippart, C., Dourov, N., He, Y., Le, Q. T., & Pireaux, J. J. (1998). Analysis of titanium dental implants after failure of osseointegration: Combined histological, electron microscopy, and X-ray photoelectron spectroscopy approach. *Journal of Biomedical Materials Research*, *43*(3), 300-312. https://doi.org/10.1002/(sici)1097-4636(199823)43:3<300::Aid-jbm11>3.0.Co;2-j

Asri, R. I. M., Harun, W. S. W., Samykano, M., Lah, N. A. C., Ghani, S. A. C., Tarlochan, F., & Raza, M. R. (2017). Corrosion and surface modification on biocompatible metals: A review. *Mater Sci Eng C Mater Biol Appl*, *77*, 1261-1274. https://doi.org/10.1016/j.msec.2017.04.102

Barros, S. P., & Offenbacher, S. (2014). Modifiable risk factors in periodontal disease: epigenetic regulation of gene expression in the inflammatory response. *Periodontol 2000*, *64*(1), 95-110. https://doi.org/10.1111/prd.12000

Bastos, M. F., de Franco, L., Garcia Tebar, A. C., Giro, G., & Shibli, J. A. (2018). Expression Levels of Semaphorins 3A, 3B, 4A, and 4D on Human Peri-implantitis. *Int J Oral Maxillofac Implants*, *33*(3), 565-570. https://doi.org/10.11607/jomi.6238

Becker, S. T., Beck-Broichsitter, B. E., Graetz, C., Dorfer, C. E., Wiltfang, J., & Hasler, R. (2014). Peri-implantitis versus periodontitis: functional differences indicated by transcriptome profiling. *Clin Implant Dent Relat Res*, *16*(3), 401-411. https://doi.org/10.1111/cid.12001

Berglundh, T., Armitage, G., Araujo, M. G., Avila-Ortiz, G., Blanco, J., Camargo, P. M., Chen, S., Cochran, D., Derks, J., Figuero, E., Hammerle, C. H. F., Heitz-Mayfield, L. J. A., Huynh-Ba, G., Iacono, V., Koo, K. T., Lambert, F., McCauley, L., Quirynen, M., Renvert, S., . . . Zitzmann, N. (2018). Peri-implant diseases and conditions: Consensus report of workgroup 4 of the 2017 World Workshop on the Classification of Periodontal and Peri-Implant Diseases and Conditions. *J Clin Periodontol*, *45 Suppl 20*, S286-S291. https://doi.org/10.1111/jcpe.12957

Berglundh, T., Gislason, O., Lekholm, U., Sennerby, L., & Lindhe, J. (2004). Histopathological observations of human periimplantitis lesions. *J Clin Periodontol*, *31*(5), 341-347. https://doi.org/10.1111/j.1600-051X.2004.00486.x

Berglundh, T., Lindhe, J., Ericsson, I., Marinello, C. P., Liljenberg, B., & Thomsen, P. (1991). The soft tissue barrier at implants and teeth. *Clin Oral Implants Res*, *2*(2), 81-90. https://doi.org/10.1034/j.1600-0501.1991.020206.x

Berglundh, T., Lindhe, J., Marinello, C., Ericsson, I., & Liljenberg, B. (1992). Soft tissue reaction to de novo plaque formation on implants and teeth. An experimental study in the dog. *Clin Oral Implants Res*, *3*(1), 1-8. https://doi.org/10.1034/j.1600-0501.1992.030101.x

Borsani, E., Salgarello, S., Mensi, M., Boninsegna, R., Stacchiotti, A., Rezzani, R., Sapelli, P., Bianchi, R., & Rodella, L. F. (2005). Histochemical and immunohistochemical evaluation of gingival collagen and metalloproteinases in peri-implantitis. *Acta Histochem*, *107*(3), 231-240. https://doi.org/10.1016/j.acthis.2005.06.002

Breitling, L. P., Yang, R., Korn, B., Burwinkel, B., & Brenner, H. (2011). Tobacco-smoking-related differential DNA methylation: 27K discovery and replication. *Am J Hum Genet*, *88*(4), 450-457. https://doi.org/10.1016/j.ajhg.2011.03.003

Brunette, D. M., Tengvall, P., Textor, M., & Thomsen, P. (2001). *Titanium in medicine: material science, surface science, engineering, biological responses and medical applications*. Berlin: Springer.

Buffoli, B., Dalessandri, M., Favero, G., Mensi, M., Dalessandri, D., Di Rosario, F., Stacchi, C., Rezzani, R., Salgarello, S., & Rodella, L. F. (2014). AQP1 expression in human gingiva and its correlation with periodontal and peri-implant tissue alterations. *Acta Histochem*, *116*(5), 898-904. https://doi.org/10.1016/j.acthis.2014.02.010

Bullon, P., Fioroni, M., Goteri, G., Rubini, C., & Battino, M. (2004). Immunohistochemical analysis of soft tissues in implants with healthy and peri-implantitis condition, and aggressive periodontitis. *Clin Oral Implants Res*, *15*(5), 553-559. https://doi.org/10.1111/j.1600-0501.2004.01072.x

Carcuac, O., Abrahamsson, I., Albouy, J. P., Linder, E., Larsson, L., & Berglundh, T. (2013). Experimental periodontitis and peri-implantitis in dogs. *Clin Oral Implants Res*, *24*(4), 363-371. https://doi.org/10.1111/clr.12067

Carcuac, O., & Berglundh, T. (2014). Composition of human peri-implantitis and periodontitis lesions. *J Dent Res*, *93*(11), 1083-1088. https://doi.org/10.1177/0022034514551754

Caton, J. G., Armitage, G., Berglundh, T., Chapple, I. L. C., Jepsen, S., Kornman, K. S., Mealey, B. L., Papapanou, P. N., Sanz, M., & Tonetti, M. S. (2018). A new classification scheme for periodontal and peri-implant diseases and conditions - Introduction and key changes from the 1999 classification. *J Clin Periodontol*, *45 Suppl 20*, S1-S8. https://doi.org/10.1111/jcpe.12935

Cesar-Neto, J. B., Duarte, P. M., de Oliveira, M. C., Casati, M. Z., Tambeli, C. H., Parada, C. A., Sallum, E. A., & Nociti, F. H., Jr. (2006). Smoking modulates interferon-gamma expression in the gingival tissue of patients with chronic periodontitis. *Eur J Oral Sci*, *114*(5), 403-408. https://doi.org/10.1111/j.1600-0722.2006.00397.x

Cesar-Neto, J. B., Duarte, P. M., de Oliveira, M. C., Tambeli, C. H., Sallum, E. A., & Nociti, F. H., Jr. (2007). Smoking modulates interleukin-6:interleukin-10 and RANKL:osteoprotegerin ratios in the periodontal tissues. *J Periodontal Res*, *42*(2), 184-191. https://doi.org/10.1111/j.1600-0765.2006.00934.x

Chapple, I. L. C., Mealey, B. L., Van Dyke, T. E., Bartold, P. M., Dommisch, H., Eickholz, P., Geisinger, M. L., Genco, R. J., Glogauer, M., Goldstein, M., Griffin, T. J., Holmstrup, P., Johnson, G. K., Kapila, Y., Lang, N. P., Meyle, J., Murakami, S., Plemons, J., Romito, G. A., . . . Yoshie, H. (2018). Periodontal health and gingival diseases and conditions on an intact and a reduced periodontium: Consensus report of workgroup 1 of the 2017 World Workshop on the Classification of Periodontal and Peri-Implant Diseases and Conditions. *J Periodontol*, *89 Suppl 1*, S74-S84. https://doi.org/10.1002/JPER.17-0719

Cho, Y. D., Kim, P. J., Kim, H. G., Seol, Y. J., Lee, Y. M., Ku, Y., Rhyu, I. C., & Ryoo, H. M. (2017). Transcriptomics and methylomics in chronic periodontitis with tobacco use: a pilot study. *Clin Epigenetics*, *9*, 81. https://doi.org/10.1186/s13148-017-0381-z

Cho, Y. D., Kim, P. J., Kim, H. G., Seol, Y. J., Lee, Y. M., Ryoo, H. M., & Ku, Y. (2020). Transcriptome and methylome analysis of periodontitis and peri-implantitis with tobacco use. *Gene*, *727*, 144258. https://doi.org/10.1016/j.gene.2019.144258

Cornelini, R., Artese, L., Rubini, C., Fioroni, M., Ferrero, G., Santinelli, A., & Piattelli, A. (2001). Vascular endothelial growth factor and microvessel density around healthy and failing dental implants. *Int J Oral Maxillofac Implants*, *16*(3), 389-393. https://www.ncbi.nlm.nih.gov/pubmed/11432658

Daubert, D., Lee, E., Botto, A., Eftekhar, M., Palaiologou, A., & Kotsakis, G. A. (2023). Assessment of titanium release following non-surgical peri-implantitis treatment: A randomized clinical trial. *J Periodontol*, *94*(9), 1122-1132. https://doi.org/10.1002/JPER.22-0716

Daubert, D. M., Pozhitkov, A. E., Safioti, L. M., & Kotsakis, G. A. (2019). Association of Global DNA Methylation to Titanium and Peri-Implantitis: A Case-Control Study. *JDR Clin Trans Res*, *4*(3), 284-291. https://doi.org/10.1177/2380084418822831

de Araujo, M. F., Etchebehere, R. M., de Melo, M. L. R., Beghini, M., Severino, V. O., de Castro Cobo, E., Rocha Rodrigues, D. B., & de Lima Pereira, S. A. (2017). Analysis of CD15, CD57 and HIF-1alpha in biopsies of patients with peri-implantitis. *Pathol Res Pract*, *213*(9), 1097-1101. https://doi.org/10.1016/j.prp.2017.07.020

de Araujo, M. F., Filho, A. F., da Silva, G. P., de Melo, M. L., Napimoga, M. H., Rodrigues, D. B., Alves, P. M., & de Lima Pereira, S. A. (2014). Evaluation of peri-implant mucosa: clinical, histopathological and immunological aspects. *Arch Oral Biol*, *59*(5), 470-478. https://doi.org/10.1016/j.archoralbio.2014.01.011

De Oliveira, N. F., Andia, D. C., Planello, A. C., Pasetto, S., Marques, M. R., Nociti, F. H., Jr., Line, S. R., & De Souza, A. P. (2011). TLR2 and TLR4 gene promoter methylation status during chronic periodontitis. *J Clin Periodontol*, *38*(11), 975-983. https://doi.org/10.1111/j.1600-051X.2011.01765.x

Derks, J., Schaller, D., Hakansson, J., Wennstrom, J. L., Tomasi, C., & Berglundh, T. (2016). Peri-implantitis - onset and pattern of progression. *J Clin Periodontol*, *43*(4), 383-388. https://doi.org/10.1111/jcpe.12535

Duarte, P. M., de Mendonca, A. C., Maximo, M. B., Santos, V. R., Bastos, M. F., & Nociti Junior, F. H. (2009). Differential cytokine expressions affect the severity of peri-implant disease. *Clin Oral Implants Res*, *20*(5), 514-520. https://doi.org/10.1111/j.1600-0501.2008.01680.x

Feinberg, A. P. (2007). Phenotypic plasticity and the epigenetics of human disease. *Nature*, *447*(7143), 433-440. https://doi.org/10.1038/nature05919

Figueiredo, L. C., Bueno-Silva, B., Nogueira, C. F. P., Valadares, L. C., Garcia, K. M. M., Filho, G., Milanello, L., Esteves, F. M., Shibli, J. A., & Miranda, T. S. (2020). Levels of Gene Expression of Immunological Biomarkers in Peri-Implant and Periodontal Tissues. *Int J Environ Res Public Health*, *17*(23). https://doi.org/10.3390/ijerph17239100

Flatebo, R. S., Johannessen, A. C., Gronningsaeter, A. G., Boe, O. E., Gjerdet, N. R., Grung, B., & Leknes, K. N. (2006). Host response to titanium dental implant placement evaluated in a human oral model. *J Periodontol*, *77*(7), 1201-1210. https://doi.org/10.1902/jop.2006.050406

Franchi, M., Bacchelli, B., Martini, D., Pasquale, V. D., Orsini, E., Ottani, V., Fini, M., Giavaresi, G., Giardino, R., & Ruggeri, A. (2004). Early detachment of titanium particles from various different surfaces of endosseous dental implants. *Biomaterials*, *25*(12), 2239-2246. https://doi.org/10.1016/j.biomaterials.2003.09.017

Fransson, C., Tomasi, C., Pikner, S. S., Grondahl, K., Wennstrom, J. L., Leyland, A. H., & Berglundh, T. (2010). Severity and pattern of peri-implantitis-associated bone loss. *J Clin Periodontol*, *37*(5), 442-448. https://doi.org/10.1111/j.1600-051X.2010.01537.x

Fretwurst, T., Buzanich, G., Nahles, S., Woelber, J. P., Riesemeier, H., & Nelson, K. (2016). Metal elements in tissue with dental peri-implantitis: a pilot study. *Clin Oral Implants Res*, *27*(9), 1178-1186. https://doi.org/10.1111/clr.12718

Fretwurst, T., Garaicoa-Pazmino, C., Nelson, K., Giannobile, W. V., Squarize, C. H., Larsson, L., & Castilho, R. M. (2020). Characterization of macrophages infiltrating peri-implantitis lesions. *Clin Oral Implants Res*, *31*(3), 274-281. https://doi.org/10.1111/clr.13568

Galindo-Moreno, P., López-Martínez, J., Caba-Molina, M., Ríos-Pelegrina, R., Torrecillas-Martínez, L., Monje, A., Mesa, F., Chueca, N., García-García, F., & O'Valle, F. (2017). Morphological and immunophenotypical differences between chronic periodontitis and peri-implantitis - a cross-sectional study. *Eur J Oral Implantol*, *10*(4), 453-463.

Ghighi, M., Llorens, A., Baroukh, B., Chaussain, C., Bouchard, P., & Gosset, M. (2018). Differences between inflammatory and catabolic mediators of peri-implantitis and periodontitis lesions following initial mechanical therapy: An exploratory study. *J Periodontal Res*, *53*(1), 29-39. https://doi.org/10.1111/jre.12483

Giro, G., Tebar, A., Franco, L., Racy, D., Bastos, M. F., & Shibli, J. A. (2021). Treg and TH17 link to immune response in individuals with peri-implantitis: a preliminary report. *Clin Oral Investig*, *25*(3), 1291-1297. https://doi.org/10.1007/s00784-020-03435-w

Goncalves, R. B., Coletta, R. D., Silverio, K. G., Benevides, L., Casati, M. Z., da Silva, J. S., & Nociti, F. H., Jr. (2011). Impact of smoking on inflammation: overview of molecular mechanisms. *Inflamm Res*, *60*(5), 409-424. https://doi.org/10.1007/s00011-011-0308-7

Gracia Villacampa, E., Larsson, L., Mirzazadeh, R., Kvastad, L., Andersson, A., Mollbrink, A., Kokaraki, G., Monteil, V., Schultz, N., Appelberg, K. S., Montserrat, N., Zhang, H., Penninger, J. M., Miesbach, W., Mirazimi, A., Carlson, J., & Lundeberg, J. (2021). Genome-wide spatial expression profiling in formalin-fixed tissues. *Cell Genom*, *1*(3), 100065. https://doi.org/10.1016/j.xgen.2021.100065

Gualini, F., & Berglundh, T. (2003). Immunohistochemical characteristics of inflammatory lesions at implants. *J Clin Periodontol*, *30*(1), 14-18. https://doi.org/10.1034/j.1600-051x.2003.300103.x

Gultekin, S. E., Senguven, B., & Karaduman, B. (2008). The effect of smoking on epithelial proliferation in healthy and periodontally diseased marginal gingival epithelium. *J Periodontol*, *79*(8), 1444-1450. https://doi.org/10.1902/jop.2008.070645

Hajishengallis, G., Chavakis, T., & Lambris, J. D. (2020). Current understanding of periodontal disease pathogenesis and targets for host-modulation therapy. *Periodontol 2000*, *84*(1), 14-34. https://doi.org/10.1111/prd.12331

He, X., Reichl, F. X., Wang, Y., Michalke, B., Milz, S., Yang, Y., Stolper, P., Lindemaier, G., Graw, M., Hickel, R., & Hogg, C. (2016). Analysis of titanium and other metals in human jawbones with dental implants - A case series study. *Dent Mater*, *32*(8), 1042-1051. https://doi.org/10.1016/j.dental.2016.05.012

Heitz-Mayfield, L. J. A., & Salvi, G. E. (2018). Peri-implant mucositis. *J Clin Periodontol*, *45 Suppl 20*, S237-S245. https://doi.org/10.1111/jcpe.12953

Hendek, M. K., Erdemir, E. O., Kisa, U., & Ozcan, G. (2015). Effect of initial periodontal therapy on oxidative stress markers in gingival crevicular fluid, saliva, and serum in smokers and non-smokers with chronic periodontitis. *J Periodontol*, *86*(2), 273-282. https://doi.org/10.1902/jop.2014.140338

Herrera, D., Sanz, M., Kebschull, M., Jepsen, S., Sculean, A., Berglundh, T., Papapanou, P. N., Chapple, I., Tonetti, M. S., Participants, E. F. P. W., & Methodological, C. (2022). Treatment of stage IV periodontitis: The EFP S3 level clinical practice guideline. *J Clin Periodontol*, *49 Suppl 24*, 4-71. https://doi.org/10.1111/jcpe.13639

Ivanovski, S., Bartold, P. M., & Huang, Y. S. (2022). The role of foreign body response in peri-implantitis: What is the evidence? *Periodontol 2000*, *90*(1), 176-185. https://doi.org/10.1111/prd.12456

Jepsen, S., Berglundh, T., Genco, R., Aass, A. M., Demirel, K., Derks, J., Figuero, E., Giovannoli, J. L., Goldstein, M., Lambert, F., Ortiz-Vigon, A., Polyzois, I., Salvi, G. E., Schwarz, F., Serino, G., Tomasi, C., & Zitzmann, N. U. (2015). Primary prevention of peri-implantitis: managing peri-implant mucositis. *J Clin Periodontol*, *42 Suppl 16*, S152-157. https://doi.org/10.1111/jcpe.12369

Jiang, L., Wang, M., Lin, S., Jian, R., Li, X., Chan, J., Dong, G., Fang, H., Robinson, A. E., Consortium, G. T., & Snyder, M. P. (2020). A Quantitative Proteome Map of the Human Body. *Cell*, *183*(1), 269-283 e219. https://doi.org/10.1016/j.cell.2020.08.036

Johnson, G. K., & Guthmiller, J. M. (2007). The impact of cigarette smoking on periodontal disease and treatment. *Periodontol 2000*, *44*, 178-194. https://doi.org/10.1111/j.1600-0757.2007.00212.x

Jung, R. E., Zembic, A., Pjetursson, B. E., Zwahlen, M., & Thoma, D. S. (2012). Systematic review of the survival rate and the incidence of biological, technical, and aesthetic complications of single crowns on implants reported in longitudinal studies with a mean follow-up of 5 years. *Clin Oral Implants Res*, *23 Suppl 6*, 2-21. https://doi.org/10.1111/j.1600-0501.2012.02547.x

Karatas, O., Balci Yuce, H., Taskan, M. M., Gevrek, F., Lafci, E., & Kasap, H. (2020). Histological evaluation of peri-implant mucosal and gingival tissues in peri-implantitis, peri-implant mucositis and periodontitis patients: a cross-sectional clinical study. *Acta Odontol Scand*, *78*(4), 241-249. https://doi.org/10.1080/00016357.2019.1691256

Karlsson, K., Derks, J., Wennstrom, J. L., Petzold, M., & Berglundh, T. (2020). Occurrence and clustering of complications in implant dentistry. *Clin Oral Implants Res*, *31*(10), 1002-1009. https://doi.org/10.1111/clr.13647

Kasnak, G., Firatli, E., Kononen, E., Olgac, V., Zeidan-Chulia, F., & Gursoy, U. K. (2018). Elevated levels of 8-OHdG and PARK7/DJ-1 in peri-implantitis mucosa. *Clin Implant Dent Relat Res*, *20*(4), 574-582. https://doi.org/10.1111/cid.12619

Kassebaum, N. J., Smith, A. G. C., Bernabe, E., Fleming, T. D., Reynolds, A. E., Vos, T., Murray, C. J. L., Marcenes, W., & Collaborators, G. B. D. O. H. (2017). Global, Regional, and National Prevalence, Incidence, and Disability-Adjusted Life Years for Oral Conditions for 195 Countries, 1990-2015: A Systematic Analysis for the Global Burden of Diseases, Injuries, and Risk Factors. *J Dent Res*, *96*(4), 380-387. https://doi.org/10.1177/0022034517693566

Katagata, Y., Takeda, H., Ishizawa, T., Hozumi, Y., & Kondo, S. (2002). Occurrence and comparison of the expressed keratins in cultured human fibroblasts, endothelial cells and their sarcomas. *Journal of Dermatological Science*, *30*(1), 1-9. https://doi.org/10.1016/S0923-1811(02)00039-7

Katz, J., Yoon, T. Y., Mao, S., Lamont, R. J., & Caudle, R. M. (2007). Expression of the receptor of advanced glycation end products in the gingival tissue of smokers with generalized periodontal disease and after nornicotine induction in primary gingival epithelial cells. *J Periodontol*, *78*(4), 736-741. https://doi.org/10.1902/jop.2007.060381

Khan, M. A., Williams, R. L., & Williams, D. F. (1996). In-vitro corrosion and wear of titanium alloys in the biological environment. *Biomaterials*, *17*(22), 2117-2126. https://doi.org/10.1016/0142-9612(96)00029-4

Kheder, W., Bouzid, A., Venkatachalam, T., Talaat, I. M., Elemam, N. M., Raju, T. K., Sheela, S., Jayakumar, M. N., Maghazachi, A. A., Samsudin, A. R., & Hamoudi, R. (2023). Titanium Particles Modulate Lymphocyte and Macrophage Polarization in Peri-Implant Gingival Tissues. *Int J Mol Sci*, *24*(14). https://doi.org/10.3390/ijms241411644

Khouly, I., Braun, R. S., Ordway, M., Aouizerat, B. E., Ghassib, I., Larsson, L., & Asa'ad, F. (2020). The Role of DNA Methylation and Histone Modification in Periodontal Disease: A Systematic Review. *Int J Mol Sci*, *21*(17). https://doi.org/10.3390/ijms21176217

Kim, Y. G., Kim, M., Kang, J. H., Kim, H. J., Park, J. W., Lee, J. M., Suh, J. Y., Kim, J. Y., Lee, J. H., & Lee, Y. (2016). Transcriptome sequencing of gingival biopsies from chronic periodontitis patients reveals novel gene expression and splicing patterns. *Hum Genomics*, *10*(1), 28. https://doi.org/10.1186/s40246-016-0084-0

Kim, Y. K., Yeo, H. H., & Lim, S. C. (1997). Tissue response to titanium plates: a transmitted electron microscopic study. *J Oral Maxillofac Surg*, *55*(4), 322-326. https://doi.org/10.1016/s0278-2391(97)90115-4

Koide, M., Maeda, H., Roccisana, J. L., Kawanabe, N., & Reddy, S. V. (2003). CytokineRegulation and the signaling mechanism of osteoclast inhibitory peptide-1 (OIP-1/hSca) to inhibit osteoclast formation. *J Bone Miner Res*, *18*(3), 458-465. https://doi.org/10.1359/jbmr.2003.18.3.458

Konermann, A., Gotz, W., Le, M., Dirk, C., Lossdorfer, S., & Heinemann, F. (2016). Histopathological Verification of Osteoimmunological Mediators in Peri-Implantitis and Correlation to Bone Loss and Implant Functional Period. *J Oral Implantol*, *42*(1), 61-68. https://doi.org/10.1563/aaid-joi-D-13-00355

Konttinen, Y. T., Lappalainen, R., Laine, P., Kitti, U., Santavirta, S., & Teronen, O. (2006). Immunohistochemical evaluation of inflammatory mediators in failing implants. *Int J Periodontics Restorative Dent.*, *26*(2), 135-141.

Kotsakis, G. A., Javed, F., Hinrichs, J. E., Karoussis, I. K., & Romanos, G. E. (2015). Impact of cigarette smoking on clinical outcomes of periodontal flap surgical procedures: a systematic review and meta-analysis. *J Periodontol*, *86*(2), 254-263. https://doi.org/10.1902/jop.2014.140452

Kroger, A., Hulsmann, C., Fickl, S., Spinell, T., Huttig, F., Kaufmann, F., Heimbach, A., Hoffmann, P., Enkling, N., Renvert, S., Schwarz, F., Demmer, R. T., Papapanou, P. N., Jepsen, S., & Kebschull, M. (2018). The severity of human peri-implantitis lesions correlates with the level of submucosal microbial dysbiosis. *J Clin Periodontol*, *45*(12), 1498-1509. https://doi.org/10.1111/jcpe.13023

Kuula, H., Salo, T., Pirila, E., Hagstrom, J., Luomanen, M., Gutierrez-Fernandez, A., Romanos, G. E., & Sorsa, T. (2008). Human beta-defensin-1 and -2 and matrix metalloproteinase-25 and -26 expression in chronic and aggressive periodontitis and in peri-implantitis. *Arch Oral Biol*, *53*(2), 175-186. https://doi.org/10.1016/j.archoralbio.2007.09.010

Lang, N. P., Berglundh, T., & Working Group 4 of Seventh European Workshop on, P. (2011). Periimplant diseases: where are we now?--Consensus of the Seventh European Workshop on Periodontology. *J Clin Periodontol*, *38 Suppl 11*, 178-181. https://doi.org/10.1111/j.1600-051X.2010.01674.x

Larsson, L., Castilho, R. M., & Giannobile, W. V. (2015). Epigenetics and its role in periodontal diseases: a state-of-the-art review. *J Periodontol*, *86*(4), 556-568. https://doi.org/10.1902/jop.2014.140559

Leite, F. R. M., Nascimento, G. G., Scheutz, F., & Lopez, R. (2018). Effect of Smoking on Periodontitis: A Systematic Review and Meta-regression. *Am J Prev Med*, *54*(6), 831-841. https://doi.org/10.1016/j.amepre.2018.02.014

Liljenberg, B., Lindhe, J., Berglundh, T., Dahlen, G., & Jonsson, R. (1994). Some microbiological, histopathological and immunohistochemical characteristics of progressive periodontal disease. *J Clin Periodontol*, *21*(10), 720-727. https://doi.org/10.1111/j.1600-051x.1994.tb00793.x

Lindhe, J., Berglundh, T., Ericsson, I., Liljenberg, B., & Marinello, C. (1992). Experimental breakdown of peri-implant and periodontal tissues. A study in the beagle dog. *Clin Oral Implants Res*, *3*(1), 9-16. https://doi.org/10.1034/j.1600-0501.1992.030102.x

Liu, Y., Liu, Q., Li, Z., Acharya, A., Chen, D., Chen, Z., Mattheos, N., Chen, Z., & Huang, B. (2020). Long non-coding RNA and mRNA expression profiles in peri-implantitis vs periodontitis. *J Periodontal Res*, *55*(3), 342-353. https://doi.org/10.1111/jre.12718

Loos, B. G., & Van Dyke, T. E. (2020). The role of inflammation and genetics in periodontal disease. *Periodontol 2000*, *83*(1), 26-39. https://doi.org/10.1111/prd.12297

Lucarini, G., Zizzi, A., Rubini, C., Ciolino, F., & Aspriello, S. D. (2019). VEGF, Microvessel Density, and CD44 as Inflammation Markers in Peri-implant Healthy Mucosa, Peri-implant Mucositis, and Peri-implantitis: Impact of Age, Smoking, PPD, and Obesity. *Inflammation*, *42*(2), 682-689. https://doi.org/10.1007/s10753-018-0926-0

Lundmark, A., Gerasimcik, N., Bage, T., Jemt, A., Mollbrink, A., Salmen, F., Lundeberg, J., & Yucel-Lindberg, T. (2018). Gene expression profiling of periodontitis-affected gingival tissue by spatial transcriptomics. *Sci Rep*, *8*(1), 9370. https://doi.org/10.1038/s41598-018-27627-3

Luo, Z., Wang, H., Sun, Z., Luo, W., & Wu, Y. (2013). Expression of IL-22, IL-22R and IL-23 in the peri-implant soft tissues of patients with peri-implantitis. *Arch Oral Biol*, *58*(5), 523-529. https://doi.org/10.1016/j.archoralbio.2012.08.006

Makihira, S., Mine, Y., Nikawa, H., Shuto, T., Iwata, S., Hosokawa, R., Kamoi, K., Okazaki, S., & Yamaguchi, Y. (2010). Titanium ion induces necrosis and sensitivity to lipopolysaccharide in gingival epithelial-like cells. *Toxicol In Vitro*, *24*(7), 1905-1910. https://doi.org/10.1016/j.tiv.2010.07.023

Mardegan, G. P., Shibli, J. A., Roth, L. A., Faveri, M., Giro, G., & Bastos, M. F. (2017). Transforming growth factor-beta, interleukin-17, and IL-23 gene expression profiles associated with human peri-implantitis. *Clin Oral Implants Res*, *28*(7), e10-e15. https://doi.org/10.1111/clr.12846

Martin, A., Zhou, P., Singh, B. B., & Kotsakis, G. A. (2022). Transcriptome-wide Gene Expression Analysis in Peri-implantitis Reveals Candidate Cellular Pathways. *JDR Clin Trans Res*, *7*(4), 415-424. https://doi.org/10.1177/23800844211045297

Martini, D., Fini, M., Franchi, M., De Pasquale, V., Bacchelli, B., Gamberini, M., Tinti, A., Taddei, P., Giarvesi, G., Ottani, V., Raspanti, M., Guizzardi, S., & Ruggeri, A. (2003). Detachment of titanium and fluorohydroxyapatite particles in unloaded endosseous implants. *Biomaterials 24*, 1309–1316.

Martins, L. R. L., Grzech-Lesniak, K., Castro Dos Santos, N., Suarez, L. J., Giro, G., Bastos, M. F., & Shibli, J. A. (2022). Transcription Factor AhR, Cytokines IL-6 and IL-22 in Subjects with and without Peri-Implantitis: A Case Control-Study. *Int J Environ Res Public Health*, *19*(12). https://doi.org/10.3390/ijerph19127434

Mercan, S., Bölükbaşı, N., Bölükbaşı, M. K., Yayla, M., & Cengiz, S. (2014). Titanium Element Level in Peri-Implant Mucosa. *Biotechnology & Biotechnological Equipment*, *27*(4), 4002-4005. https://doi.org/10.5504/bbeq.2013.0007

Meyer, U., Buhner, M., Buchter, A., Kruse-Losler, B., Stamm, T., & Wiesmann, H. P. (2006). Fast element mapping of titanium wear around implants of different surface structures. *Clin Oral Implants Res*, *17*(2), 206-211. https://doi.org/10.1111/j.1600-0501.2005.01184.x

Mijiritsky, E., Ferroni, L., Gardin, C., Peleg, O., Gultekin, A., Saglanmak, A., Delogu, L. G., Mitrecic, D., Piattelli, A., Tatullo, M., & Zavan, B. (2019). Presence of ROS in Inflammatory Environment of Peri-Implantitis Tissue: In Vitro and In Vivo Human Evidence. *J Clin Med*, *9*(1). https://doi.org/10.3390/jcm9010038

Mirani, F., Maffini, A., Casamichiela, F., Pazzaglia, A., Formenti, A., Dellasega, D., Russo, V., Vavassori, D., Bortot, D., Huault, M., Zeraouli, G., Ospina, V., Malko, S., Apinaniz, J. I., Perez-Hernandez, J. A., De Luis, D., Gatti, G., Volpe, L., Pola, A., & Passoni, M. (2021). Integrated quantitative PIXE analysis and EDX spectroscopy using a laser-driven particle source. *Sci Adv*, *7*(3). https://doi.org/10.1126/sciadv.abc8660

Mirbod, S. M., Ahing, S. I., & Pruthi, V. K. (2001). Immunohistochemical study of vestibular gingival blood vessel density and internal circumference in smokers and non-smokers. *J Periodontol*, *72*(10), 1318-1323. https://doi.org/10.1902/jop.2001.72.10.1318

Moeintaghavi, A., Arab, H. R., Rahim Rezaee, S. A., Naderi, H., Shiezadeh, F., Sadeghi, S., & Anvari, N. (2017). The Effects of Smoking on Expression of IL-12 and IL-1beta in Gingival Tissues of Patients with Chronic Periodontitis. *Open Dent J*, *11*, 595-602. https://doi.org/10.2174/1874210601711010595

Mombelli, A., Hashim, D., & Cionca, N. (2018). What is the impact of titanium particles and biocorrosion on implant survival and complications? A critical review. *Clin Oral Implants Res*, *29 Suppl 18*, 37-53. https://doi.org/10.1111/clr.13305

Mouzakiti, E., Pepelassi, E., Fanourakis, G., Markopoulou, C., Tseleni-Balafouta, S., & Vrotsos, I. (2011). The effect of smoking on the mRNA expression of MMPs and TIMP-1 in untreated chronic periodontitis patients: a cross-sectional study. *J Periodontal Res*, *46*(5), 576-583. https://doi.org/10.1111/j.1600-0765.2011.01375.x

Nagashima, K., Zheng, J., Parmiter, D., & Patri, A. K. (2011). Biological tissue and cell culture specimen preparation for TEM nanoparticle characterization. *Methods Mol Biol*, *697*, 83-91. https://doi.org/10.1007/978-1-60327-198-1_8

Nagy, G., Whitlow, H. J., & Primetzhofer, D. (2022). The scanning light ion microprobe in Uppsala – Status in 2022. *Nuclear Instruments and Methods in Physics Research Section B: Beam Interactions with Materials and Atoms*, *533*, 66-69. https://doi.org/10.1016/j.nimb.2022.10.017

Nakajima, T., Amanuma, R., Ueki-Maruyama, K., Oda, T., Honda, T., Ito, H., & Yamazaki, K. (2008). CXCL13 expression and follicular dendritic cells in relation to B-cell infiltration in periodontal disease tissues. *J Periodontal Res*, *43*(6), 635-641. https://doi.org/10.1111/j.1600-0765.2008.01042.x

Nelson, K., Hesse, B., Addison, O., Morrell, A. P., Gross, C., Lagrange, A., Suarez, V. I., Kohal, R., & Fretwurst, T. (2020). Distribution and Chemical Speciation of Exogenous Micro- and Nanoparticles in Inflamed Soft Tissue Adjacent to Titanium and Ceramic Dental Implants. *Anal Chem*, *92*(21), 14432-14443. https://doi.org/10.1021/acs.analchem.0c02416

Nociti, F. H., Jr., Casati, M. Z., & Duarte, P. M. (2015). Current perspective of the impact of smoking on the progression and treatment of periodontitis. *Periodontol 2000*, *67*(1), 187-210. https://doi.org/10.1111/prd.12063

Noronha Oliveira, M., Schunemann, W. V. H., Mathew, M. T., Henriques, B., Magini, R. S., Teughels, W., & Souza, J. C. M. (2018). Can degradation products released from dental implants affect peri-implant tissues? *J Periodontal Res*, *53*(1), 1-11. https://doi.org/10.1111/jre.12479

Oh, J. M., Kim, Y., Son, H., Kim, Y. H., & Kim, H. J. (2023). Comparative transcriptome analysis of periodontitis and peri-implantitis in human subjects. *J Periodontol*. https://doi.org/10.1002/JPER.23-0289

Olander, J., Ruud, A., Wennerberg, A., & Stenport, V. F. (2022). Wear particle release at the interface of dental implant components: Effects of different material combinations. An in vitro study. *Dent Mater*, *38*(3), 508-516. https://doi.org/10.1016/j.dental.2022.01.001

Olmedo, D. G., Nalli, G., Verdu, S., Paparella, M. L., & Cabrini, R. L. (2013). Exfoliative cytology and titanium dental implants: a pilot study. *J Periodontol*, *84*(1), 78-83. https://doi.org/10.1902/jop.2012.110757

Olmedo, D. G., Paparella, M. L., Spielberg, M., Brandizzi, D., Guglielmotti, M. B., & Cabrini, R. L. (2012). Oral mucosa tissue response to titanium cover screws. *J Periodontol*, *83*(8), 973-980. https://doi.org/10.1902/jop.2011.110392

Orbak, R., Erciyas, K., & Kaya, H. (2003). Flow-cytometric analysis of T-lymphocyte subsets after different treatment methods in smokers and non-smokers with chronic periodontitis. *Int Dent J*, *53*(3), 159-164. https://doi.org/10.1111/j.1875-595x.2003.tb00741.x

Ozdemir, B., Ozmeric, N., Elgun, S., & Baris, E. (2016). Smoking and gingivitis: focus on inducible nitric oxide synthase, nitric oxide and basic fibroblast growth factor. *J Periodontal Res*, *51*(5), 596-603. https://doi.org/10.1111/jre.12338

Paknejad, M., Bayani, M., Yaghobee, S., Kharazifard, M. J., & Jahedmanesh, N. (2015). Histopathological evaluation of gingival tissue overlying two-stage implants after placement of cover screws. *Biotechnology & Biotechnological Equipment*, *29*(6), 1169-1175. https://doi.org/10.1080/13102818.2015.1066234

Palmer, R. M., Wilson, R. F., Hasan, A. S., & Scott, D. A. (2005). Mechanisms of action of environmental factors--tobacco smoking. *J Clin Periodontol*, *32 Suppl 6*, 180-195. https://doi.org/10.1111/j.1600-051X.2005.00786.x

Papapanou, P. N., Sanz, M., Buduneli, N., Dietrich, T., Feres, M., Fine, D. H., Flemmig, T. F., Garcia, R., Giannobile, W. V., Graziani, F., Greenwell, H., Herrera, D., Kao, R. T., Kebschull, M., Kinane, D. F., Kirkwood, K. L., Kocher, T., Kornman, K. S., Kumar, P. S., . . . Tonetti, M. S. (2018). Periodontitis: Consensus report of workgroup 2 of the 2017 World Workshop on the Classification of Periodontal and Peri-Implant Diseases and Conditions. *J Clin Periodontol*, *45 Suppl 20*, S162-S170. https://doi.org/10.1111/jcpe.12946

Passi, P., Zadro, A., Galassini, S., Rossi, P., & Moschini, G. (2002). PIXE micro-beam mapping of metals in human peri-implant tissues. *J Mater Sci Mater Med*, *13*(11), 1083-1089. https://doi.org/10.1023/a:1020309108950

Pettersson, M., Kelk, P., Belibasakis, G. N., Bylund, D., Molin Thoren, M., & Johansson, A. (2017). Titanium ions form particles that activate and execute interleukin-1beta release from lipopolysaccharide-primed macrophages. *J Periodontal Res*, *52*(1), 21-32. https://doi.org/10.1111/jre.12364

Pettersson, M., Pettersson, J., Johansson, A., & Molin Thoren, M. (2019). Titanium release in peri-implantitis. *J Oral Rehabil*, *46*(2), 179-188. https://doi.org/10.1111/joor.12735

Pjetursson, B. E., Thoma, D., Jung, R., Zwahlen, M., & Zembic, A. (2012). A systematic review of the survival and complication rates of implant-supported fixed dental prostheses (FDPs) after a mean observation period of at least 5 years. *Clin Oral Implants Res*, *23 Suppl 6*, 22-38. https://doi.org/10.1111/j.1600-0501.2012.02546.x

Pontoriero, R., Tonelli, M. P., Carnevale, G., Mombelli, A., Nyman, S. R., & Lang, N. P. (1994). Experimentally induced peri-implant mucositis. A clinical study in humans. *Clin Oral Implants Res*, *5*(4), 254-259. https://doi.org/10.1034/j.1600-0501.1994.050409.x

Rakic, M., Radunovic, M., Petkovic-Curcin, A., Tatic, Z., Basta-Jovanovic, G., & Sanz, M. (2022). Study on the immunopathological effect of titanium particles in peri-implantitis granulation tissue: A case-control study. *Clin Oral Implants Res*, *33*(6), 656-666. https://doi.org/10.1111/clr.13928

Rao, A., Barkley, D., Franca, G. S., & Yanai, I. (2021). Exploring tissue architecture using spatial transcriptomics. *Nature*, *596*(7871), 211-220. https://doi.org/10.1038/s41586-021-03634-9

Revathi, A., Borras, A. D., Munoz, A. I., Richard, C., & Manivasagam, G. (2017). Degradation mechanisms and future challenges of titanium and its alloys for dental implant applications in oral environment. *Mater Sci Eng C Mater Biol Appl*, *76*, 1354-1368. https://doi.org/10.1016/j.msec.2017.02.159

Rezavandi, K., Palmer, R. M., Odell, E. W., Scott, D. A., & Wilson, R. F. (2002). Expression of ICAM-1 and E-selectin in gingival tissues of smokers and non-smokers with periodontitis. *J Oral Pathol Med*, *31*(1), 59-64. https://doi.org/10.1046/j.0904-2512.2001.joptest.doc.x

Richter, G. M., Kruppa, J., Munz, M., Wiehe, R., Hasler, R., Franke, A., Martins, O., Jockel-Schneider, Y., Bruckmann, C., Dommisch, H., & Schaefer, A. S. (2019). A combined epigenome- and transcriptome-wide association study of the oral masticatory mucosa assigns CYP1B1 a central role for epithelial health in smokers. *Clin Epigenetics*, *11*(1), 105. https://doi.org/10.1186/s13148-019-0697-y

Roediger, M., Miró, X., Geffers, R., Irmer, M., Huels, A., Miosge, N., & Gersdorff, N. (2009). Profiling of Differentially Expressed Genes in Peri-implantitis and Periodontitis in vivo by Microarray Analysis. *Journal of Oral Biosciences*, *51*(1), 31-45. https://doi.org/10.1016/s1349-0079(09)80018-2

Safioti, L. M., Kotsakis, G. A., Pozhitkov, A. E., Chung, W. O., & Daubert, D. M. (2017). Increased Levels of Dissolved Titanium Are Associated With Peri-Implantitis - A Cross-Sectional Study. *J Periodontol*, *88*(5), 436-442. https://doi.org/10.1902/jop.2016.160524

Sanz, M., Alandez, J., Lazaro, P., Calvo, J. L., Quirynen, M., & van Steenberghe, D. (1991). Histo-pathologic characteristics of peri-implant soft tissues in Branemark implants with 2 distinct clinical and radiological patterns. *Clin Oral Implants Res*, *2*(3), 128-134. https://doi.org/10.1034/j.1600-0501.1991.020305.x

Sanz, M., Herrera, D., Kebschull, M., Chapple, I., Jepsen, S., Beglundh, T., Sculean, A., Tonetti, M. S., Participants, E. F. P. W., & Methodological, C. (2020). Treatment of stage I-III periodontitis-The EFP S3 level clinical practice guideline. *J Clin Periodontol*, *47 Suppl 22*(Suppl 22), 4-60. https://doi.org/10.1111/jcpe.13290

Schlegel, K. A., Eppeneder, S., & Wiltfang, J. (2002). Soft tissue findings above submerged titanium implants--a histological and spectroscopic study. *Biomaterials*, *23*(14), 2939-2944. https://doi.org/10.1016/s0142-9612(01)00423-9

Schliephake, H., Reiss, G., Urban, R., Neukam, F. W., & Guckel, S. (1993). Metal release from titanium fixtures during placement in the mandible: an experimental study. *Int J Oral Maxillofac Implants*, *8*(5), 502-511.

Schmidt, J. C., Jajjo, E., Berglundh, T., & Zitzmann, N. U. (2020). Periodontitis lesions in smokers and non-smokers. *Eur J Oral Sci*, *128*(3), 196-203. https://doi.org/10.1111/eos.12693

Schminke, B., Vom Orde, F., Gruber, R., Schliephake, H., Burgers, R., & Miosge, N. (2015). The pathology of bone tissue during peri-implantitis. *J Dent Res*, *94*(2), 354-361. https://doi.org/10.1177/0022034514559128

Schwarz, F., Derks, J., Monje, A., & Wang, H. L. (2018). Peri-implantitis. *J Clin Periodontol*, *45 Suppl 20*, S246-S266. https://doi.org/10.1111/jcpe.12954

Senturk, R. A., Sezgin, Y., Bulut, S., & Ozdemir, B. H. (2018). The effects of smoking on the expression of gelatinases in chronic periodontitis: a cross-sectional study. *Braz Oral Res*, *32*, e114. https://doi.org/10.1590/1807-3107bor-2018.vol32.0114

Setyawati, M. I., Khoo, P. K., Eng, B. H., Xiong, S., Zhao, X., Das, G. K., Tan, T. T., Loo, J. S., Leong, D. T., & Ng, K. W. (2013). Cytotoxic and genotoxic characterization of titanium dioxide, gadolinium oxide, and poly(lactic-co-glycolic acid) nanoparticles in human fibroblasts. *J Biomed Mater Res A*, *101*(3), 633-640. https://doi.org/10.1002/jbm.a.34363

Seyfang, M., Dreyhaupt, J., Wiegreffe, C., Rudolph, H., Luthardt, R. G., & Kuhn, K. (2022). Quantification of MRP8 in immunohistologic sections of peri-implant soft tissue: Development of a novel automated computer analysis method and of its validation procedure. *Comput Biol Med*, *148*, 105861. https://doi.org/10.1016/j.compbiomed.2022.105861

Seymour, G. J., Gemmell, E., Lenz, L. J., Henry, P., Bower, R., & Yamazaki, K. (1989). Immunohistologic analysis of the inflammatory infiltrates associated with osseointegrated implants. *Int J Oral Maxillofac Implants*, *4*(3), 191-198. https://www.ncbi.nlm.nih.gov/pubmed/2639119

Sonmez, S., Canda, T., Ozkara, E., & Ak, D. (2003). Quantitative evaluation of the vasculature and fibronectin localization in gingival connective tissue of smokers and non-smokers. *J Periodontol*, *74*(6), 822-830. https://doi.org/10.1902/jop.2003.74.6.822

Souto, G. R., Queiroz-Junior, C. M., Costa, F. O., & Mesquita, R. A. (2014). Effect of smoking on immunity in human chronic periodontitis. *Immunobiology*, *219*(12), 909-915. https://doi.org/10.1016/j.imbio.2014.08.003

Souza, J. C., Barbosa, S. L., Ariza, E. A., Henriques, M., Teughels, W., Ponthiaux, P., Celis, J. P., & Rocha, L. A. (2015). How do titanium and Ti6Al4V corrode in fluoridated medium as found in the oral cavity? An in vitro study. *Mater Sci Eng C Mater Biol Appl*, *47*, 384-393. https://doi.org/10.1016/j.msec.2014.11.055

Stahl, P. L., Salmen, F., Vickovic, S., Lundmark, A., Navarro, J. F., Magnusson, J., Giacomello, S., Asp, M., Westholm, J. O., Huss, M., Mollbrink, A., Linnarsson, S., Codeluppi, S., Borg, A., Ponten, F., Costea, P. I., Sahlen, P., Mulder, J., Bergmann, O., . . . Frisen, J. (2016). Visualization and analysis of gene expression in tissue sections by spatial transcriptomics. *Science*, *353*(6294), 78-82. https://doi.org/10.1126/science.aaf2403

Suarez-Lopez Del Amo, F., Rudek, I., Wagner, V. P., Martins, M. D., O'Valle, F., Galindo-Moreno, P., Giannobile, W. V., Wang, H. L., & Castilho, R. M. (2017). Titanium Activates the DNA Damage Response Pathway in Oral Epithelial Cells: A Pilot Study. *Int J Oral Maxillofac Implants*, *32*(6), 1413-1420. https://doi.org/10.11607/jomi.6077

Taskan, M. M., & Gevrek, F. (2020). PPAR-gamma, RXR, VDR, and COX-2 Expressions in gingival tissue samples of healthy individuals, periodontitis and peri-implantitis patients. *Niger J Clin Pract*, *23*(1), 46-53. https://doi.org/10.4103/njcp.njcp_349_19

Tawse-Smith, A., Ma, S., Duncan, W. J., Gray, A., Reid, M. R., & Rich, A. M. (2017). Implications of Wear at the Titanium-Zirconia Implant-Abutment Interface on the Health of Peri-implant Tissues. *Int J Oral Maxillofac Implants*, *32*(3), 599-609. https://doi.org/10.11607/jomi.5014

Tawse-Smith, A., Ma, S., Siddiqi, A., Duncan, W. J., Girvan, L., & Hussaini, H. M. (2012). Titanium Particles in Peri-Implant Tissues: Surface Analysis and Histologic Response. *Clinical Advances in Periodontics*, *2*(4), 232-238. https://doi.org/10.1902/cap.2012.110081

Tomar, S. L., & Asma, S. (2000). Smoking-Attributable Periodontitis in the United States: Findings From NHANES III. *Journal of Periodontology*, *71*(5), 743-751. https://doi.org/10.1902/jop.2000.71.5.743

Tomasi, C., Leyland, A. H., & Wennstrom, J. L. (2007). Factors influencing the outcome of non-surgical periodontal treatment: a multilevel approach. *J Clin Periodontol*, *34*(8), 682-690. https://doi.org/10.1111/j.1600-051X.2007.01111.x

Tonetti, M. S., Greenwell, H., & Kornman, K. S. (2018). Staging and grading of periodontitis: Framework and proposal of a new classification and case definition. *J Periodontol*, *89 Suppl 1*, S159-S172. https://doi.org/10.1002/JPER.18-0006

Tonetti, M. S., & Sanz, M. (2019). Implementation of the new classification of periodontal diseases: Decision-making algorithms for clinical practice and education. *J Clin Periodontol*, *46*(4), 398-405. https://doi.org/10.1111/jcpe.13104

Toyooka, T., Amano, T., & Ibuki, Y. (2012). Titanium dioxide particles phosphorylate histone H2AX independent of ROS production. *Mutat Res*, *742*(1-2), 84-91. https://doi.org/10.1016/j.mrgentox.2011.12.015

Traweek, S. T., Liu, J., & Battifora, H. (1993). Keratin gene expression in non-epithelial tissues. Detection with polymerase chain reaction. *Am J Pathol*, *142*(4), 1111-1118. https://www.ncbi.nlm.nih.gov/pubmed/7682761

Venza, I., Visalli, M., Cucinotta, M., De Grazia, G., Teti, D., & Venza, M. (2010). Proinflammatory gene expression at chronic periodontitis and peri-implantitis sites in patients with or without type 2 diabetes. *J Periodontol*, *81*(1), 99-108. https://doi.org/10.1902/jop.2009.090358

Voggenreiter, G., Leiting, S., Brauer, H., Leiting, P., Majetschak, M., Bardenheuer, M., & Obertacke, U. (2003). Immuno-inflammatory tissue reaction to stainless-steel and titanium plates used for internal fixation of long bones. *Biomaterials*, *24*(2), 247-254. https://doi.org/10.1016/s0142-9612(02)00312-5

Wachi, T., Shuto, T., Shinohara, Y., Matono, Y., & Makihira, S. (2015). Release of titanium ions from an implant surface and their effect on cytokine production related to alveolar bone resorption. *Toxicology*, *327*, 1-9. https://doi.org/10.1016/j.tox.2014.10.016

Wheelis, S. E., Gindri, I. M., Valderrama, P., Wilson, T. G., Jr., Huang, J., & Rodrigues, D. C. (2016). Effects of decontamination solutions on the surface of titanium: investigation of surface morphology, composition, and roughness. *Clin Oral Implants Res*, *27*(3), 329-340. https://doi.org/10.1111/clr.12545

White, P. C., Hirschfeld, J., Milward, M. R., Cooper, P. R., Wright, H. J., Matthews, J. B., & Chapple, I. L. C. (2018). Cigarette smoke modifies neutrophil chemotaxis, neutrophil extracellular trap formation and inflammatory response-related gene expression. *J Periodontal Res*, *53*(4), 525-535. https://doi.org/10.1111/jre.12542

Williams, C. G., Lee, H. J., Asatsuma, T., Vento-Tormo, R., & Haque, A. (2022). An introduction to spatial transcriptomics for biomedical research. *Genome Med*, *14*(1), 68. https://doi.org/10.1186/s13073-022-01075-1

Wilson, T. G., Jr., Valderrama, P., Burbano, M., Blansett, J., Levine, R., Kessler, H., & Rodrigues, D. C. (2015). Foreign bodies associated with peri-implantitis human biopsies. *J Periodontol*, *86*(1), 9-15. https://doi.org/10.1902/jop.2014.140363

Wimmer, I., Troscher, A. R., Brunner, F., Rubino, S. J., Bien, C. G., Weiner, H. L., Lassmann, H., & Bauer, J. (2018). Systematic evaluation of RNA quality, microarray data reliability and pathway analysis in fresh, fresh frozen and formalin-fixed paraffin-embedded tissue samples. *Sci Rep*, *8*(1), 6351. https://doi.org/10.1038/s41598-018-24781-6

Wu, Y. Y., Cao, H. H., Kang, N., Gong, P., & Ou, G. M. (2013). Expression of cellular fibronectin mRNA in adult periodontitis and peri-implantitis: a real-time polymerase chain reaction study. *Int J Oral Sci*, *5*(4), 212-216. https://doi.org/10.1038/ijos.2013.65

Zhang, Q., Liu, J., Ma, L., Bai, N., & Xu, H. (2020). Wnt5a is involved in LOX-1 and TLR4 induced host inflammatory response in peri-implantitis. *J Periodontal Res*, *55*(2), 199-208. https://doi.org/10.1111/jre.12702

Zhou, H., Chen, D., Xie, G., Li, J., Tang, J., & Tang, L. (2020). LncRNA-mediated ceRNA network was identified as a crucial determinant of differential effects in periodontitis and periimplantitis by high-throughput sequencing. *Clin Implant Dent Relat Res*, *22*(3), 424-450. https://doi.org/10.1111/cid.12911

Zitzmann, N. U., Berglundh, T., Marinello, C. P., & Lindhe, J. (2001). Experimental peri-implant mucositis in man. *J Clin Periodontol*, *28*(6), 517-523. https://doi.org/10.1034/j.1600-051x.2001.028006517.x